Durham E-Theses

Adaptive Three-Stage Controlled Islanding to Prevent Imminent Wide-area Blackouts

SHAO, HONGBO

How to cite:

SHAO, HONGBO (2016) *Adaptive Three-Stage Controlled Islanding to Prevent Imminent Wide-area Blackouts*, Durham theses, Durham University. Available at Durham E-Theses Online: http://etheses.dur.ac.uk/11410/

Use policy

The full-text may be used and/or reproduced, and given to third parties in any format or medium, without prior permission or charge, for personal research or study, educational, or not-for-profit purposes provided that:

- a full bibliographic reference is made to the original source
- a link is made to the metadata record in Durham E-Theses
- the full-text is not changed in any way

The full-text must not be sold in any format or medium without the formal permission of the copyright holders.

Please consult the full Durham E-Theses policy for further details.

Academic Support Office, Durham University, University Office, Old Elvet, Durham DH1 3HP
e-mail: e-theses.admin@dur.ac.uk Tel: +44 0191 334 6107
http://etheses.dur.ac.uk

Adaptive Three-Stage Controlled Islanding to Prevent Imminent Wide-area Blackouts

Hongbo Shao

A thesis submitted for the degree of Doctor of Philosophy

School of Engineering and Computing Science
Durham University
United Kingdom

2015

Abstract

Power blackouts are a recurring problem worldwide, and research in this area continues to focus on developing improved methods for their prediction and prevention. Controlled islanding has been proposed as a last resort action to save the network before imminent blackouts when the usual means fail in an unexpected manner. Successful controlled islanding has to deal with three important issues that are involved in the implementation of islanding: when to island, where to island and what to do after islanding is implemented in each island.

This thesis presents a framework that combines all three issues to achieve successful islanding based on wide area measurement systems (WAMS). In addition, this thesis focuses on the question of when to island. This question is critical to the success of the three-stage controlled islanding scheme because the possible issues of false dismissal and false alarm have to be handled. In false dismissal, islanding is triggered too late. However, the potentially unstable system is still allowed to operate, and this unstable system, which could have survived, may cause uncontrolled cascading blackouts. In false alarm, islanding is triggered too early, and an originally stable system is forced to split into islands, resulting in unnecessary disruption and economic loss. Thus, the early recognition and identification of "the point of no return" before blackout is inevitable. The single machine equivalent (SIME) method is adopted online to predict transient stability during cascading outages that would shortly lead to blackouts, giving support in decisions about when to island in terms of transient instability. SIME also evaluates dynamic stability after islanding and ensures that the selected island candidates are stable before action is taken. Moreover, in this thesis, the power flow tracing-based method provides all possible islanding cutsets, and SIME helps to identify the one that has the best transient stability and minimal power flow disruption. If no possible island cut set exists, corrective actions through tripping critical generators or load shedding are undertaken in each island.

The IEEE 10-generator, 39-busbar power system and 16-generator 68-busbar system are used to demonstrate the entire framework of the controlled islanding scheme. The performance of each methodology involved in each stage is then presented.

Declaration

No part of this thesis has been submitted elsewhere for any other degree or qualification. The content of this thesis is all my own work unless referenced to the contrary in the text.

Copyright © 2015 Hongbo Shao.

"The copyright of this thesis rests with the author. No quotation from it should be published without the prior written consent of the author and information derived from it should be acknowledged".

Acknowledgement

My EPSRC-funded PhD research began in January, 2011. The work described in this thesis was completed with the assistance of many people who deserve my gratitude.

First, I would like to thank my supervisor, Professor Janusz Bialek. I will never forget his knowledge, guidance and responsibility in conducting research and sharing life experiences. His enthusiasm and patience in research constantly inspired me to overcome challenges when obstacles occurred. I could not have completed this research project without his help.

I would also like to thank my colleagues, Dr Patrick McNabb, Dr Sean Norris and Dr Zhenzhi Lin. They shared their experience and knowledge with me in this research project, and they gave me their friendly support and assistance. Because of the constructive discussions with them and their helpful comments, my research project progressed every day.

Finally, I would like to thank my family—Yufu Shao, Huixia Song and Zihui Shao. Thanks for your understanding and support of my decision when I was at a crossroads in my life.

Publications

Conference Papers:

- **H. Shao**, Z. Lin, S. Norris and J. Bialek, "Application of Emergency-Single Machine Equivalent method for cascading outages," *18th Power Systems Computation Conference*, Wroclaw, Poland. Aug. 2014.
- Z. Lin, S. Norris, **H. Shao** and J. Bialek, "Transient stability assessment of controlled islanding based on power flow tracing," *18th Power Systems Computation Conference*, Wroclaw, Poland. Aug. 2014.
- **H. Shao**, S. Norris, Z. Lin and J. Bialek, "Determination of when to island by analysing dynamic characteristics in cascading outages," *IEEE PowerTech Conference*, Grenoble, France. Jun. 2013.
- S. Norris, **H. Shao** and J. Bialek, "Considering voltage stability in preventive islanding," *IEEE PowerTech Conference*, Grenoble, France. Jun. 2013.
- **H. Shao** and J. Bialek, "When to island in the controlled islanding scheme to prevent imminent wide-area blackouts," *47th International Universities' Power Engineering Conference*, London, UK. Sep. 2012.

Journal Papers:

- Z. Lin, S. Norris, **H. Shao** and J. Bialek, "Controlled islanding: comparison between power flow tracing and slow coherency based approaches," *IEEE Transactions on Smart Grid*. To be submitted in Mar. 2016.
- **H. Shao**, Z. Lin, S. Norris and J. Bialek, "Adaptive three-stage controlled islanding to prevent imminent wide-area blackouts," *IEEE Transactions on Power Systems*. To be submitted in Mar. 2016.
- Z. Lin, **H. Shao**, S. Norris and J. Bialek, "Improved slow coherency based islanding considering transient stability margins," *IEEE Transactions on Power Systems*. To be submitted in Mar. 2016.

Contents

List of Figures

List of Tables

Acronyms and Abbreviations

AVR	Automatic Voltage Regulator
ANN	Artificial Neural Network
BAs	Balancing Areas
CC	Corrective control
CT	Current Transformer
CSR	Critical Splitting Rule
CIT	Critical Islanding Time
CMR	Critical Machine Ranking
COA	Centre of Angles
DT	Decision Tree
DR	Distance Relay
DSA	Dynamic Security Assessment
EAC	Equal Area Criterion
EEAC	Extended Equal Area Criterion
EC	Emergency control
HVDC	High Voltage Direct Current
IDMT	Inverse Definite Mean Time
IS	Islanding Strategies
KE	Kinetic Energy
LMP	Locational Marginal Price

MLRM	Multi-Linear Regression Models
OMIB	One Machine Infinite Bus
OBDD	Ordered Binary Decision Diagram
OC	Operation Condition
OEL	Over Excitation Limiter
OST	Out-of-Step Tripping
PMU	Phasor Measurement Unit
PC	Preventive Control
PSM	Plug Scale Multiplier
PSB	Power Swing Blocking
PSAT	Power System Assessment Tool
PE	Potential Energy
PF	Power Flow
RPR	Reactive Power Reserve
SIME	SIngle Machine Equivalent
SCADA	Supervisory Control And Data Acquisition
TSO	Transmission System Operator
TDS	Time Domain Simulation
UCTE	Union for Coordination of Transmission of Electricity
UFLS	Under-Frequency Load-Shedding
UVLS	Under-Voltage Load-Shedding

UEL	Under Excitation Limiter
ULTC	Under-Load Tap Changer
VSM	Voltage Stability Margin
WAMS	Wide Area Measurement Systems
WLS	Weighted Least-Squares

Nomenclature

A	The set of all remaining machines
a	Its equivalent of A, aggregated machine
A_1 / A_{acc}	Kinetic energy
A_2 / A_{dec}	Potential energy
B	Susceptance
E_i	Voltage behind d-axis transient reactance
E_G	Voltage on generator side
E_M	Voltage on motor side
G	Conductance
H	Inertia constant
I	Faulted current that relay monitors
I_N	Nominal current of relay
I^2R	Power loss
i_f	Field current
J	Inertia of the turbine/generator set
M_i	Inertia coefficient
$PSM \cdot I_N$	Pickup current
P_e	Electrical power

P_m	Mechanical power
P_R	Transmitted active power
P_g	Active power produced by generator
P_{eO}	Pre-breaker $P-\delta$ curve
P_{eP}	Post-breaker $P-\delta$ curve
Q_R	Local injected reactive power
Q_g	Reactive power produced by generator
S	The set of machines composing the critical cluster of machines
s	Its equivalent of S, aggregated machine
T_m	Mechanical torque provided by the turbine
T_e	Electrical torque reacted by the generator
T_S	Synchronizing torque coefficient
$T_S\Delta\delta$	Synchronizing torque component
T_D	Damping torque coefficient
$T_D\Delta w$	Damping torque component
t_u	Time to instability
Δt	Time interval
V_g	Voltage at the generator bus
V_R	Receiving end voltage

v_{ref_0}	Reference voltage of AVR
w_0	Generator angular speed
X_T	Overall reactance of generator, transmission line and motor
x	Reactive power reserve
x_d	d-axis reactance of generator
x_q	q-axis reactance of generator
y	Voltage stability margin
Y	Reduced admittance matrix to generator nodes
$Y_{ij}\left(\theta_{ij}\right)$	Modulus (argument) of *ij*th element of Y
Z_{LD}	Load demand
δ_o	Orginal steady state rotor angle
δ_m	Generator rotor angle
δ_u	OMIB unstable equilibrium angle
δ_{clear}	Generator angle when protective devices take actions to clear the fault
β	Best vector of coefficients
γ	OMIB acceleration at $t = t\left(\delta_o^+\right)$
η	Transient stability margin
λ^*	Measured cascading propagation factor
ε	Estimation errors

Chapter 1:

Introduction

In recent decades, the reliability of electrical power systems has become more and more demanding because the profit-driven maximum utilisation of network and environment-driven high penetration of generation distribution have reduced the security margin and led to the high possibility of blackouts under severe disturbances. In addition, the lack of effective communication between neighbouring operators in the transfer of power across borders also may jeopardize the system's security, which caused the blackout that occurred in Italy in 2003 [1]. Consequently, the occurrence of blackouts has spread around the world in recent decades, most of which were caused cascading outages, such as the India blackout in 2012 [2][3] and the US/Canada blackout in 2003 [4]. The malfunction of protection and the lack of proper protection integration deteriorated, causing cascading outages in these cases. Normally, blackouts are imminent when the usual methods in the widely used three-defence-line scheme fail, which are preventive control, emergency control and corrective control [5]. Under these circumstances, controlled islanding is proposed as a last resort to prevent blackouts and help the system to survive [6]-[8]. This controlled islanding scheme has three stages that must be considered before action is taken: 1) When to island? 2) Where to island? 3) After islanding, the dynamic stability in each island is evaluated.

1.1 Research Background and Objective

This research is an engineering project that aims to develop methodologies to prevent the occurrence of blackouts by splitting the transmission network into several islands when a blackout is imminent. In order to make the controlled islanding scheme perform successfully, a few questions have to be properly addressed. Because islanding is already a huge disturbance, proper islanding cutsets should be provided without worsening the state of the system. In addition, the designed islands should be triggered at the correct moment as last resort, and the islands formed after splitting the network should maintain a power balance between generation and demand without violating

static and dynamic constraints, such as the thermal current limits of transmission lines and transient stability. Based on different spectra of research, the project is accordingly divided into three stages [15]:

- Stage 1: When to island?

The question of when to island is of crucial importance because islanding too early causes an unnecessary, heavy intervention with enormous economic loss. However, waiting too long would lead to a blackout [6]. Thus, the early recognition and identification of the point of no return before a blackout is very important. Previous research in [7][8] used a trained decision tree (DT) based on off-line simulation data from a specific system to decide when to island. However, DT-based methods are not flexible in their application for different power systems with continuously updated system topology [6]. Similarly, in [9] a probability analysis was proposed based on measurement data of previous blackout events to decide whether the cascading failures would propagate in a network. However, the use of probability theory is still risky in real-time operations [6].

This thesis aims to answer the question when is "the point of no return" by using the single machine equivalent (SIME) method [10]-[14] when controlled islanding has to be activated. In this work, we assume that blackouts are caused by cascading outages, and the point of no return is the last tripped line, which results in transient instability. In fact, blackouts are characterised by several features, such as voltage collapse, frequency collapse and transient instability in cascading outages. However, in this thesis, we concentrate on transient instability because the majority of the known, previous blackouts were preceded by severe power swings. By applying SIME online, we aim to find an a priori transient stability indicator during cascading outages and adapt to the controlled islanding scheme to support decision making of islanding implementation in terms of transient instability. SIME transforms the multi-machine system into a two-machine dynamic equivalent, and then it is further reduced to a one-machine infinite bus (OMIB) system [10]-[14]. The transient stability issue is then reduced to a single equation to compare the kinetic energy and the potential energy during dynamic change under contingencies, which is based on the well-known equal area criterion. In addition, the on-line application of SIME relies on real-time information from wide area

measurement systems (WAMS). SIME monitors the system's status and updates its calculation results, so it could predict whether the system is driven to transient instability after assuming that the next expected tripped line is actually tripped. The identification of the next expected tripped line is based on the thermal threshold of the lines and the thermal characteristics of the protection installed on the lines [15]. If SIME indicates that the system will be transiently stable after the assumed line is tripped, then the order of implementing the controlled islanding has to wait for the performance of the other existing control. In the meantime, the status of the system's stability continues to be monitored and assessed after the next expected line is tripped. If the a priori transient indicator shows transient instability after tripping the next expected line, then the order will be given immediately to split the network into the designed islanding cutsets once the next expected line is actually tripped.

- Stage 2: Where to island?

In previous research, the ordered binary decision diagram (OBDD), slow coherency and spectral clustering-based method were proposed to solve this issue. In [16]-[18] the OBDD-based method aimed to provide all the possible splitting strategies to satisfy the required constraints, such as synchronisation, power balance and rated limits. In [19]-[23], spectral graph theory-based islanding methods were proposed. The basic principle was to use graph eigenvalue analysis to provide the intrinsic structure of the power system and obtain information to identify the transmission lines that led to the creation of islands. In [24]-[27], the slow coherency-based method was used to provide islanding cutsets by first identifying the coherent generator groups and then searching for minimal cutsets having a minimal power flow imbalance in each controlled island. However, the identification of coherent groups of machines is based on small-signal linearized analysis around a certain operating point. The operating point may shift away because of large-scale dynamic changes, and system splitting may follow the invalid slow-coherency groups. Even worse, there may be resulting transient instability in each formed island after splitting. In this thesis, power flow tracing-based islanding cutsets are used, which are then adapted to the three-stage controlled islanding scheme. The power flow tracing-based method in [28][29] provides a new approach to splitting strategies in controlled islanding. It is based on the proportional sharing principle, which starts from disturbed nodes to identify the power flow between any two nodes in

the system. When the power flow is known, the nodes with heavier power flow between them are regarded as strongly connected, and they should stay connected in controlled islanding. Nodes with less power flow in between them or weakly connected nodes are considered cut through for islanding. Compared to the slow coherency-based method, in the power flow tracing method, the performance of power flow disruption, minimal generation-load imbalance and subsequent transient stability in islands is highlighted. In real situations, although protection, such as load or generation shedding, helps stabilize the formed islands, we do not consider it as the focus of this research.

- Stage 3: Evaluation of dynamic stability in each island after islanding

Because islanding is a huge disturbance to the system, intentional splitting has to ensure that it will not affect customers in using electrical power in originally healthy islands after islanding. Therefore, successful controlled islanding not only relies on splitting the entire network into smaller islands with the best possible generation/load power balance, but also has to ensure that the selected islanding cutsets are transiently stable before the order for intentional splitting order is given to the system operator. As mentioned earlier, SIME helps to identify the point of no return in cascading line trips, in which the last line trip leads to transient instability and the system's collapse. When this is detected by an a priori SIME indicator, the islanding order has to wait to be activated until the last line is tripped. Therefore, another important concern before splitting is to make sure that the selected power flow tracing-based islanding cutsets are transiently stable by using SIME before the assumed last expected tripped line has been actually tripped. If SIME indicates that one or more islanding cut sets are unstable, these candidates are discarded and then the power-flow-tracing-based method provides another candidate. Subsequently, SIME continues assessing the transient status until the newly provided islanding cutsets are determined to be transiently stable. If no possible island with transient stability is provided, further actions have to be taken, such as load shedding and generator tripping, in order to achieve a power balance in the island and bring the sub-system back to a safe operating condition.

1.2 Contribution to Knowledge

This thesis contributes to the existing knowledge by developing methods to use in three different stages to solve the problem and by proposing a framework that closely

connects these three stages for an online application that prevents blackouts as a last resort of corrective control.

First and most important, a framework consisting of these three closely connected stages in a controlled islanding scheme for online application is proposed. In this framework, SIME and the power flow tracing method are used and further developed. Subsequently, they are adapted to the three-stage controlled islanding scheme. The case study results showed that when to island was determined through the identification of the point of no return by using SIME. The calculation results of using SIME matched the time domain simulation. In addition, the disturbance could be contained in the sick island by using power flow tracing and forming only two islands to stabilise imminent blackouts. SIME was also used to assess transient stability in each island after islanding.

Transient stability assessment tools, such as SIME, are conventionally applied in cases of three phase-to-ground faults. In this application, once the multi-machine system is transferred to the OMIB equivalent, then the issue of transient stability assessment is decided by when the fault is cleared. It is well known that before the fault is cleared, some generators keep accelerating to gain kinetic energy, which is stored in the generators, and the generator angles continue to increase. Therefore, a critical clearing time is essential to decide whether the generators can be brought back to synchronism with the other generators when the fault is cleared. The comparison of both kinetic energy and potential energy during the three conditions of pre-fault, during-fault and post-fault is a dynamic process that is subject to the applied critical clearing time. However, in cases of line trip, only the two conditions of pre-trip and post-trip exist without the involvement of a contingency clearing action. The occurrence of the gained kinetic energy and potential energy is irrelevant to the critical clearing time. In other words, the obtained maximal kinetic energy and the potential energy are fixed each time a single line is tripped. In this thesis, the novelty of using SIME under such circumstances is that SIME is formulated during the line trip cases instead of traditional fault application cases, and then it is adapted to cascading line outages, which occur shortly before blackouts. Thus, after each line trip, the specific stability margin could be computed, and it could tell how far the current operating condition is from the transient instability boundary. Based on the obtained a-priori transient stability indicator, decisions about islanding can be taken in terms of the transient instability during

cascading outages. In addition, in order to increase the accuracy for online application, the results of the SIME calculation results are updated every short-time interval, which relies on the online WAMS system. In the decision tree (DT) method, the decision to island relies on a large number of off-line trained databases. The DT method is time-consuming and inflexible because it has to be trained every time it is applied to a different power system. In this thesis, a new method based on SIME calculates the transient stability margin very quickly because it relies on only a single equation based on a well-known criterion of equal area. Moreover, it is flexible enough to be applied in different power systems to decide when to island in terms of transient instability during cascading outages.

Regarding where to island, a novel method for power flow tracing, which was developed in Durham, was applied in [28][29]. The main author was Dr Sean Norris, I collaborated as a team member and contributed to this research in our group. Contribution in this part is that in order to identify the best optimal islands, three constraints consisting of power disruption, power imbalance and voltage change have been raised as a team member in developing power flow tracing based islanding solution. Based on the islanding cutsets obtained from power flow tracing, SIME will be further applied in sub-system to assess the post-islanding transient stability in order to successfully delivery this three-stage controlled islanding scheme. The power flow tracing method is location dependent and aims to contain the spread of disturbance, leaving only two islands in the entire power network. One island contains the disturbance, and the other one ensures that the remaining healthy network is intact. The method starts by looking at the bus where the disturbance occurs and then identifies the cutting boundary around the sick bus. Because power flow tracing allows the determination of the power flow contribution on each bus, we know how much the neighbouring bus was dependent on the source bus of the disturbance in terms of real power. Their dependency was expressed based on the receiving end and the sending end of the power around the bus. If the neighbouring bus is heavily dependent on the sick bus, then they are strongly connected. The strongly connected bus is contained in the island where the sick bus is located until the power flow tracing identifies the most weakly connected bus, which is considered the cutting boundary between the sick island and the remaining healthy island. Compared with previous methods, the

advantage of forming two islands by using power flow tracing is that it avoids unnecessary cuts that might lead to an overall reduction in security. In addition, it prevents possible asynchronous regions from occurring. It is difficult if too many islands need to be resynchronised after islanding. Another advantage of power flow tracing is that the input signal relies only on the information about power flow, which is easily obtained from the online measurement or the state estimator.

Furthermore, in this thesis, SIME is applied to each island. It aims to assess the operating condition and make sure that the sub-system in each island is transiently stable before the islanding can be implemented. Previous research has not investigated this issue. Although the system is intended to be split in order to affect the customers as little as possible, there is no guarantee that an exact power balance can be achieved between the generation and the load in each island. Therefore, under this situation, SIME is applied to assess whether the sub-system in each island is transient stable. If so, then the order of the controlled islanding scheme could be given subsequently. Otherwise, further action in the unstable island has to be taken, such as load shedding or generator tripping.

Chapter 2:

Blackouts and Prevention

Before beginning the research on controlled islanding, it is important and necessary to review recent blackouts that have occurred worldwide, such as the India blackout (2012) [2][3], the California blackout (2011) [30], the Brazil blackout (2009) [31], the US/Canada blackout (2003) [4], the Denmark/Sweden blackout (2003) [32][33] and the Italy blackout (2003) [34]. The main objective of this chapter is to investigate how and why these blackouts still happen despite the high level of security in the operation of power systems. In addition, the chapter addresses the current methods of control used in industrial practice to prevent blackouts and discusses whether these measures are sufficient and effective in preventing blackouts.

2.1 Introduction

This chapter discusses our motivation for developing the methods used in the controlled islanding scheme to prevent blackouts. It is easily assumed that blackouts rarely happen because the current transmission system was designed with high levels of security and reliability. A large number of advanced protection schemes have been installed for each asset, and preventive or corrective control schemes have been designed to ensure the security of the system. This smart design of transmission systems seems to ensure that blackouts can be prevented even if faults occur. However, in recent decades, several blackouts have happened across the globe, such as the India blackout in 2012, the California blackout in 2011, Brazil blackout in 2009 and the US/Canada blackout in 2003. This chapter begins by reviewing these blackout cases and exploring the reasons that these blackouts occurred.

An interconnected power system has several merits. It can increase the system's robustness to improve frequency stability and reduce its susceptibility to voltage oscillation. It also connects high generation areas and high demand areas to improve the

management of the power balance. In addition, the deregulated market demands that systems be interconnected to optimise the trade of power flow across different regions. However, renewable energy development has introduced wide deployment into the system, which might have affected the security of power systems. Moreover, because of economic development, heavy demands have been placed on power systems that were not originally designed for increased loads. In particular, the liberalization of the electrical market usually leads to increases in the trade of power flow across the tie lines between different systems or the borders between different countries. There often is no unified governance of power flow trade across those areas because there are many system operators, and each operator considers and assesses the system security in their own region, rather than assessing the stability of the entire system [35][36]. Hence, traditional closely connected systems are not aware of other operating conditions because of the lack of communication and information exchange, such as in the disturbance in Germany (2003) [34]. This disturbance caused a frequency separation in the European network, which led to three different frequency areas. Circumstances such as these cannot facilitate the development of future power systems, and they may lead to new problems. When the tie lines across borders are tripped, each region's power imbalance could lead to new cascading outages, causing transient instability before the system collapses. This occurred in the recent blackouts across the world, which is discussed in the following section.

2.2 Recent Blackouts in Power Systems

The most recent blackouts occurred as follows: the Turkey blackout on 31 March 2015, the San Diego blackout on 26 December 2014 and the Bangladesh blackout on 1 November 2014. However, the specific reasons for those blackouts are still under investigation, and no full technical reports have yet been published. In this section, we discuss the evolution of blackout events and analyse other recent blackouts across the globe that occurred from 2012 to 2013, such as the India blackout in 2012, the California blackout in 2011 and so on.

2.2.1 India blackouts on 30 and 31 July 2012

The India blackout was a typical cascading case, occurring twice 30 and 31 July 2012 [2][3]. It affected 600 million people and half of India was without electricity. In July 2012, the synchronously connected Indian main power network, the NEW Grid, was the blackout area, which consisted of the North Region (NR), the East Region (ER), the West Region (WR) and the Northeast Region (NER). The South Region (SR) is a separate power network run by a different system operator and is asynchronously connected with the NEW Grid via a high voltage direct current (HVDC) line. Figure 2.1 below shows the four affected regions on India's NEW Grid on 31 July 2012.

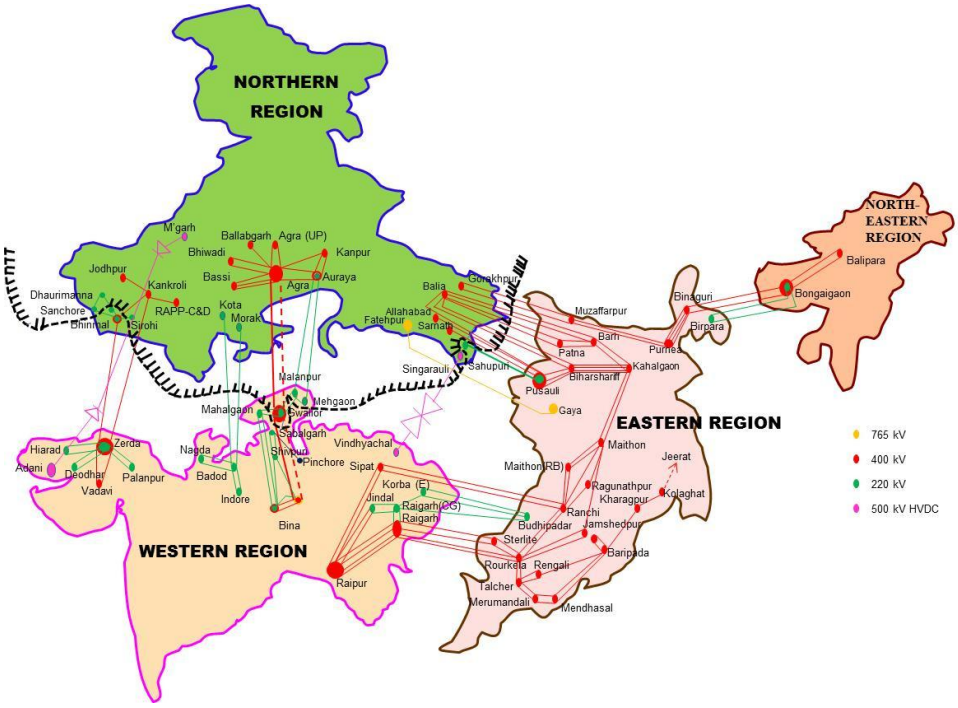

Figure 2.1*: India's NEW Grid power system separation on 31 July 2012 [2].*

NR is a high demand area, and is heavily dependent on the power supply from the WR. In fact, the Indian aging power system facilities and network design capacity hardly meet the peak load demand annually because of rapid economic development, particularly in the summer of 2012. Because of the extremely hot weather and heavier demand for power in the agricultural area in the north, the consumption of electricity reached a historical record. In four areas (Haryana, Rajasthan, Uttar Pradesh and Punjab) the power consumption was severely over scheduled in the power delivery from WR by 14%, 18%, 6% and 6%. In this situation, two 400 kV tie lines connecting the NR and

WR were overloaded and then were tripped quickly by the overcurrent protection. Because a large amount of power flow from the WR had to go to the NR through the ER, the NR began to lose synchronism with the WR. Figure 2.2 shows the frequency as the NR and WR moved apart at around 2:33:12 in the early morning of July 30. In addition, the angular separation between NR and WR started to increase. The remaining tie lines connecting the NR and the WR were then tripped incrementally by the distance protection in Zone 2 and Zone 3, which was caused by load encroachment or power swings. Consequently, the NR was isolated from the WR, and the generators in the NR lost synchronism completely. They were tripped immediately until the whole power system in the NR collapsed. In the case of the blackout in India, transient instability played a significant role before leading to blackout. Hence, the observation and predication of losing synchronism is vital to prevent imminent blackouts.

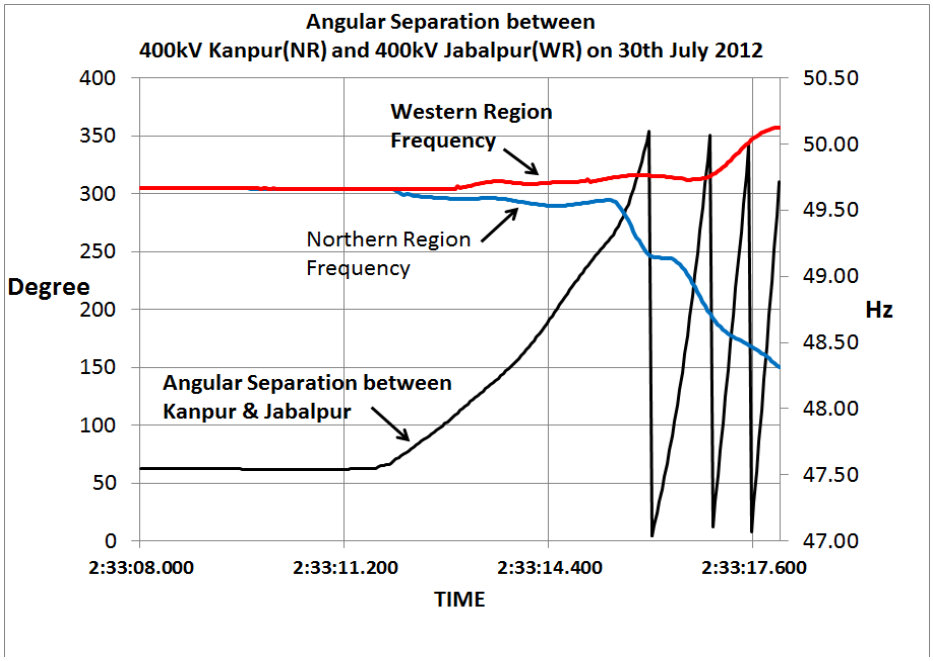

Figure 2.2: *Frequency profile from data measurement of phasor measurement units (PMUs) [3].*

In order to restore the power system in NR, India decided to increase the power delivery from the ER to the NR. However, the huge load demand in the NR caused the tie lines between NR and ER to overload again. The system operator failed to shed some load in the NR before some NR–ER tie lines were tripped. The tripped tie lines transferred the burden of power flow onto the other neighbouring lines. Subsequently,

the six 400 kV-rating tie lines connecting the NR and the ER were all tripped, leading to a complete blackout in the NR, ER and NER on the second day after the first blackout.

The lesson we can learn from the India blackouts is that deregulation requires different system operators to work closely and communicate effectively. Especially for tie lines across borders, overloading status has to be identified early and cleared immediately.

2.2.2 California blackout on 8 September 2011

The California blackout on 8 September 2011 is another typical case of a cascading blackout [30]. This eleven-minute system disturbance affected around 2.7 million people in the Pacific Southwest. On that day, one 500 kV high-voltage transmission corridor connecting North Gila and Hassayampa (NG-H) was tripped, which initiated the cascading blackout. However, this was not the only reason for the cascading outages. Indeed, the system designed by the Western Electricity Coordinating Council (WECC) was capable of surviving under an N-1 contingency condition. Although this NG-H line was also tripped, it did not cause cascading outages. However, because the demand in San Diego was at the peak level, the sudden trip of a major east-west transmission line instantaneously redistributed the power flow across the system. The power flow redistribution during the peak demand level in San Diego caused a voltage drop and equipment overload to the north of the southwest power link (SWPL), resulting in the overloading of three 230/92 kV transformers and a line (Path 44) in Southern California.

Surprisingly, during the eleven-minute disturbance before the imminent blackouts, the system operator in the WECC failed to give an effective order. Consequently, the uncontrolled cascading outages spread because of the facilities were overloaded. Finally, the trips of the transmission lines caused the transient instability of the system. When the generators lost synchronism, they were tripped by the corresponding protection devices, which resulted in a cascading blackout in the California area.

2.2.3 Brazil blackout on 10 November 2009

The Brazil blackout in 2009 was a typical incident involving the loss of synchronism in the generator angles, which resulted from cascading outages [31]. It happened within eight seconds after the first fault, and it lost 24,436 MW of demand, which accounted for 40% of the required national load.

At 22:13 pm on 10 November 2009, three 765 kV transmission lines connecting Itabera and Ivaipora were tripped incrementally one by one because of the fault applied to them. Subsequently, one 500 kV tie line and two 230 kV tie lines between the South Region and Southeast Region in Brazilian National Interconnected Power System (NIPS) were overloaded and quickly tripped by the distance protection. The power system between the South Region and the Southeast Region started oscillating via the 500 kV Londrina-Becausesisi-Araraquara (L-B-A) tie line. In the next 1 second and 2 seconds after the first fault, one 230 kV and eleven 440 kV transmission lines, respectively, inside the Southeast Region were tripped by the distance protection because of the power swings, The Southeast Region completely lost synchronism with the North Region and the Northeast Region. The frequency in the Southeast Region dropped significantly, and the load shedding protection scheme started shedding loads in this region while trying to bring system frequency back to the nominal level of 60 Hz. However, some lines continued being tripped because of the over-voltage protection placed on them after the load shedding in Southeast Region. Then eight seconds after the initial fault, the generators in the Southeast Region were tripped after completely losing synchronism, which led to the blackout.

The lesson we can learn from the Brazil blackout is that when the system's generator angles start oscillating during uncontrolled cascading outages, such as in the case of the L-A-A tie line between the South Region and the Southeast Region, it is uncertain whether the system will be transiently stable if further cascading contingency occurs. Therefore, it is important that the transient stability assessment indicator is obtained to help the system operator deal with this issue before the generators completely lose synchronism and are tripped by the protection devices, thereby resulting in the system's collapse.

2.2.4 US/Canada Blackouts on 14 August 2003

This US/Canada blackout occurred in large areas of the northeastern US and southeastern Canada, which affected approximately 50 million people [4]. During this event, over 400 transmission lines were tripped, and at least 263 power plants with more than 531 individual generating units were shut down on that day. The process of the blackout was based on cascading events that can be classified into the four typical stages [4] described below:

- **Weakened condition:** Between 12:05 and 13:31, three generating units, which were separately located in Conesville, Greenwood and the Eastlake region, amounting to 12,757 MW were out of service on August 14 because of routine maintenance. Although this was not the direct cause of blackout, to some extent, the unavailability of these individual generators caused the power flow in the system to reroute, and it probably caused some critical transmission lines to approach their operating limits.

- **Triggering event:** At 15:05, a tree flashover occurred in the Harding-Chamberlain 345-kV transmission line. However, the control room engineers did not know about it because the alarm and logging system in the FirstEnergy Corp.'s control room failed before the cascade started. Because no action was taken, this line was quickly tripped.

- **Slow cascading progression:** After the failure of the Harding-Chamberlain line, the power flow in this line was shared by the neighbouring lines, which led to overloading in the neighbouring parallel lines. The overload was cleared by tripping the paralleled lines, which led to further overloads until another four neighbouring lines failed at 16:05. Figure 2.3 shows this increased line loading caused by the neighbouring line trip.

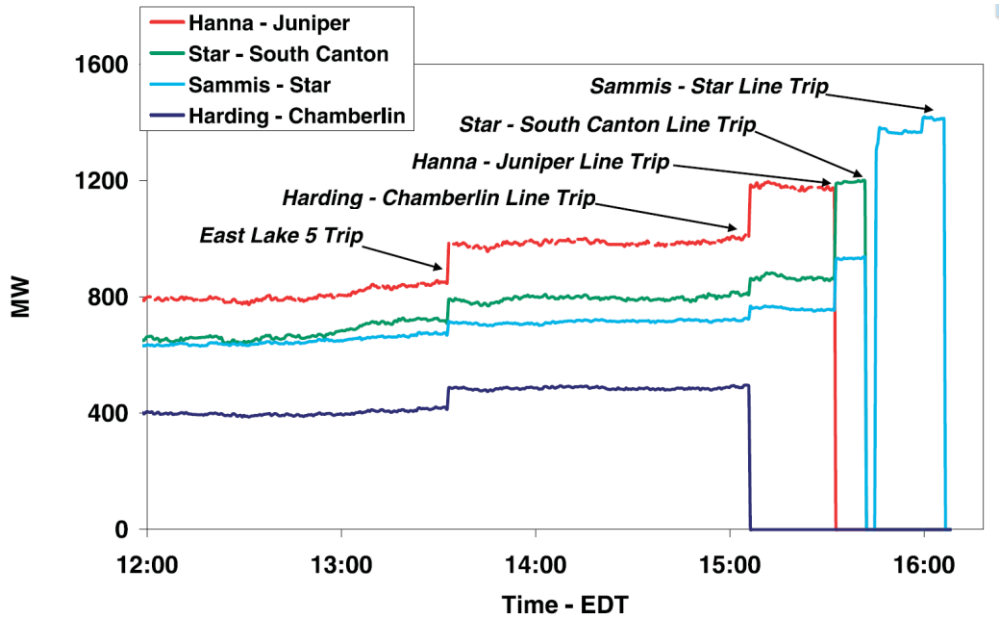

Figure 2.3: *Power flow redistribution on FirstEnergy Corp.'s 345-kV lines [4].*

However, in fact, each of these lines tripped, not because of overloading protection, but because the big sag caused by the overload hit overgrown and untrimmed trees. The Harding-Chamberlin line, Hanna-Juniper line and Star-South line failed separately with power flow at only 44%, 88% and 93%, respectively, of the normal and emergency line ratings. The current information on the system, such as active power flow, could have been acquired and displayed by Supervisory Control and Data Acquisition (SCADA) within a few seconds in a cycle. In this stage, each occurrence of these cascading events was dependent on the earlier one or more events. Figure 2.4 shows that the voltages declined at the 138-kV buses in five regions during the cascading outages, which could also have been measured by SCADA when several 345-kV lines and one 138-kV line was tripped before the local blackouts occurred.

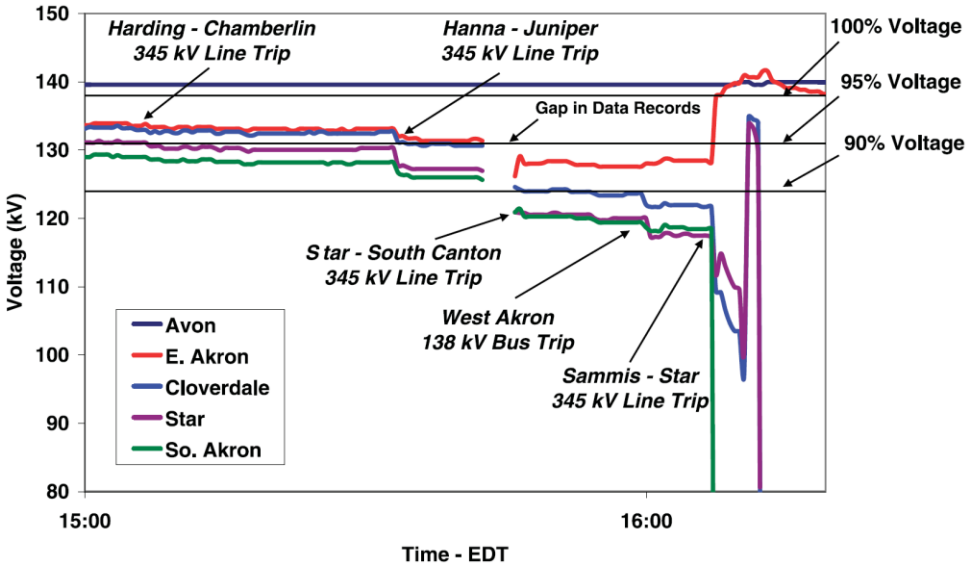

Figure 2.4: *Voltages on FirstEnergy Corp.'s 138-kV lines: impacts of line trips [4].*

- **Fast cascading progression:** Fast cascading occurred between 16:09 and 16:12. Within no more than three minutes, hundreds of transmission lines and generators successively tripped, leading to widespread blackouts. The speed of the cascading is shown in Figure 2.5.

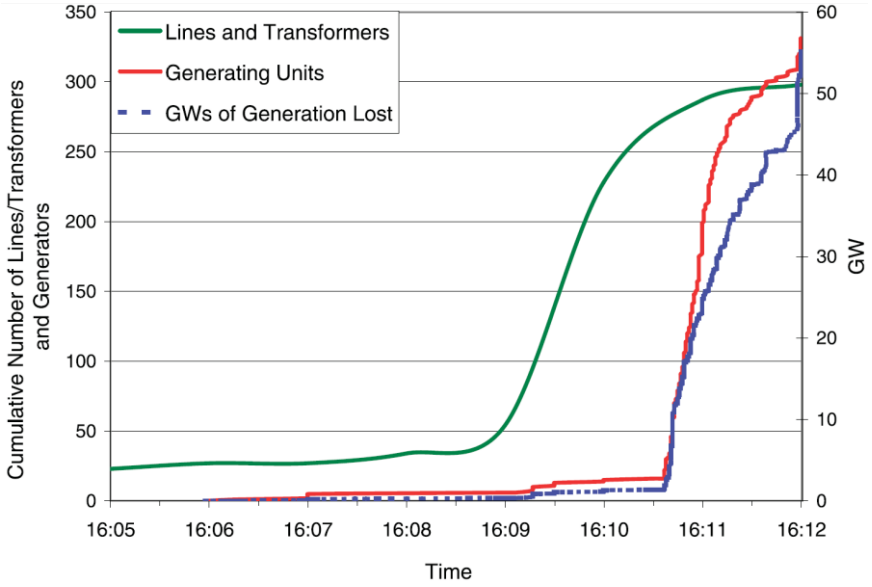

Figure 2.5: *Rate of line and generator trips during the cascade [4].*

During this period, power swings and voltage fluctuations caused the transmission lines to detect high currents and low voltages. The measured apparent impedance obtained might have entered the operating characteristic zone of the protection relays, which

were not able to discriminate the impedance change between the faults and the power swings. Therefore, the transmission lines were tripped successively by the distance relay in zone 3. Meanwhile, the generators were tripped in order to protect themselves from severe power swings, which could damage the generators. Moreover, during this fast cascading period, because several outages occurred simultaneously in the interconnected system, the original protection setting of the relays for the transmission lines, generators, under-voltage load shedding and under-frequency load shedding [4] might not have been accurately coordinated and integrated, which would have accelerated the cascading events.

Hence, the US/Canada blackout was also caused by cascading outages. The final tripping of the generators because of the loss of synchronism resulted in the loss of power supply, and the entire system collapsed. The lessons that we can learn from the US/Canada blackouts are that in addition to the overloading, the line hit trees that were inadequately trimmed. Furthermore, no action was taken after the initial line tripping events because of the failure of the FirstEnergy Corp.'s control room, the overreaching distance relays in zone 2 and zone 3 [4], and the lack of coordination and integration between the generator protection system and the transmission line protection system in different areas, which combined to accelerate the widespread blackouts.

2.2.5 Denmark/Sweden Blackouts on 23 September 2003

The Scandinavian blackouts affected 5 million people who lost power in Eastern Denmark and Southern Sweden. The process of this blackout can also be described in four stages [32]:

- **Weakened condition:** At 12:30, one 1.2 GW generating unit at the Oskarshamn power station, which was located on the southeastern grid, tripped because of technical problems. Suddenly, the north-south power flow on the west side of the network increased because the power flow was rerouted to satisfy the southern demand.

- **Triggering event:** At 12:35, one switching device broke apart at the Horred substation.

- **Sequence of events:** The triggering even caused four 400 kV lines and two units (1,800 MW) at the Ringhals Nuclear Power Station to be tripped. Suddenly, the system was operating under the N-7 contingency situation, but the system had not been designed to deal with this condition. The heavy loss of generation and transmission on the southern grid caused heavy power flows on the remaining transmission lines from north to south in Sweden. Consequently, voltages started to drop. They then were maintained by the local power plants before they finally collapsed, which is shown in Figure 2.6. Because shown in Figure 2.6, oscillation existed in both voltage and frequency, which also indicated the oscillation of the generator angles. Both voltage and frequency are related to the generator angle, and their oscillation is caused by the oscillation of the generator angle itself. The measurements of current, voltage, frequency are time-synchronized, which are taken as phasor measurement units (PMUs) in WAMS at pre-selected locations and stored in the data concentrator every 20 milliseconds.

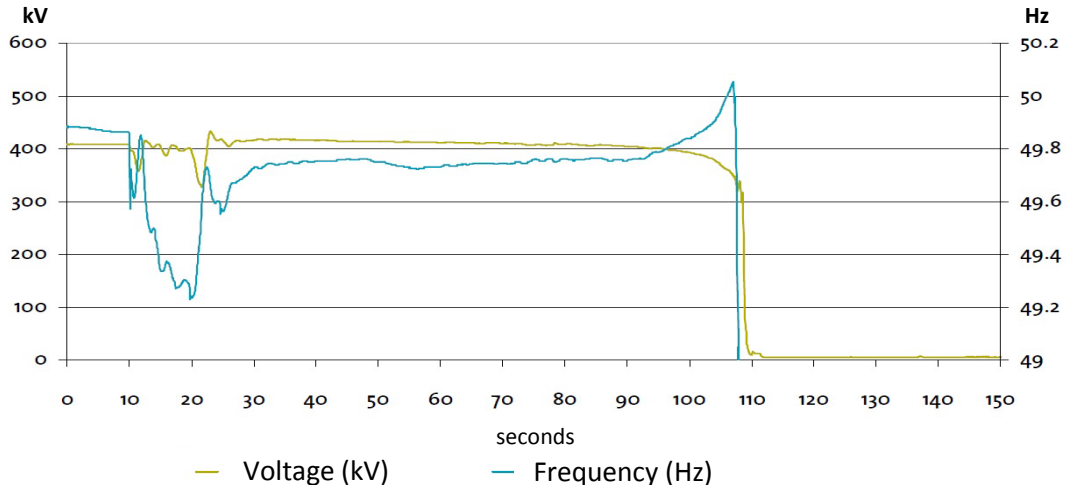

Figure 2.6: *Voltage and frequency acquired by WAMS at 400 kV connection between southern Sweden and eastern Denmark [33].*

- **Blackouts:** Between 12:35 and 12:37, because of the deficit in generation within the southern subsystem, the huge imbalance in generation and demand caused the frequency and voltage to drop further. False faults with high current and low voltage on the 400 kV transmission lines in southern Sweden were detected during the power swings, and they were tripped by distance relays in zone 3. Then the power plants

shut down, and blackouts occurred in southern Sweden and eastern Denmark, causing this area to separate from the remaining network.

Coincidently, several unexpected outages occurred simultaneously after the system was operating under the widely used "N-1" security criterion, which deteriorated the system's operating security margin and forced the system to run under the N-7 contingency, which led to blackouts within two minutes.

Therefore, the N-k (k>1) security requirements should be adapted in an increasingly stressed system to reduce the likelihood of simultaneous and multiple faults.

2.2.6 Italy Blackouts on 28 September 2003

Because the power supply is not self-sufficient, Italy imports power from France, Switzerland, Austria and Slovenia. Italy's generation deficit equals 24% of the country's total energy demand. Italy's blackouts on 28 September 2003 affected the entire country, and 57 million people lost 27 GW in power supply [34].

- **Weakened condition:** At 15:00, Italy imported 6.7 GW of power, which was 25% of the country's total load. However, there was 300 MW power more than originally scheduled, which caused an overload on the Swiss border in the Silis-Soazza transmission line.

- **Triggering event:** At 15:01, a major 380-kV tie line between Italy and Switzerland was highly loaded at approximately 86% of its maximum capacity, which led to line sag caused by the gradual heating process of the conductors. The decreases distance between the conductors and the ground violated the security distance and caused a tree flashover. After the first tie line was tripped, its load was taken up by the neighbouring 380 kV Silis-Soazza line, which then was operating at around 110% of its nominal capacity.

- **Sequence of events:** (1) At 15:11, the transmission system operator (TSO), Swiss ETRANS, informed Italy's national power grid (GRTN) of the request by phone to reduce the importation by 300 MW. GRTN complied with the request within 10 minutes. Despite several internal countermeasures taken by Swiss, unfortunately, it was not enough to relieve the overloads. (2) At 15:25, the overloading Sils-Soazza

line tripped after 24 minutes because of tree flashover. Meanwhile, the Italian grid lost synchronism with the main grid of the Union for Coordination of Transmission of Electricity (UCTE) because of the generation deficit. Because of the overloads, the remaining lines connected to Italy were simultaneously tripped by the protection devices. Figure 2.7 shows the decrease in frequency with the cascading outages in Italy:

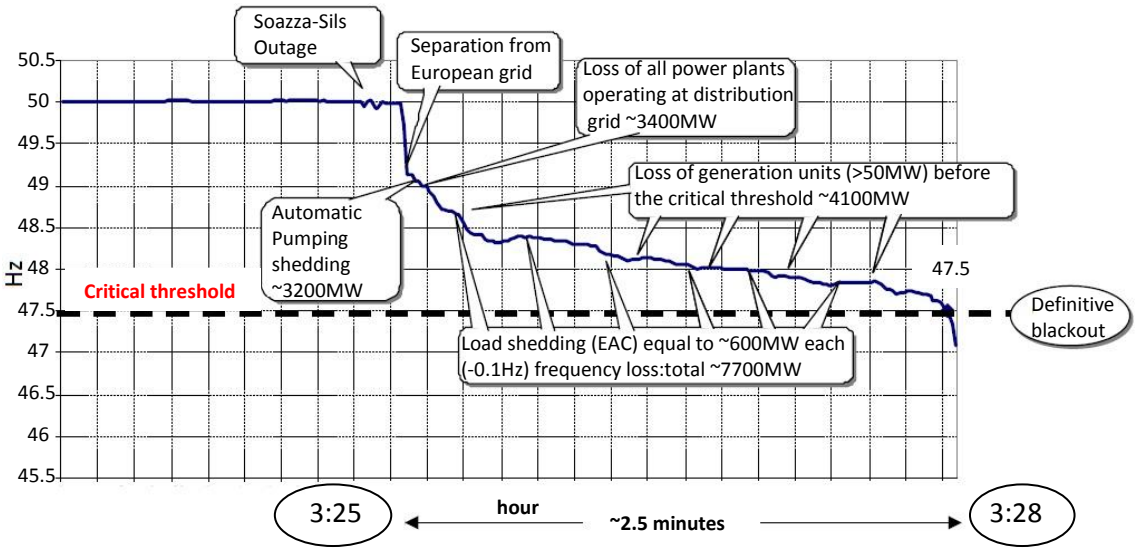

Figure 2.7: *Frequency behaviour in Italy in the transitory period [34].*

- **Blackout:** At 15:27, the Italian system was not able to operate separately from the UCTE network because of the deficit in self-sufficiency and the breakdown. The entire Italian system collapsed, causing a nationwide blackout.

Shortly before the blackout occurred, Italy's power system had a generation deficit and lost transient stability with the UCTE network. One of the main lessons learned from the Italian blackout is that system-wide analyses and security criteria research in every country are required because there is an increasing number of cross-border power trading and most contingencies occur in the tie lines between two countries or two regions. However, in Europe, countries and regions operate and manage their own grids separately subject to individual security criteria. Furthermore, there is a lack of online coordination and exchange of information between the interdependent utilities in each country.

2.2.7 UCTE Disturbance on 3 November 2006

In the UCTE system, there are high power transfers between countries from east to west because northern Germany exports sufficient wind generation to meet the demand in the east.

- **Weakened condition:** These strong power flows were interrupted during the event. On 3 November, the energy supplier E.ON received a request from a shipyard to disconnect a double circuit 380 kV Diele-Conneferde line in northern Germany later that day. At 21:38, 4 November, E.ON turned off the line without analysing the updated N-1 security criterion, which resulted in a significant increase in the power flow in the Landesbergen-Wehrendorf line from 600 MW to around 1,300 MW.

- **Triggering event:** At 22:07, alarms of high power flows occurred, and E.ON decided to couple a busbar to decrease the current without online simulations. Nevertheless, the current continued to increase, causing the line to be tripped, which led to overloads on other lines. These were tripped simultaneously by the distance protection. Before 22:07, attempts at re-dispatch actions failed because the required increase in power output at some power plants that were already operating at the maximum generation level was impossible to achieve.

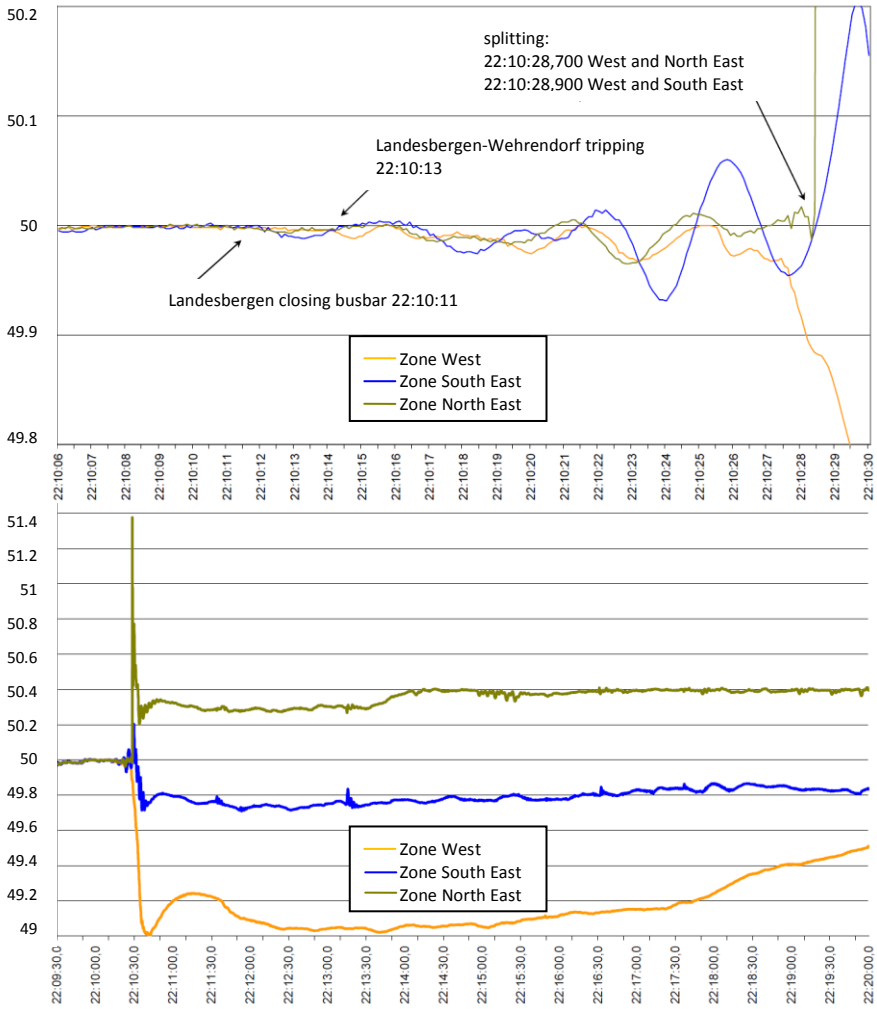

Figure 2.8: *Frequency recordings received by WAMS before and after area split [34].*

- **Disturbance:** At 22:10, the UCTE system split into three regions with different frequencies. Figure 2.8 shows the variances in the frequencies in the three regions before and after the separation of the UCTE network. In the western subsystem, a load generation imbalance of about 8.9 GW in the generation deficit led the frequency to decline to 49 Hz. In the northeast subsystem, the frequency initially increased to 51.4 Hz and then decreased to 50.4 Hz because the over-frequency protection tripped the wind generators in order to recover the frequency. Because shown in Figure 2.8, the frequency oscillation was equivalent to the oscillation of the generator angles in three areas. Therefore, transient oscillation in the UCTE network before losing stability also occurred in this disturbance.

Similarly, the N-1 security criterion was not fulfilled in the German grid [34] because there were an increasing number of power transfers across the borders of the UCTE. Therefore, instead of individual grid security, a wide-area system security assessment was required. Moreover, the insufficient internal TSO coordination [34] should have been enhanced because the time it took to switch off the double circuit line was earlier than the scheduled one was, and the other directly involved TSOs were late in communicating with the German TSO after switching off, which left insufficient time to check the system's security operation.

2.2.8 Conclusion to the blackout cases

Based on the review of the previous blackouts, the time scale in terms of evolvement can be divided into four stages [32]:

- **Pre-event conditions:** extreme weather, stressful system condition and weakened network topology

- **Triggering events:** various kinds of N-1 or N-k (k>1) contingencies with internal faults, such as tree flashover in the US/Canada blackout (2003), failure of the switching device at substation in Sweden/Denmark blackout (2003), another tree flashover in the Italy blackout (2003) and mal-operation without simulation before taking action in the UCTE disturbance (2006)

- **Pre-collapse events:** power swings, overloads, voltage drop, frequency variation and transient instability

- **Nature of collapse:** cascading tripping of system components

Based on the review of the causes and process of these previous blackouts, it can be confirmed that most occurred when the system was secure but under high stress [37] caused by overloads in transmission lines that could be tripped successively. Many blackouts are triggered by the simultaneous occurrence of a credible contingency and an internal fault [37], such as the mal-operation and malfunction of protection devices, which strengthen the effect of the credible contingency in the system. Shortly thereafter, one or more healthy components in the grid are tripped without the timely removal of

the internal faults. Therefore, one routine incident becomes a major problem that could lead to a cascading blackout that is out of control. In all these recent blackout cases, the cascading outages that occurred first were caused by overloading on transmission lines. The further tripping of the system's components then exacerbated the disturbances. The systems finally collapsed because generating units were tripped because of the loss of transient stability. Therefore, transient stability during cascading status is the most important factor when a blackout is imminent. In this research project, we mainly focus on transient stability during the cascading process.

2.3 Conventional Prevention Methods for Blackouts

2.3.1 Power system security criteria

2.3.1.1 N-1 and N-D criteria

In power systems, N-k contingency analysis has been widely used as the criterion of industry practice and fundamental security to govern and assess the operation of a network, which allows the system to keep running when components fail. The widely used current N-1 security standard requires a system to continue operating satisfactorily after any one outage of the system's N components. Similarly, the N-D security criterion allows one system to work healthily without being affected by the loss of double circuit line and highly risky paired N components in the power grid [38], which is currently used in UK. In order to ensure that all these credible contingencies will not lead to cascading outages, which are the main reason for blackouts, such as the typical blackouts that occurred in India (2012), California (2011) and US/Canada (2003), during outage planning stage, the system operators have to analyse a large number of "what-if" contingencies to check for possible intolerances.

2.3.1.2 Why We Need These Security Criteria

In the central control room of a power grid, the system operators have to monitor the network operating state continuously and ensure that the system works in healthy conditions. They also need to implement an economic dispatch to optimize each generating unit's output to achieve the goal of minimising the cost of the power system

operation. This economic dispatch allows competitive generators to generate more power at the cheapest locational marginal price (LMP). There will be more transactions between these generators and demands in long-distance transmission lines, which could put more pressure on these transmission lines and even make them operate at the maximum capacity, thus threatening the system's security. Therefore, a balance between minimising the cost of operation and the fear of blackouts [37] is essential for the secure operation of power grids.

In order to solve this conflict and help the system operator to better dispatch the generating units' output, organisations such as the Reliability Councils in the USA or European Network of Transmission System Operators for Electricity (ENTSOE) in Europe developed rules that the transmission utilities and operators should follow at all times. The basic principle of these rules is that the system should operate at a level within a sufficient security margin. Moreover, credible contingencies that occur in the network should not lead to cascading outages or system instability. This regulation is reasonable because power systems are inevitably affected by routine maintenance and unpredictable faults and failures. However, it is impossible to ensure that the system is able to endure all credible contingencies. Normally, the likelihood that multiple outages will occur simultaneously is too low to be considered. Hence, most security rules need a system to withstand the loss of any component in the network, such as the N-1 security criterion, which was produced in this environment.

2.3.1.3 Why Blackouts Still Happen Despite Observance of the N-1 Criterion

The blackouts that occurred in India, California, Brazil and US/Canada raised the question of why they happened despite the N-1 security criterion rule. Because previously discussed, the current N-1 criterion may no longer be adequate to assess the vulnerability of the cascading outages because after the first credible contingency occurs, the system may no longer be N-1 secure. However, it is still possible that independent and unrelated internal failures would follow the credible outage. These internal failures could trigger the cascading failures that lead to widespread blackouts. In addition, there could be other contributing factors, such as communication failure (e.g., the US/Canada blackout in 2003). Another main reason is that each administrative area or state applies the N-1 security criteria within their own territory. Thus, it cannot be guaranteed that N-1 security criteria will work on a wide scale. An increasing

number of transactions take place across the borders of these balancing areas (BA) [39]. Each BA looks no further than its own border to perform the N-1 contingency analysis and always ensures that its individual network satisfies the N-1 security criteria within each BA. The case of the Indian NEW Grid power system is a typical example. The North Region of India required a large amount of power flow from neighbouring areas across the tie lines. However, there was no unified system security assessment between different operators, and there was lack of information exchange between them. If these credible contingencies occurred simultaneously in adjacent BAs, the system in each BA would still be secure. However, they ignored the impact of credible contingencies, which perhaps violated the N-1 security criterion that every BA should connected to the others, which inevitably led to cascading failures.

Therefore, the system security criteria should be tightened to adapt this deregulation of crossing every BA, such as N-2. An even higher-order contingency analysis should be conducted in the future because of the increasing capacity of transmission lines. Furthermore, simply building more transmission lines without adjusting the contingency rule cannot enhance the security level of the power system and reduce the likelihood of blackouts [37].

2.3.2 Three-defence-lines in the power system

The cascading blackouts that occurred worldwide in recent decades made us reconsider the flaws in the current defence against blackouts. These events also raised questions, one of which concerns the currently used methods to prevent blackouts and the role each method plays in different stages of imminent blackouts. It is useful to review the widely used three-defence-lines criteria [5] against blackouts to better adapt the controlled islanding scheme. The US/Canada blackout on August 14 is a typical example. Figure 2.9 below shows the typical evolution of the US/Canada cascading blackouts.

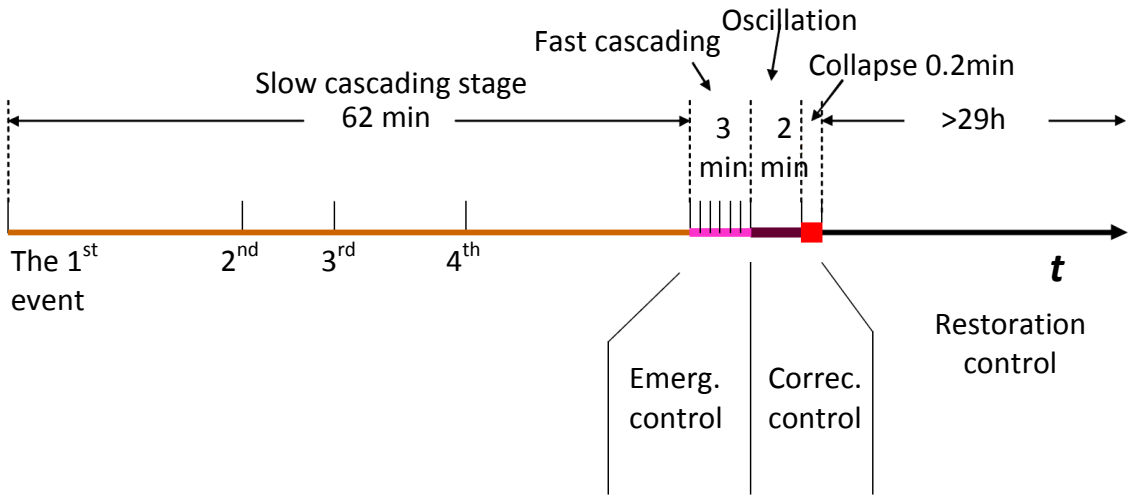

Figure 2.9: *Typical evolution of US/Canada cascading blackouts [5].*

In Figure 2.9, the time axis shows that the process was divided into four stages: slow cascading, fast cascading, oscillation and collapse, each of which had a time interval. Moreover, each period corresponded to the relevant control action, which attempted to return the system to the normal operating point. During the slow cascading stage, preventive control (PC) was activated, which is an open-loop control and requires the operators to make a decision based on the signal alarm received to return the system to a renewed stability domain. The protection devices were probably involved in this process. However, the PC control stage sometimes fails because of the mal-operation or malfunction of the protection devices, such as in the UCTE case in 2003 where operators should have limited the line loadings at a level that allowed credible contingency to occur without violating the system's security rule under the pre-contingency condition. However, they wrongly coupled the busbar after receiving the high current alarm. In the case of the US/Canada blackout in 2003, even the operation control room failed. During the fast cascading stage, emergency control (EC) came into effect, which is a close-loop feed-forward control that automatically switches equipment on or off based on the pre-contingency protection design. However, the EC control stage sometimes fails because of the lack of coordination and integration between the generators and transmission lines' protection device in complicated power grids. During the oscillation stage, corrective control (CC) takes the final steps for the system's survival by using under-voltage load-shedding (UVLS), under-frequency load-shedding (UFLS) and out-of-step protection [5], which isolates the affected region. All control failures in this three-defence-line may lead to widespread blackouts.

It can be confirmed that the performance of the islanding scheme as a last-resort action after the failures of the usual preventive means against imminent blackouts has a limited window of operation. As shown in Figure 2.9, only 2.2 minutes were left to encounter oscillation and collapse and probably even less time in the other cases. Therefore, the early and fast recognition of the transformation from disturbances to blackouts is critical to decisions about when to island. Moreover, the early detection of variations in some signals, such as voltage and frequency, could indicate that blackouts are imminent.

2.3.3 Voltage collapse prevention

In these blackouts, some dynamic phenomena occurred during the cascading outages, such as voltage drop and frequency oscillation. Frequency oscillation is also related to generator angle oscillation. The following section describes the occurrence of these dynamic phenomena during the cascading contingencies in the blackouts reviewed in this thesis.

Although voltage collapse occurs in all blackouts, voltage change is a local phenomenon, and its collapse occurs only in a small area when there is no efficient reactive power supply and the active demand is huge, such as in the cases of Denmark/Sweden (2003) and Greece (2004) [40][41]. There are usually several precursors before the occurrence of voltage collapse, such as low voltage profiles, insufficient reactive power supply and high reactive power flow in transmission lines. In most situations, the voltage collapse is accelerated by several unexpected and undesired single or multiple contingencies. In order to understand how these precursors satisfy the voltage collapse conditions that lead to blackouts, let us begin by explaining the P-V and Q-V curves shown in Figure 2.10 and Figure 2.11.

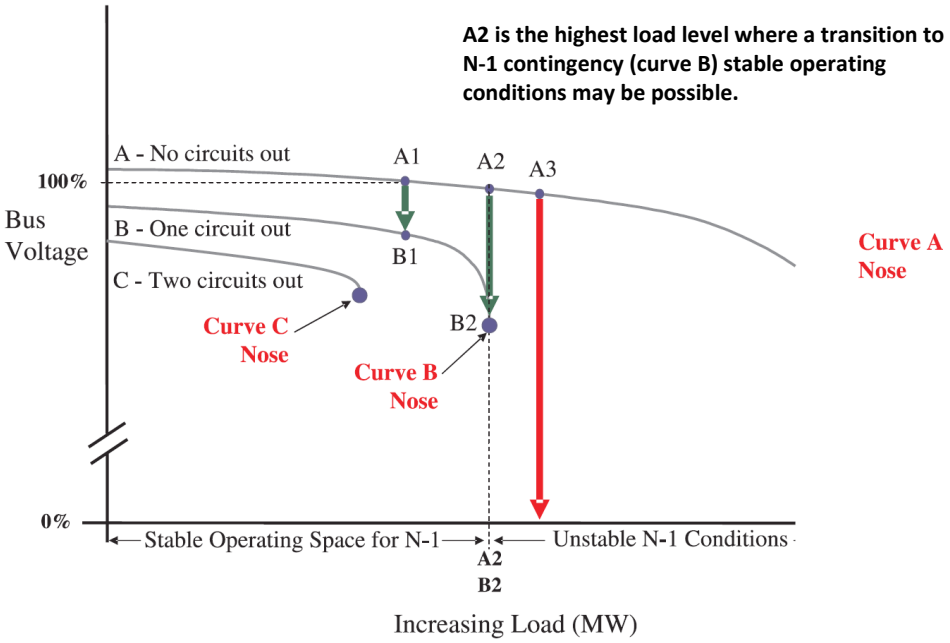

Figure 2.10: *Real power-voltage (P-V) curves [4].*

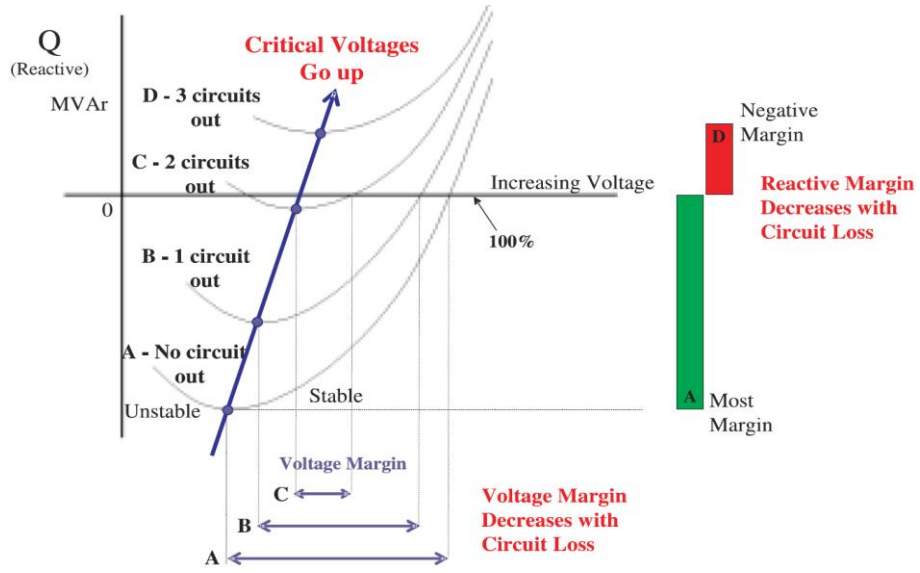

Figure 2.11: *Reactive power-voltages (Q-V) curves [4].*

Generally, the busbar voltage should be maintained at the rating voltage, which is much higher than the critical voltage shown as the curved noses in both figures. However, when the load increases significantly, causing high power flow and stressing the system, the voltage surrounding the high demand area will decrease gradually, as shown in Figure 2.10. When the load continues to increase, the voltage decreases and probably crosses the critical voltage, leading to the voltage collapse. During that period, if the

reactive power is adequate in the high demand area, the situation will be relieved, and the voltage will increase until it is maintained at a steady state. However, if a contingency happens simultaneously, as shown in Figure 2.10, the previously stable voltage may cross the critical voltage in the new network, leading to local blackouts and affecting the high power flow in the remaining system. This local blackout caused by voltage collapse occurred in the Denmark/Sweden blackout (2003). As shown in Figure 2.6, the voltage collapse in the local area further affect the entire system and resulted in more cascading trips because of the power imbalance.

Therefore, a sufficient reactive source in the high demand area is critical to maintain the voltage level. Normally, voltage should be maintained at a level with a large voltage margin. In addition, there should be a large reactive power injection margin to prevent the consequences of unexpected circuit outages. As shown in Figure 2.11, these voltage margins and reactive margins will decrease with the loss of circuits, which causes the voltage to approach the critical limit and even exceed it, which leads to local blackouts.

2.3.4 Frequency collapse prevention

In addition to significant voltage drops before imminent blackouts, frequencies usually also have great variation. Examples are the frequency collapse in the Italian case (2003) and the frequency disturbance in the UCTE case (2003).

Under stable operation, the frequency across the whole network remains at 50 Hz. However, this numerical value always varies because of the second-to-second imbalance between generation and demand. Therefore, frequency could be an indicator of power balance. If there is deficit of generation, the speed (frequency) of the rotor will decrease, which triggers the turbine to increase power to drive the rotor automatically via feedback control and vice versa. This control action consists of three control performances (Figure 2.12): primary control, secondary control and tertiary control [42], which prevent the continuous decrease in frequency caused by the deficit in generation and maintain it at a stable level.

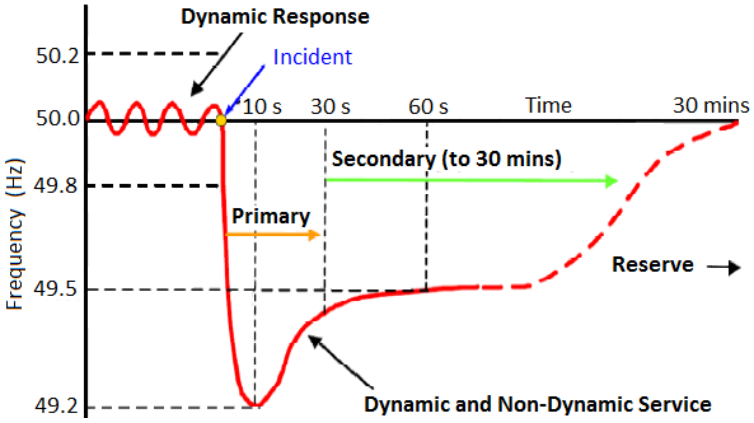

Figure 2.12: *Frequency regulation intervals subject to a disturbance [42].*

However, in extreme conditions, these control actions do not always succeed in maintaining the frequency. In situations of under frequency, as a last resort, load-shedding (UFLS) will come into effect after the region has been isolated. In this formed islanding, the frequency drops to 49.3 Hz. UFLS will shed the pre-designated customers in steps in order to stabilize the power balance within the island to prevent the local blackout. The Italian frequency collapse shown in Figure 2.7 is an example. After the outages of all of transmission lines connected to Italy, the Italian system lost synchronism and operated separately from the UTCE. Because there was a deficit of 24% in this island's generation, the frequency decreased significantly. Concurrently, several UFLSs were implemented to maintain the frequency, which was not effective because of simultaneously occurring problem, such as electrical instability and voltage collapse [34]. When the frequency drops to 47.5 Hz, the under-frequency protection relays will be triggered to prevent damage to the generators, thus leading to local blackouts within the islands. Because frequency collapses are global phenomena and the frequencies at each node are always the same, it could reflect either a total power balance or imbalance in the entire system. However, the significant change in frequency does not indicate which part of the system has problems until the uncontrolled islands are formed. The frequencies within each island are separated, such as in the UTCE disturbance case (2006). Moreover, even in a steady state, frequencies change because of the electricity consumption behaviour of individuals. Hence, a dynamic power balance is rarely achieved. Therefore, frequency is more likely to be a post-event reflection signal instead of a precursor.

2.4 Summary

This chapter described a series of blackout incidents that occurred in power systems across the globe in recent decades. The analysis included the process of the events that lead to blackouts. From the operational point of view, the biggest issue in these blackout cases is that there were too many system operators in the interconnected network. Moreover, there was a lack of effective coordination, information exchange and overall unified system security assessment. The Italy blackout in 2003 is an example. When Italy national power grid GRTN identified that in its own power network there were 300 MW more power imported from Switzerland, it took more than two minutes for the Swiss operator to take action after a phone call made by GRTN regarding this issue. In addition, there were not enough operators trained to deal with an emergency. In the UCTE disturbance in 2006, the E.ON operator disconnected a 380 kV line in order to let one shipyard to go through. However, because it was done without a security analysis, it caused overloading on the Landesbergen-Wehrendorf line. Subsequently, the system operator aimed to decrease the current on the overloading line but wrongly coupled a busbar without a pre-event online simulation, triggering cascading outages.

Moreover, from the technical point of view, the current transmission system has a very advanced design. The system's state can be monitored in the control room through direct measurement by using WAMS and indirect calculation. Each facility in the system can be protected by various systems to avoid damage. Remote control action can also be implemented to adjust the system's status, such as reactive power adjustment to satisfy voltage constraints and loading shedding or generator tripping to satisfy the requirement of system frequency. System demand forecasting is planned for both the short run and the long run in order to enhance the system's reliability. However, an unexpected lack of coordination always exists in these smart-designed corrective controls, especially when the original system configuration changes during cascading outages. In addition, hidden faults in the system will become apparent under extreme conditions, which also deteriorate the safety of the system.

This chapter outlined system security criteria and traditional prevention schemes against system collapse or blackouts. Also discussion includes methods used to counter voltage drop and frequency drop. However, in the blackouts described earlier, the poor

operation of traditional controls because of the lack of integration failed to ensure the survival of the system in the cascading progress, especially when several faults occurred simultaneously. In addition, the malfunction of the distance relays in zone 2 and zone 3 also contributed to several blackouts, which will be discussed further in Chapter 6. Therefore, under such circumstances, a new three-stage controlled islanding scheme against blackouts at the top level of the system is proposed. This scheme will be used as a last resort action to prevent blackouts from occurring when the usual means fail.

In addition, the review of major blackouts in recent decades indicated that they were caused by cascading outages. They began when the lines were tripped because of line overloading, and they ended when the generator was tripped when synchronism was lost, which directly led to the blackouts. Furthermore, because of the dynamic characteristics of the cascading process, the voltage oscillation and frequency oscillation that were observed through online measurement were caused by the oscillation of the generator angle. Therefore, the online assessment of transient stability is the most important contribution to preventing blackouts and a vital indicator in predicting imminent blackouts. This thesis focuses on the issue of transient stability during cascading blackouts.

Chapter 3:

Power System Security Assessment

In this chapter, the security assessment in the power system is described, particularly transient stability because it occurs significantly in the cascading outages before imminent blackouts and could be an indicator of when to island. In addition, in order to adopt the controlled islanding scheme online, the latter has to align with current systems of security assessment. Hence, it is necessary to review security assessment in traditional power systems. This assessment aims to detect the degree of risk and test the systems' ability to survive imminent disturbances or contingencies without interrupting the customer service. This security assessment usually relates to the robustness of the system and its operating conditions. It also depends on the contingent probability and severity of disturbances.

In the past, conceptual terms in [43], such as security, reliability and stability, have been used to describe a power system's capability to survive all kinds of disturbances. The overall and long-term objective is reliability, which ensures the satisfactory design and operation of a power system. Therefore, in order to be reliable, the system must be secure most of the time. In order to be secure, the system must be stable against other contingencies that may occur and lead to instability problems in terms of overloading, voltage and transient issues. However, in the long run, one fact must be faced: Any system with high reliability, security or stability will still be challenged by periods of severe insecurity under unexpected disturbances. Therefore, offline outage planning and online continuous security assessment according to the security criteria are important for the current and future security of power systems.

3.1 Power System Security

3.1.1 Factors affecting system security assessment

Ensuring secure operation in a safe and economic manner in a power system is already a primary objective. However, with the development of traditional electrical power industries to operate in the liberalised electrical market, an increasing number of factors have become sources of system disturbances that affect the security of system operations. These factors not only reduce the robustness of the power system but also decrease the secure predictability of system operations. These factors include aging transmission infrastructure, large numbers of penetration of renewable generation, market-driven electrical power transaction, and so forth.

3.1.2 Direct method of stability analysis

Dynamic security assessment (DSA) in a power system requires a correct and timely analysis to decide whether the current operating system is able to satisfy the reliability and security criteria in both transient and steady-state conditions in all credible contingencies [43][44]. In an operating environment, a secure system can assess all aspects of the power system that affect system stability issues in both pre-contingency and post-contingency states, including thermal loading of power elements (e.g., transformer, transmission lines etc.), frequency and voltage variation and other forms of stability (i.e., generators' power angle). Historically, security assessment has been conducted in an off-line operating environment where the performance of steady-state and transient stability is tested based on all kinds of forecasted contingencies using tools such as power flow computation and time-domain simulation. Transient stability assessment has been investigated for many decades, such as in research to adapt an offline tool to an online tool. Traditionally, time-domain simulation uses numerical integration to calculate the during-fault and post-fault trajectories of the generator's behaviour. The generator's behaviour is then used to decide whether the system's stability can be maintained. This conventional approach is time consuming and can only be used in the off-line analysis of transient stability. However, the off-line analysis of the current power system is still not desirable in an online operating environment. On one hand, an online application based on the results of an off-line analysis is

conservative in accuracy and leads to a trade-off between safety and business. On the other hand, the amount of offline analysis required can be significantly reduced compared with the online analysis using online measurements from the WAMS system.

Under such circumstances, a direct method [45]-[58] was developed to assess transient stability for online application purposes. Compared with the time-domain approach, the direct method only integrates in the during-fault system and does not integrate in the post-fault system. When the fault is cleared, the direct method determines whether the system is transiently stable by comparing the system's energy with a calculated threshold value. In other words, the stability issue involves determining whether the initial point of post-fault trajectory is inside the stability boundary, which is formed by an acceptable stable equilibrium point (SEP). However, this direct method is subject to one assumption [47]: the pre-fault SEP has to be inside the stability region of a desired post-fault SEP. Although this energy function-based direct method has advantages compared with the conventional time-domain approach, such as fast computation and an exact stability margin, some challenges remain. Regarding the simplified transient stability model, research has shown that it is too impractical for use in real power system applications. In [49], the direct method was used to handle more complicated power system models by constructing a numerical energy function.

The direct method has undergone several stages in its historical development. Initially, the famous equal area criterion in one-machine-infinite busbar system was proposed for stability analysis. Based on this energy concept, the critical clearing angle could be obtained without solving the differential equations in the conventional approach. This energy-based concept then was extended to a multi-machine system. Subsequently, Lyapunov's idea, which was associated with LaSalle's invariance principle [52][53] was proposed to estimate the region of stability and critical clearing time. However, the difficulty was that in order to obtain the critical clearing time, the threshold value that the fault trajectory reaches in the region of stability must be determined. Subsequent research proposed finding all unstable equilibrium points around the stable equilibrium point in order to estimate the critical clearing time [54]. However, finding all unstable equilibrium points is not an easy task. The closest unstable equilibrium point (UEP) method and the controlling UEP method [47] were proposed and developed in the late 1960s and 1980s, respectively. In the closest UEP method, during-fault trajectory is not

taken into account. Therefore, this method cannot provide an accurate approximation of the region of stability, resulting in severe conservativeness. In order to reduce the conservativeness of the closet UEP method, the controlling UEP method was proposed, which takes into account the during-fault trajectory and provides an accurate approximation of the region of stability. Its stability assessment results are much more accurate than the results obtained by the closed UEP method are [47][50]. However, the disadvantage of the controlling UEP method is that in some cases, it is still challenging to find the controlling UEP associated with the during-fault trajectory [47][50].

The potential energy boundary surface (PEBS) was proposed by Kakimoto [55] to obtain critical energy and estimate critical clearing time without calculating the unstable equilibrium points. The critical energy is defined as the first local maximum of the potential energy along the fault-on trajectory. The research results in [56] showed that the PEBS method yields a good estimation of the critical clearing time. However, in some cases, this method produces non-conservative results of the critical clearing time. Such results are not desirable because online application systems may have already lost transient stability, so it cannot be included in the calculation.

The boundary controlling unstable (BCU) method, which is the most popular direct method, was proposed in 1990s by Chiang [48][57]. The BCU method is based on the PEBS method. However, its accuracy is guaranteed by a precise definition based on dynamic system theory. Compared with the PEBS method, the BCU method provides conservative results of the first swing assessment, and it always guarantees the first swing stability.

In conclusion, many advances have been made in direct methods, but many challenges remain. These direct methods are still not suitable for the analysis of multi-swing transient stability. Another limitation of the direct method is that the initial condition of the post-fault system is essential for online application, and these initial data must be available in advance. However, the data can only be obtained beforehand through the time-domain approach. Moreover, the limitation of all of these direct methods [45]-[58] is that they are based on an inherent characteristic: the pre-fault SEP must be inside the boundary of the post-fault SEP. Otherwise, the stability issue has to reply to the conventional time-domain approach for verification. Another challenge is the accuracy

of the assessment of transient stability. Research on all these direct methods and the numerical energy function [59] has attempted to achieve that objective. The reliability of the direct method is linked to the reliability of computing the controlling UEP for every contingency. All these direct methods have demonstrated uniqueness from a theoretical perspective. However, from a practical perspective, the task of computation is still challenging.

In addition, the direct methods face the same issue of finding the Lyapunov functions, especially when detailed models are considered, such as realistic generator models and load models. Hybrid methods [10]-[14] have been proposed, which aim to take advantage of both direct methods and the conventional methods. Direct methods guarantee fast calculation speed in building computation algorithms, while the conventional method obtains realistic data from a detailed model, which is used in the calculation of the direct method. Hybrid methods currently used are EEAC and SIME, which will be thoroughly discussed in Chapter 7 and Chapter 8. Moreover, these methods are used in this thesis to assess online transient stability in the controlled islanding scheme.

3.1.3 Online dynamic security assessment

The off-line DSA approach will be implemented in the outage planning stage. Numerous N-1 (N-D applied in UK) contingency analyses and computations need to be executed and updated continuously before the forecasted contingent conditions occur. However, these forecasted contingent conditions might never happen, and they might not include all of possible contingencies because the system's components and configuration may change in the real time phase. Therefore, based on the obtained offline DSA results, the online DSA [44] has to be continued in the real time phase in the control room. System stability in terms of all security aspects under the current updated operation condition (OC) is computed online as it occurs with sufficient time and speed either to trigger the control devices automatically or to let the system operators take action with enough time left if the analysed contingency is shown to be potentially insecure. This approach scans the system continuously for a potential problem that results from the analyses of N-1 or even N-k (k>1) contingencies, and the planned outages are assessed for maintenance purposes in a process that is similar to the

sweeping behaviour of a radar mechanism. Figure 3.1 shows an overview of the mechanism of this online DSA approach. Different components have different functions in achieving the online security assessment.

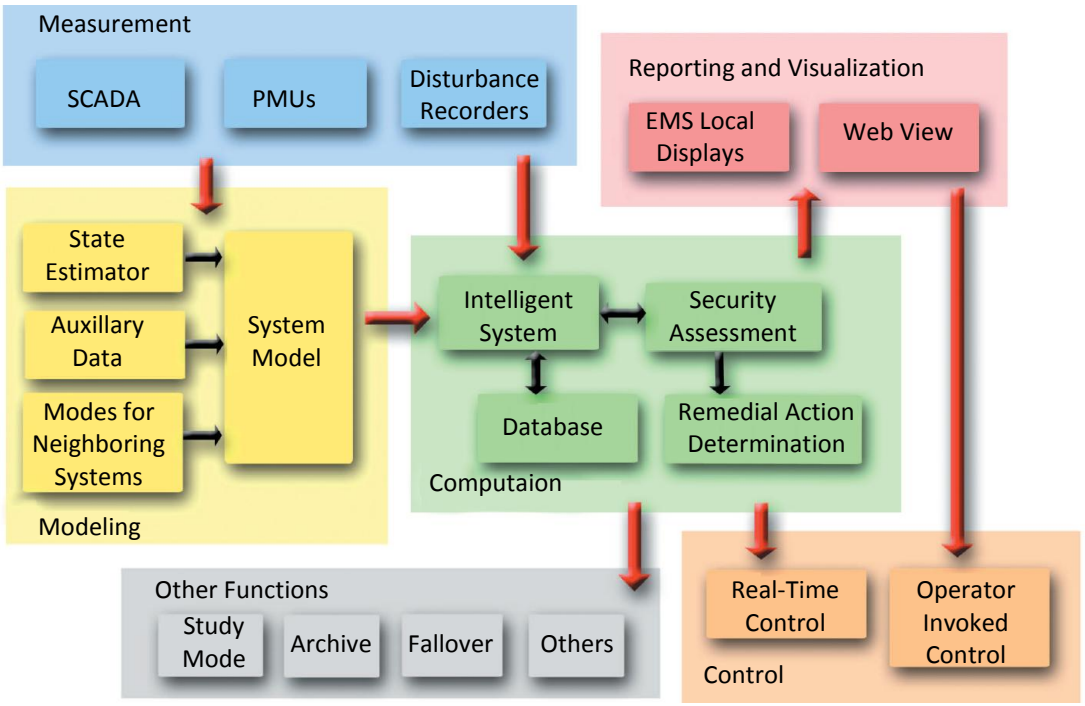

Figure 3.1: *Online dynamic security assessment system mechanism [44]*

Figure 3.1 shows all components in the DSA system, including measurement, modelling, computation, reporting, visualization, other functions and control. In measurement, important data in the actual system's OC, such as voltage, current, phase angle, can be obtained from SCADA in real time for use in computation. These signals are received as inputs and then implanted in the state estimators and dynamic models for use in the power flow and dynamic computation. The analytical solutions will assess the security of the pre-fault operating condition if planned outages are undertaken. In addition, in the planning stage, post-fault operating conditions also have to be considered if the operating condition is changed to assume that a fault happened in order to satisfy the system's N-1 security criteria. In addition, post-fault actions have to be signalled to the control room if these assumed faults occur in real time. For example, if the post fault indicates an overloading issue, a corresponding decrease in power generation from certain generators has to be implemented to alleviate the overloading problem before it reaches the post-fault rating of lines and to return the reduced power flow to the pre-

fault rating. If transient instability occurs between the energy-importing area and the energy-exporting area, then the pre-agreed generators in the energy-exporting area will be asked by the system operator to decrease their generation in order to solve the transient instability issue. Various security criteria regarding the thermal overloading of transmission lines, steady-state voltage excursion, voltage change excursion and transient stability and so forth are shown in Figure 3.2. Figure 3.2 illustrates the security region in a two-dimensional nomogram to represent operating margin for a case of two generation groups in the interconnected system.

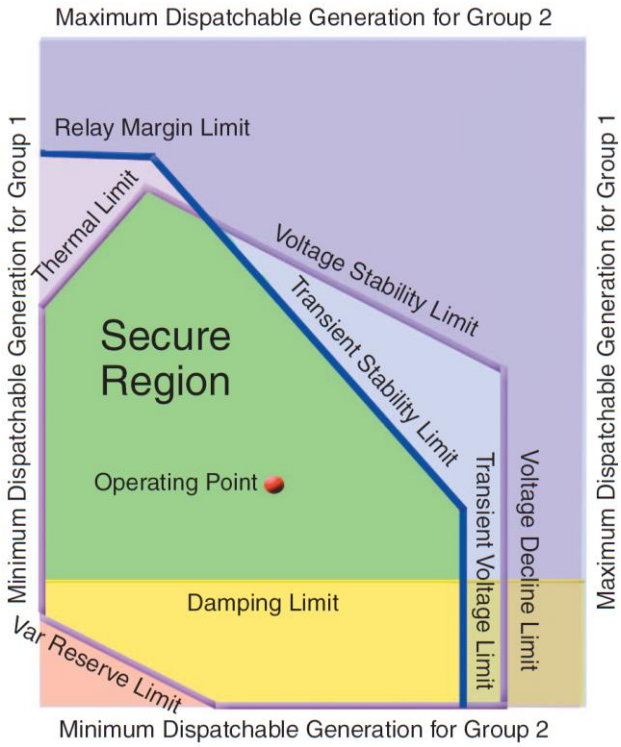

Figure 3.2: *Security margin nomogram under current OC [44]*.

The online DSA determines the assumed contingencies or disturbances that will result in an insecure condition in the power system. When these events happen, the remedial control actions will counter the insecure situation and return the system to another secure OC. In addition, other functions are also involved in the online DSA system, such as the study mode, archive, system monitoring and maintenance functions. These functions could be used to store data periodically and selectively from the on-line system for off-line study and post-event analysis. They could also be used to monitor the performance of the DSA system.

3.1.4 Security in system operations

Because the demand for electrical power has been increasing in recent decades, in addition to the profit-driven incentive, power systems are gradually operating closer to their stability limits. Therefore, power system operation has become more challenging. In [60], the normal operating state in power system is defined as needing to satisfy the following requirements:

- Power balance between generation and demand satisfied by the capacity constraints of individual generators
- Frequency dynamic variation within a prescribed range
- Steady-stage voltage limit and voltage change limit satisfied
- No overloading apparatus

All these requirements are expressed in the form of a set of equality constraints and a set of inequality constraints. The objective of the operators is to keep the system under a normal operating condition. They will choose to take preventive control actions to achieve this goal. However, in practice, such actions are not enough to maintain the system's security. For instance, a disturbance may cause an emergency that may lead to cascading failures, thus deteriorating the security of the entire system. Thus, correct control in real time is also important in maintaining a system in a normal operating state.

3.1.5 Power system security criteria

Assume that a set of disturbances are given to a system one at a time. If the system continues to maintain a normal operating state without any action taken, it is said to be secure. Actually, the system cannot avoid being affected by disturbances, such as lightning strikes on transmission lines, mechanic failures of the system's components and so on. Therefore, the system has to be designed to withstand these unexpected contingencies while continuing to be secure. Currently, the fundamental N-1 and N-D or even N-k (k>1) security criteria are widely used. The definitions of these criteria and the reasons that are required are explained in Chapter 2.

3.1.6 Analysis of power system security

As previously mentioned, the analysis of system security relates to the robustness of the power system, the system's current operating conditions and the severity of possible disturbances. Typically, two important aspects need to be considered in the analysis of the power system: static security analysis and dynamic security analysis [43]. For example, when a system is subjected to a disturbance, it is important for the system to settle to a new operating condition without violating the physical stability constraints after removing the disturbance. This also implies that during the transition period to the new operating condition, the system has to survive by satisfying all dynamic constraints resulting from the disturbance.

The static security analysis aims to determine the security of the steady state operating condition after the disturbances by checking that the system components' ratings are at normal level and determining whether the voltage limits are violated. The dynamic security analysis aims to analyse the system's stability during the dynamic progress, including voltage stability, frequency stability and the stability of the generators' power angle, which are integral components of security assessment.

Both analyses and all stability issues involved in the security of the power system are shown in Figure 3.3:

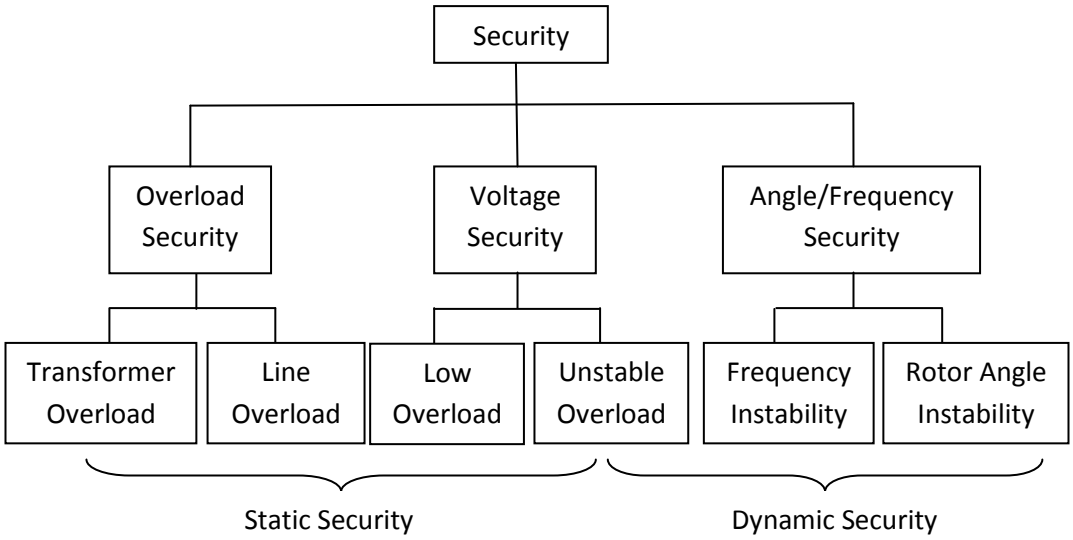

Figure 3.3: *Categories of the power system's security [61].*

3.2 Power System Stability

3.2.1 Classification of power system stability

Modern power systems are a high-order and multivariable network with dynamic changes that depend on various devices with different characteristics and ratings. Stability is just a condition in which several equilibria are not violated. When these equilibriums are destroyed by a set of disturbances, a long-sustained imbalance may cause instability in its many components, which can lead to the collapse of the system.

Because of their complexity, power systems are subject to various forms of instability. Stability issues can be divided into categories, which are shown in Figure 3.4:

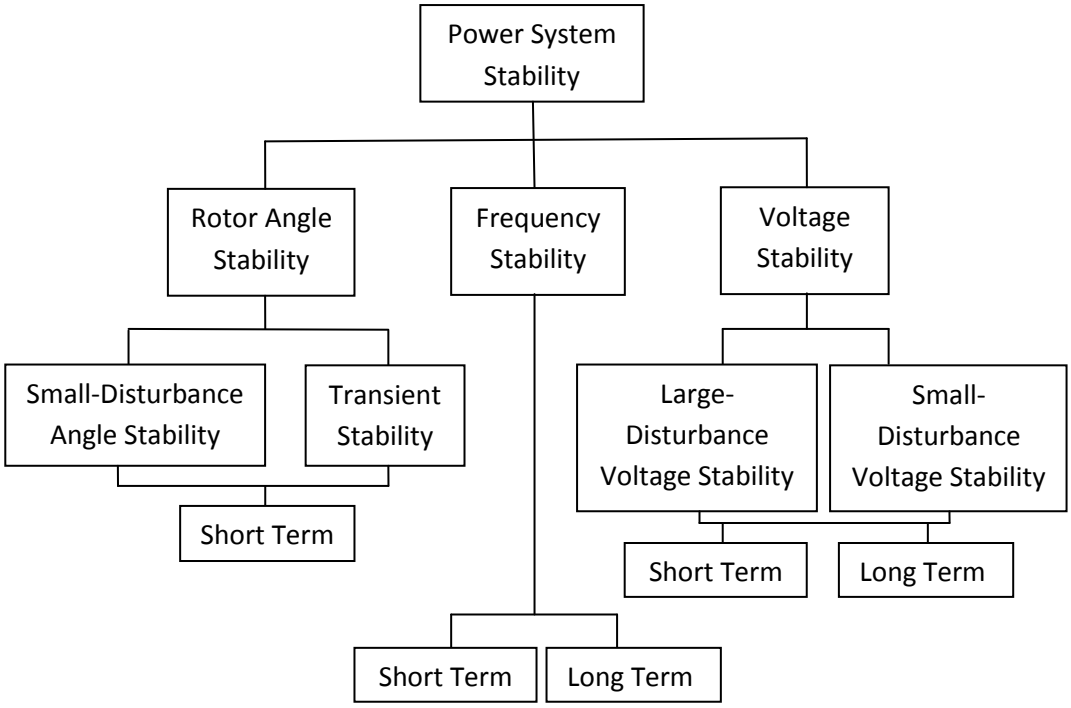

Figure 3.4: *Classification of power system stability [43]*.

Figure 3.4 shows an overview of potential instabilities in the power system. These are classified based on a few contributing factors that need to be considered, including the physical consequences of instability, system variables, severity of disturbances that influence the analysis of dynamic modelling, predication of stability, and the time span that is used for assessment of stability. Generally, all three kinds of instability could happen during cascading blackouts. Transient stability and voltage or frequency

oscillation could trip more components of the system and accelerate the speed of the cascade. The following section explains the principle of transient stability.

3.2.2 Rotor angle stability in the generator

Rotor angle stability is the ability of synchronous generators in an interconnected system to maintain synchronism, that is, continue to be "in step" after being subjected to a disturbance. Rotor angle stability depends on the ability of synchronous generators to maintain or restore the equilibrium between electromagnetic torque and mechanical torque to prevent the angular swings of some generators from being increased during oscillation to cross a certain limit. Consequently, it causes these generators to lose synchronism with the remaining generators in the network, which leads to instability. Newton's famous second law describes three different kinds of torque working against each other, which is shown in the following equation [62]:

$$J\frac{d\omega_m}{dt}+T_D=T_t-T_e \tag{2.1}$$

where J is the inertia of the turbine/generator set, ω_m is rotor shaft velocity, T_t is the torque provided by the turbine, T_e is the electrical torque reacted by the generator and T_D is damping torque accounting for the mechanical loss caused by rotational friction.

In the steady state, turbine torque T_t is equal to the sum of the electrical toque T_e and the damping torque T_D. In other words, the net mechanical torque T_m is equal to the turbine torque subtracting the damping torque, while the generator's rotor angular speed is the synchronism speed at ω_{sm}, as shown in the following equations:

$$T_t=T_e+T_D \quad \text{or} \quad T_m=T_t-T_D=T_e \tag{2.2}$$

$$T_D=D_d\omega_{sm} \tag{2.3}$$

where D_d is the coefficient of the damping torque.

Under a disturbance, the net mechanical torque and the electrical torque will lose their

balance. If $T_m > T_e$, then the rotor accelerates at a higher rotor angular velocity; if $T_m < T_e$, then the rotor decelerates at a lower rotor angular velocity. Therefore, the generator rotor's angular velocity can be expressed as the sum of the angular synchronism speed plus the angular deviation during a disturbance, as shown in the following equation:

$$\omega_m = \omega_{sm} + \Delta\omega_m = \omega_{sm} + \frac{d\delta_m}{dt} \tag{2.4}$$

Substituting equations (2.2), (2.3), (2.4) into (2.1) yields

$$J\frac{d^2\delta_m}{dt^2} + D_d\left(\omega_{sm} + \frac{d\delta_m}{dt}\right) = T_t - T_e \tag{2.5}$$

Based on (2.3) moving $D_d\omega_{sm}$ to the right side of (2.5) yields

$$J\frac{d^2\delta_m}{dt^2} + D_d\frac{d\delta_m}{dt} = T_m - T_e \tag{2.6}$$

Because the torque can be expressed as the power over angular velocity, then in terms of power, the right-hand side of (2.6) can be given as

$$J\frac{d^2\delta_m}{dt^2} + D_d\frac{d\delta_m}{dt} = \frac{P_m}{\omega_m} - \frac{P_e}{\omega_m} \tag{2.7}$$

where P_m is the mechanical power of the rotating shaft produced by the turbine in the generator, while P_e is the generator's electrical power driven by demand. Multiplying synchronous angular speed ω_{sm} on both sides of (2.7) yields

$$J\omega_{sm}\frac{d^2\delta_m}{dt^2} + \omega_{sm}D_d\frac{d\delta_m}{dt} = \frac{\omega_{sm}}{\omega_m}P_m - \frac{\omega_{sm}}{\omega_m}P_e \tag{2.8}$$

Because the synchronous angular speed ω_{sm} is close to the rotor's angular velocity during a disturbance, $\omega_m \approx \omega_{sm}$ could be obtained to make the coefficients of P_m and P_e in (2.8). The famous swing equation of the generators can then be expressed as follows:

$$M_m \frac{d^2\delta_m}{dt^2} = P_m - P_e - D_m \frac{d\delta_m}{dt} \tag{2.8}$$

where $M_m = J\omega_{sm}$ which represents angular momentum of rotor at synchronous speed; $D_m = \omega_{sm} D_d$ which represents damping coefficient.

The swing equation (2.8) represents the dynamic behaviour of generators during a disturbance. It also has subsequence influence on governing the parameters in the system because of the change in generator angles, such as power flow and voltage.

In (2.8), the angular momentum of the rotor can be expressed by the normalized inertia constant H. The inertia constant is defined as the ratio of stored kinetic energy at synchronous speed in mega joules over generator rating S_n in megavolt-amperes, as follows:

$$H = \frac{0.5J\omega_{sm}^2}{S_n} \tag{2.9}$$

The unit of H is seconds. The inertia constant physically interprets how long the stored kinetic energy in the rotor at synchronous speed takes the generator to reach an equivalent amount of electrical energy when operating at its MVA rating power output.

If electrical radians and electrical radians per second are used to express power angle and angular speed, then they can be expressed by associating with number of poles p in the generator as follows:

$$\delta = \frac{\delta_m}{p/2};\ \omega_s = \frac{\omega_{sm}}{p/2} \tag{2.10}$$

Substituting (2.9) and (2.10) into (2.8) gives

$$\frac{2HS_n}{\omega_s} \frac{d^2\delta}{dt^2} = P_m - P_e - D\frac{d\delta}{dt} \tag{2.11}$$

where $D = 2D_m / p$ and D is defined as the damping coefficient. In addition, the inertia

coefficient M and damping power P_D are defined as follows:

$$M = \frac{2HS_n}{\omega_s}, \quad P_D = D\frac{d\delta}{dt} \tag{2.12}$$

Therefore, the common form of the swing equation can be expressed as

$$M\frac{d^2\delta}{dt^2} = P_m - P_e - P_D \tag{2.13}$$

This aspect of stability is influenced by the dynamics of the generator rotor angles and the power-angle relationships, which are shown in Figure 3.5.

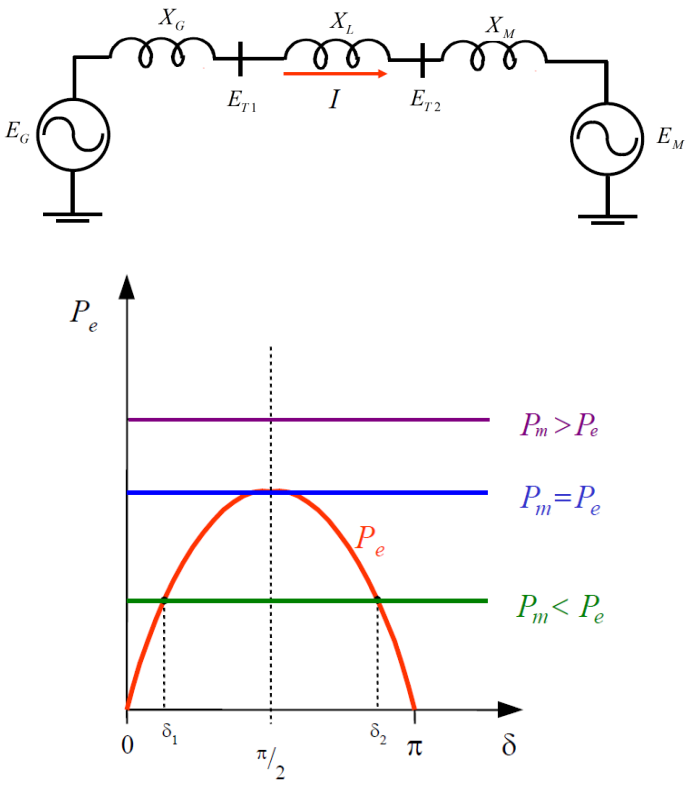

Figure 3.5: *Idealized model and power-angle curve [63].*

In Figure 3.5, the idealized model on the left shows a simple system that can be used to determine the power versus the angle relationship, which is shown as the power-angle curve on the right in Figure 3.5. The sending and receiving voltages V_S, V_R can be expressed as follows [62][63]:

$$V_S = E_G \angle \delta \,,\; V_R = E_M \angle 0 \tag{2.14}$$

where E_G represents voltage on the generator side, and E_M represents voltage on the motor side; δ is the generator angle. The current flowing on the circuit I can then be expressed as follows:

$$I = \frac{E_G \angle \delta - E_M \angle 0}{jX_T} = \frac{E_G \cos\delta - E_M + jE_G \sin\delta}{jX_T} \tag{2.15}$$

where $X_T = X_G + X_L + X_M$ and X_T denote the overall reactance of the generator, transmission line and motor. The sending end real power P_S and reactive power Q_S can be obtained as follows:

$$P_S + jQ_S = V_S I^* = E_G(\cos\delta + j\sin\delta)\frac{E_G \cos\delta - E_M - jE_G \sin\delta}{-jX_T} \tag{2.16}$$

After simplification, (2.16) becomes

$$P_S + jQ_S = \frac{E_G E_M \sin\delta + j(E_G^2 - E_G E_M \cos\delta)}{X_T} \tag{2.17}$$

Because the line is assumed to be loss less without resistance, the power transferred from the generator to the motor P is equal to the real power dispatched from the sending end and the real power received at the receiving end. This is described by the following equation [63]:

$$P = P_S = P_R = \frac{E_G E_M}{X_T}\sin\delta \tag{2.18}$$

A fundamental factor in rotor angle stability is shown in Figure 3.5, where the power output of synchronous generators varies with the change in their rotor angles. In the steady-state condition, equilibrium exists between the electromagnetic torque and the mechanical torque, and the rotating speed of generators remains constant. When the system is disturbed, the equilibrium will be reset to find another balance point. During this oscillation process, the rotor will accelerate and decelerate until it achieves a new equilibrium between the electromagnetic torque and mechanical torque if it can be

found before the loss of synchronism.

During the process of oscillation, if one generator temporarily runs faster than another, the angular position of the rotor relative to that of the slower one will advance. The resulting rotor angle difference will then transfer part of the load from the slow machine to the fast machine, which tends to reduce speed difference and rotor separation [64]. Figure 3.5 shows that the power-angle relationship is highly nonlinear especially beyond 90 degrees that the rotor angle reaches to. The gap of angular separation is increased, which is performed by a decrease in power transfer, so this will further increase the power separation until the fast-running generator goes across the unstable equilibrium generator angle $\delta^{\lim}$ shown in Figure 3.6. The rotor angle cannot go back and synchronism with the rest of network is lost.

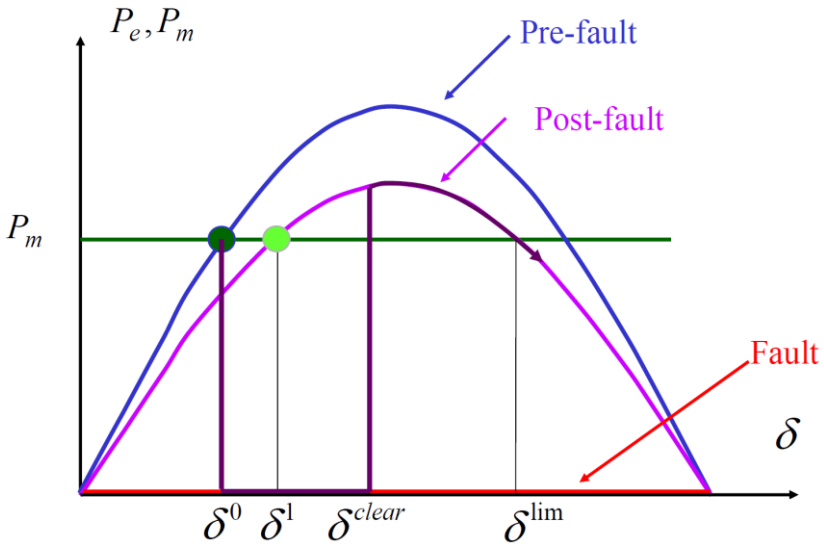

Figure 3.6: *Evolution of the state of the system [63].*

A critical question about the transient stability of the rotor angle concerns whether it can move from one steady state operating point to another without being unstable in a large disturbance. One machine and the infinite bus system shown in Figure 3.6 are examples:

- Before the fault, the power angle of the generator is shown as δ^o.

- During the fault, which occurs at the terminal of the generator, the electrical power P_e suddenly drops to zero, and the voltage is zero.

- Consequently, the power angle δ increases because the mechanical power is much bigger than the electrical power ($P_m > P_e = 0$).

- Let the increasing power angle δ be equal to δ_{clear} when protective devices take actions to clear the fault.

- After the protective devices trip the faulted component, the system configuration changes while the impedance in the transmission lines changes. A new post-fault power angle curve is produced as shown in Figure 3.6.

- Power angle δ continues to increase because of momentum obtained during the fault. In addition, because the electrical power is bigger than the mechanical power ($P_e > P_m$), the rate of increase in the power angle gradually slows.

- Power angle δ reaches its maximum value when the momentum is exhausted.

- Because the electrical power is still bigger than the mechanical power ($P_e > P_m$), the power angle δ starts to decrease toward to δ^1 in order to achieve a power balance.

- Power angle oscillates around δ^1 until damping lets it settle at δ^1, which means that the system obtains another stable operating condition in the post-fault power angle curve.

Based on the description of the transient period of the generators' power angle, the system will be stable if δ never exceeds $\delta^{\lim}$, which is shown as follows:

$$\delta^{\max} < \delta^{\lim} \tag{2.19}$$

Because we know, if the power angle δ increases beyond $\delta^{\lim}$, the mechanical power will again be greater than the electrical power ($P_m > P_e$). The turbine and generator re-accelerate infinitely until the generator loses synchronism because there is no chance that the electrical power could be bigger than mechanical power once the power angle crosses $\delta^{\lim}$. This constraint can be translated into a practical stability criterion, which is called the equal area criterion, which was described in [62]-[64]. It is a simple,

observed criterion based on the concept of stored kinetic energy, which is illustrated in Figure 3.7.

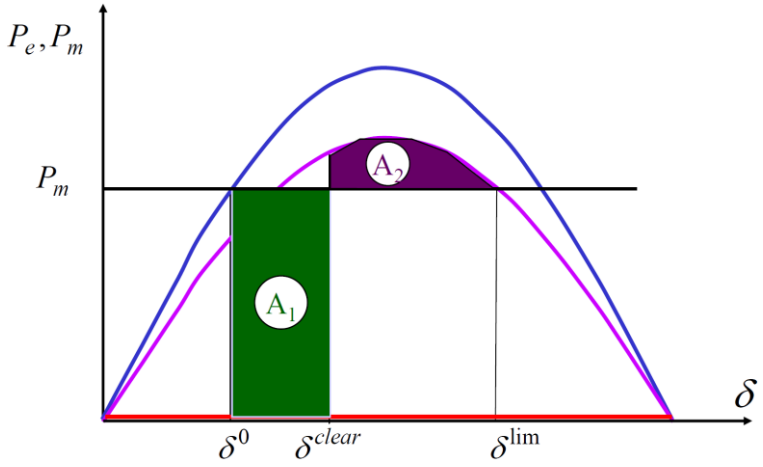

Figure 3.7: *Equal area criterion [63].*

In order to maintain the system's stability, the increased kinetic energy A_1 during the fault must be exhausted by the injected kinetic energy A_2 during the post-fault period before the power angle δ reaches $\delta^{\lim}$. The largest and most critical value of the power angle is δ^{clear} to ensure $A_1 = A_2$. Therefore, the protective devices have to take action to clear the faults before δ reaches δ^{clear}. This angle is called the critical clearing angle [62]-[64]. Accordingly, the system will be stable if the actual clearing angle δ^{clear} never exceeds δ^{crit}, which is shown as follows:

$$\delta^{clear} < \delta^{crit} \tag{2.20}$$

This equal area criterion provides us with a method to calculate the critical clearing angle δ^{crit}, which can be used to determine whether the system will be stable. However, in practice, the power angle cannot be measured and controlled directly. It depends on the loading of the system and the characteristics of the fault [64]. Therefore, a more practical and feasible way to determine whether the system will be stable or not is to compare kinetic energy and potential energy by using the extended equal area criterion (EEAC) and the single machine equivalent (SIME), which are discussed in detail in Chapter 7 and Chapter 8, respectively. EEAC and SIME are also used in the assessment

of online transient stability during cascading outages and in decisions regarding the correct time to implement the islanding scheme.

In reality, transient instability is a critical issue in the power transfer between two weakly interconnected areas; however, this transient instability can also be improved to some extent. For example, in the UK power system, a large amount of power flow needs to be transferred to heavily loaded areas in England from Scotland, which is mostly produced by renewable energy because of the CO2 emission target set by the UK government. However, the Scotland network and the England/Wales network are weakly connected by two 400 kV DC along the west and east coasts. The conventional generators between both areas often oscillate with each other and even lose synchronism if the threshold value of the power transfer across the boundary is violated. A few means have been proposed to address the transient stability issue, such as decoupling the Scotland-England network using VSC-HVDC [65]. Alternatively, a series of braking resistors [66] could be used to improve the stability of low-inertia synchronous generators. Currently, series compensators are installed on each 400 kV transmission line, and a new HVDC transmission line is under construction to improve the power transfer from Scotland to England in order to manage the high penetration of renewable energy transfer. However, this could increase the vulnerability of the network to transient instability because of the connection to the low inertia of wind farms [67], resulting in the reduced inertia of the system.

3.3 Summary

This chapter describes the traditional security assessments of the power system and its online operation. Every planned outage for asset maintenance or system enhancement first has to be assessed offline during the planning stage before its handover to the control room in the real time phase. This offline assessment is based on the operation condition in which planned outages actually take place; moreover, the worst faults happen around these planned outages. This well-known assessment is called the N-1 security criterion, and it is widely used in industrial practice. In fact, the UK applies the N-D security criterion, which takes into account a double circuit fault when assessing system security, making the system more secure. Pre/post thermal issue, voltage step change, transient stability and fault level will be assessed during offline DSA. The

outage planners have to make sure that the security issues in the planned outages under the worst fault scenario will not be violated. Otherwise, the system operators may lose money in buying generation in order to satisfy the N-1 system's security criterion. When the offline DSA is complete, the assessment results will be delivered to the control room a day in advance. In the next 24 hours, the control room will reassess the planned outages in real time. Although the assessment is closer to real time, the results are more accurate, the operating condition may vary because of changes in system configuration, generation and demand forecast. Therefore, in real-time system operation, the condition of the system is monitored and DSA is conducted, such as in N-1 contingency analysis. This N-1 contingency will be updated every few minutes.

In addition, this chapter outlined the development of the direct method of assessing transient stability and highlighted the advantages of new online transient stability methods compared with conventional time-domain approach using numerical integration. Finally, EEAC and SIME used in direct methods are discussed. In this thesis, these are used to assess transient stability in order to decide when to island in the controlled islanding scheme. Transient instability has occurred in most blackouts across the world in recent decades, such as the US/Canada blackout (2003). The chapter also provides background information regarding transient stability, including the well-known power swing equations, power-delta curve and equal area criterion, shows how this equal area criterion works under a fault scenario.

Based on the fundamental principle of transient stability, the methodology of transient stability assessment EEAC and SIME are described in detail in Chapter 7 and Chapter 8, respectively. These assessments are used in the online transient stability prediction to solve the when-to-island issue. EEAC and SIME will be used to extend the application of the equal area criterion from a simple single-machine infinite busbar system to a realistic multi-machine system.

Chapter 4:

Review of Islanding Methods

N-k contingency analysis is widely used in power systems because it is the industry standard in governing and assessing the operation of a network to allow it to keep operating when its components fail. Power systems are usually operated according to the N-1 security criteria with a sufficient security margin, which historically has proved to deliver a satisfactory level of reliability. In addition, an enormous number of conventional protection relays are designed to ensure that their own important equipment, such as generators, transmission lines and so on, is not damaged by faults and disturbances. However, because of the lack of coordination of protection in different interconnected areas and in maintaining widespread system stability, uncontrolled islanding occurs in most circumstances through tripping the tie line relays while simultaneously separating the system into unplanned out-of-control islands, thus leading to blackouts. In this situation, one strategy used to prevent blackout is the proposed preventive island scheme. In this scheme, a system is split into smaller islands so that the size of the blackout and its effects are minimized. An essential question concerns when an islanding scheme should be activated. Islanding too early would mean an unnecessarily heavy intervention, whereas waiting too long would mean that a blackout could happen. The other question concerns where to island. The proposed scheme aims to find boundaries to split the whole network and prevent the cascading contingencies from spreading into the remaining areas. In this chapter, we will review previous islanding methods regarding these two issues in the controlled islanding scheme.

4.1 When to Island?

In previous research regarding when to island, controlled islanding [6]-[8],[68] used the DT-based method as a strategy to split the network intentionally into pre-designed islands based on the characteristics of the predictive signals received to trigger the out-of-step relays installed on the tie lines. In [7] the power angles of generators and rotor

velocities during severe disturbances were selected as predictors to train DT to determine whether the system is potentially unstable. In [68] the voltage phase angles, angular velocities and accelerations measured at critical high voltage busbars were chosen as predictors to train DT to decide when to island. In [8], the inputs of trained DT were measured in apparent resistances *R* and their rates of change *Rdot.* The output indicated the operating condition of the system. A combination of one-shot control actions would be triggered if the *R-Rdot*-based trained DT predicted that the blackouts were imminent. Before reviewing these DT-based methods, it is necessary to describe the DT method.

4.1.1 Decision Tree Method

The decision tree (DT) technique uses a small number of variables or predictors to classify the objective under the identified critical splitting rule (CSR) that could affect the objective more directly and efficiently [68]. In power systems, the application of DT describes the prediction model of the system stability problem through creating a database that consists of a huge number of cases. Each case is described by pre-designated predictive signals the objectives of which are affected by these predictors. Figure 4.1 represents a DT structure with five internal nodes and six terminal nodes. Each internal node is usually divided into two successors. During the classification process, the CSR will be asked to identify the predictors and decide in which classification branch the successor should be placed. In Figure 4.1, the predictors are demonstrated by voltage phase angles and angular change velocities. For each terminal node that has no successors, a final classification will be obtained based on the majority of cases trained previously for the objective. For example, Figure 4.1 shows at the terminal node the final number of cases belonging to this classification. The black bar represents the percentages of the “stable” systems , and the grey bar represents the percentages of the “unstable” systems in this classification.

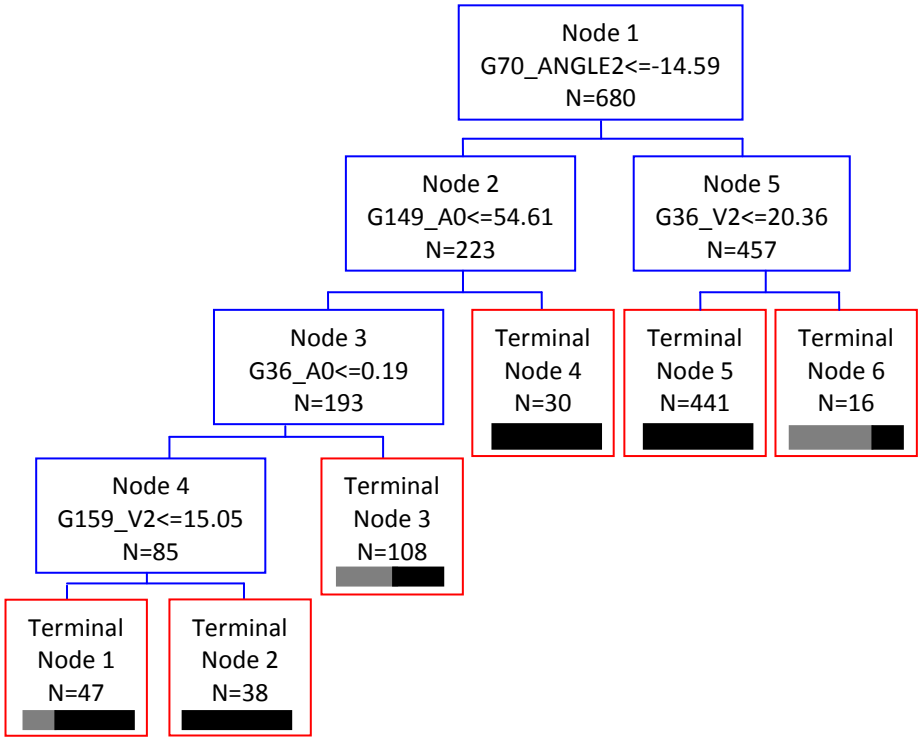

Figure 4.1: *A decision tree with five internal nodes and six terminal nodes [68].*

Thus, in power systems, DT is an effective, simply structured model that offers readability in conducting security assessments. The predication results can be obtained by comparing the predictors with the threshold of the CSR. Predictors such as voltage phase angles can also be read directly from the phase measurement unit (PMU) installed on buses.

4.1.2 DT-based Controlled Islanding Scheme

The process of training a DT not only determines the predictors affecting the objective in known cases but also predicts the objective in unknown cases. Therefore, in order to enhance the prediction ability and robustness and accuracy of DTs, several offline simulations are required, which enable the DT to be well trained based on simulation or historical data before performing the online application. Figure 4.2 shows the DT-based controlled islanding strategy.

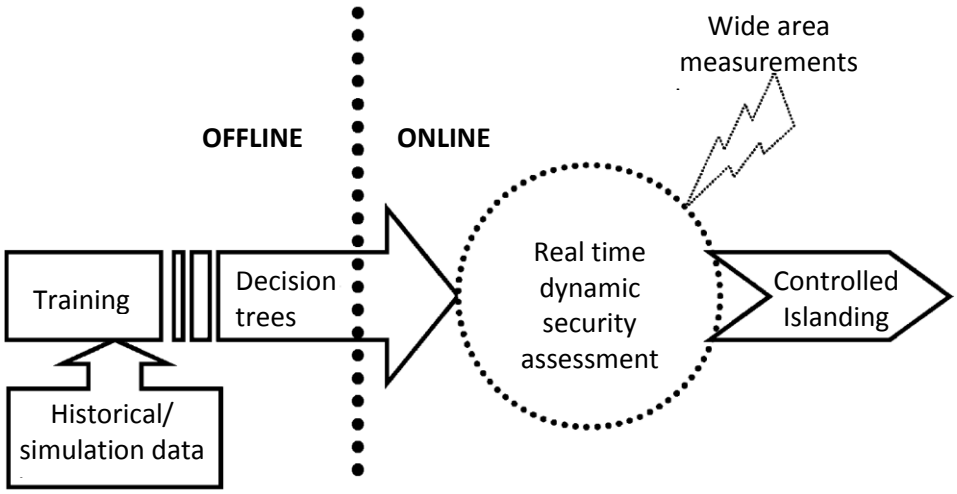

Figure 4.2: *DT-based controlled islanding strategy [7]*.

When the trained DT has been built from the current database at a given operating point, it has to be updated at certain time intervals to improve its prediction ability and adapt it to unknown and unforeseen cases [68]. The offline updated DT then can determine when to island by checking whether the predictive signals obtained from the online measurement of the wide-area PMU violate the threshold set in CSR. During the simulation process of training the DT, software, such as the Transient Security Assessment Tool has been used [7][68] to simulate issues in transient stability. Powerflow and Short-circuit Analysis have also been used [68] to help generate operating conditions.

The flowchart in Figure 4.3 shows how the DT-based method works in [68] regarding when to island in the entire controlled islanding scheme:

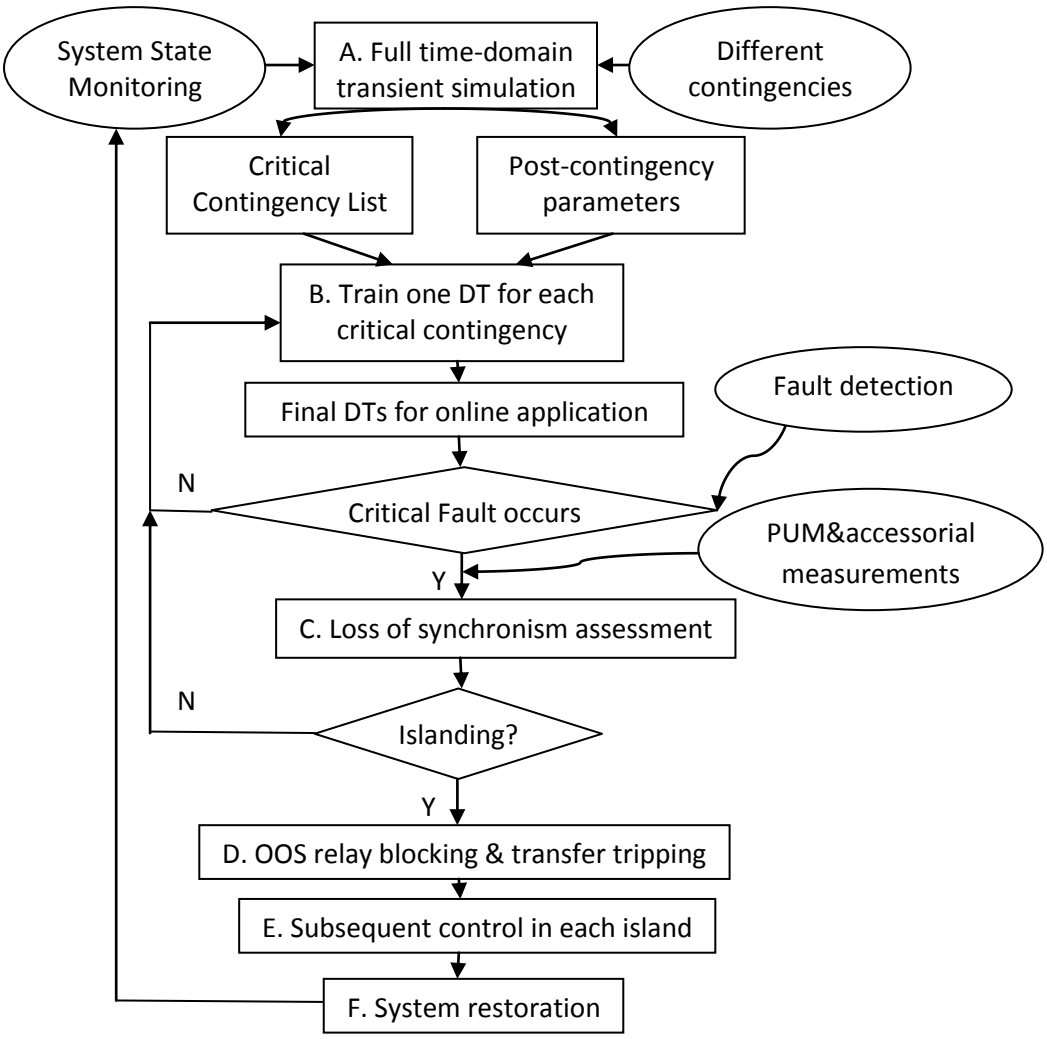

Figure 4.3: *Proposed DT-based controlled islanding scheme [68]*.

As shown in Figure 4.3, there are several stages in the DT-based controlled islanding scheme. In Stage A, several second contingencies under the N-1 credible operating condition are used to implement time-domain transient simulation and identify the critical contingency that may result in the loss of synchronism or cascading outages. In fact, because there are thousands of combinations of these contingencies, completing these simulations is time consuming. Moreover, some contingencies may have no effect to the system. Therefore, only contingencies in [68] that occurred on high voltage busbars and transmission lines will be selected for transient simulation. In Stage B, predictors will be selected to train the DTs. Because each of these critical contingencies leads to different instability problems, it is better to train one DT for each contingency in order to enhance accuracy and implement the controlled islanding scheme correctly. In Stage C, the final offline trained DTs are used in a real time operation, where a fault

detection that occurred in system will be checked to determine whether this contingency is on the critical contingency list. A correspondingly trained DT will be checked to determine whether the predictor signals received from PMU violate the threshold of CSR in this DT. If an unstable assessment is obtained from the output of the DT, then it will trigger the pre-designated out-of-step relays to separate the network into the pre-designed islands. In next three stages—D, E and F—a series of control actions will be undertaken to maintain the frequency and voltage stability in each island. After the disturbance effect is diminished or disappeared, the tripped transmission lines will reconnect the whole system based on the restoration procedure.

4.1.3 DT building procedure

In order to build the DT in a certain system, N-k contingency analysis used to build a database. The following four-step procedure is used to build a DT:

1. Implement an N-1 contingency analysis scan to check if the chosen system model satisfies the N-1 security criterion.

    - The first contingencies are set to be faults on each bus, and the faulted lines are tripped by protection in order to remove the fault.

    - Use the simulation results to check if any N-1 contingency cases will cause an out-of-step power swing.

2. Implement N-2 contingency analysis at the high voltage buses and find the second problematic contingency that will lead to out-of-step power swings in the system. Then add the critical contingencies to the list.

    - There will be an enormous number of combinations of these two contingencies. In practice, it is quite difficult to execute all these cases for transient simulations; consequently, this will increase the computation burden. Therefore, only high voltage lines are chosen for N-2 contingency analysis because they carry higher power flow, and its loss may lead to a critical and serious impact on the power system.

- In real power systems, the simultaneous occurrence of two line contingencies is very rare under the N-1 operating condition. Normally, these contingencies happen incrementally. Therefore, the N-2 line contingency is set accordingly. First, the first line with a fault is tripped before the time-domain simulation. The power flow is then re-dispatched to represent a new operating condition. Next, another fault is added on the second line, which should be tripped after three cycles. Finally, the time-domain simulation is conducted to check whether the system is stable after the two line contingencies.

3. A database could be built based on the simulation results of all listed critical contingencies occurring in different cases, including different operating conditions, different sequences of occurrence of two contingency lines, different fault locations on lines and so forth.

- In order to obtain DTs that are correct and robust, a large number of simulation cases are required following the critical contingencies.

- The operating conditions should be provided by the system operators to represent the lowest and highest load levels during each month. In addition, the provided load levels should be changed within +/- 10% of the original value to obtain more operating conditions without changing the network's topology and component status. Therefore, different power flows in the system could be obtained based on these operating conditions, which represent a system in different steady states.

- Based on the results ("secure" or "insecure") obtained from the time-domain simulation, the post-contingency phase angles are collected in six-cycle-time after the line contingency. Angular velocity and angular acceleration are calculated and recorded as predictors in order to build the database.

4. Find the CSRs from the database form and obtained DT.

- Each predictor chosen could potential become one CSR. Many CSRs could have the same performance in predicting the out-of-step power swings occurring in the network.

- There will be a large number of predictors because there are six predictive signals on each high voltage bus, including voltage phase angle, phase angular speed, phase angular acceleration, voltage magnitude, magnitude change velocity and magnitude change acceleration.

4.1.4 Case study of building a DT in a 14-busbar system

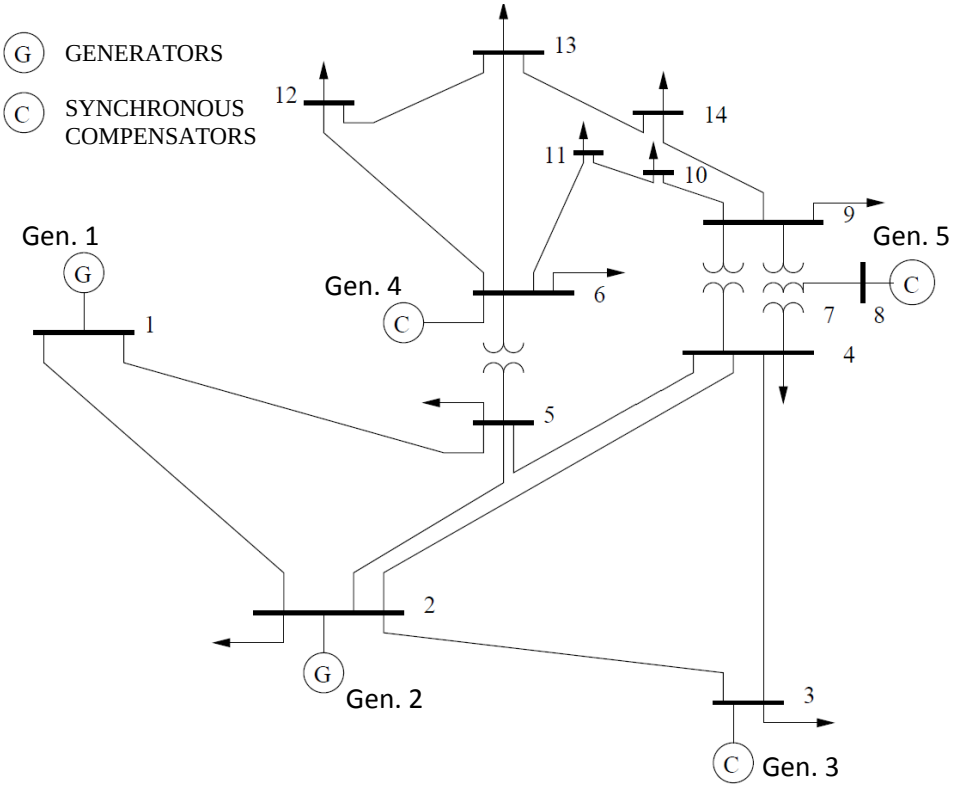

Figure 4.4: *IEEE 14-busbar system [69]*.

In this case study of offline DT training, an IEEE 14-busbar system (Figure 4.4) is built using the MATLAB-based Power System Assessment Tool (PSAT). Finally, the cases of N-3 critical contingencies that lead to out-of-step power swings after running the time-domain simulation are identified. The data collection is then initiated. Further transient cases should be implemented in order to train DT correctly and robustly. This could be obtained through changing the sequences of the line contingencies, creating more operating conditions by changing the load levels at the +/- 10% range of their original values without changing the network topology. Possible predictors in the 14-busbar system are the voltage phase angle, voltage magnitude change velocity and acceleration at each high voltage bus, which are shown in Table 4.1:

Table 4.1: *Database created in 14-busbar system for building DT.*

Stable (S) or Unstable (U)	**U (Line 1-2,1-5,2-3)**	S (Line 1-2,2-3,1-5)	S (Line 2-3,1-5,1-2)	**U(Line 2-3,2-4,4-5)**	S (Line 2-3,4-5,2-4)	**U (Line 2-4,4-5,2-3)**
Bus1-Angle 1	**1.7223**	0.25951	0.30463	**9.3459**	11.112	**10.456**
Bus1-Angle 2	**2.0935**	0.78217	0.83710	**12.883**	13.472	**12.651**
Bus1-Angle 3	**2.2304**	1.6870	1.7647	**17.946**	19.019	**17.451**
Bus1-V1	**3.7115**	5.2266	5.3247	**35.370**	23.601	**21.951**
Bus1-V2	**1.3693**	9.0484	9.2757	**50.636**	55.465	**48.004**
Bus1-a0	**-23.442**	38.218	39.510	**152.65**	318.64	**260.53**
Bus2-Angle 1	**-96.958**	-14.609	-17.150	**8.2742**	10.803	**9.6135**
Bus2-Angle 2	**-117.85**	-44.033	-47.125	**11.578**	12.146	**10.978**
Bus2-Angle 3	**-125.56**	-94.971	-99.344	**16.562**	17.528	**15.563**
Bus2-V1	**-208.94**	-294.23	-299.76	**33.033**	13.427	**13.646**
Bus2-V2	**-77.089**	-509.39	-522.18	**49.845**	53.825	**45.845**
Bus2-a0	**1318.5**	-2151.5	-2224.3	**168.12**	403.98	**322.00**
Bus3-Angle 1	**-126.29**	-27.517	-37.340	**-46.344**	-47.266	**-36.174**
Bus3-Angle 2	**-152.74**	-53.434	-58.772	**-68.719**	-69.999	**-59.384**
Bus3-Angle 3	**-169.44**	-101.43	-104.32	**-91.069**	-102.06	**-88.812**
Bus3-V1	**-264.46**	-259.18	-214.32	**-223.76**	-227.33	**-232.10**
Bus3-V2	**166.97**	-479.97	-455.50	**-223.50**	-320.64	**-294.28**
Bus3-a0	**4314.3**	-2207.9	-2411.7	**2.6120**	-933.09	**-621.79**
Bus4-Angle 1	**-115.52**	-21.654	-28.145	**-41.502**	-43.053	**-35.907**
Bus4-Angle 2	**-137.17**	-50.208	-54.165	**-61.041**	-63.021	**-54.280**
Bus4-Angle 3	**-148.75**	-100.22	-103.67	**-80.734**	-91.578	**-78.784**
Bus4-V1	**-216.49**	-286.29	-260.20	**-195.39**	-199.69	**-183.73**
Bus4-V2	**-115.80**	-500.10	-495.04	**-196.93**	-285.57	**-245.04**
Bus4-a0	**1006.9**	-2138.1	-2348.4	**-15.438**	-858.82	**-613.12**
Bus5-Angle 1	**-113.78**	-20.611	-26.727	**2.1148**	3.0852	**2.4102**
Bus5-Angle 2	**-134.97**	-49.474	-53.275	**3.5694**	4.0247	**3.4101**
Bus5-Angle 3	**-145.97**	-99.684	-103.20	**8.3016**	9.8201	**7.8399**
Bus5-V1	**-211.87**	-288.63	-265.49	**14.545**	9.3954	**9.9991**
Bus5-V2	**-110.04**	-502.09	-499.24	**47.322**	57.954	**44.298**
Bus5-a0	**1018.3**	-2134.6	-2337.6	**327.77**	485.58	**342.99**

Assume that line contingencies occur on high-voltage buses. In the six cases, three cases result in unstable systems, which are shown in the simple database provided in Table 4.1. After the comparison and analysis of these data, the results shown that a few predictors were able to be CSRs. Simply, in this case, a single CSR is enough to predict the system results ("stable" or "unstable"). These include Bus3-V2>-320, Bus3-a0>-930, Bus4-V2>-280 and Bus4-a0>-850. For instance, the first CSR is used to build the DT shown in Figure 4.5:

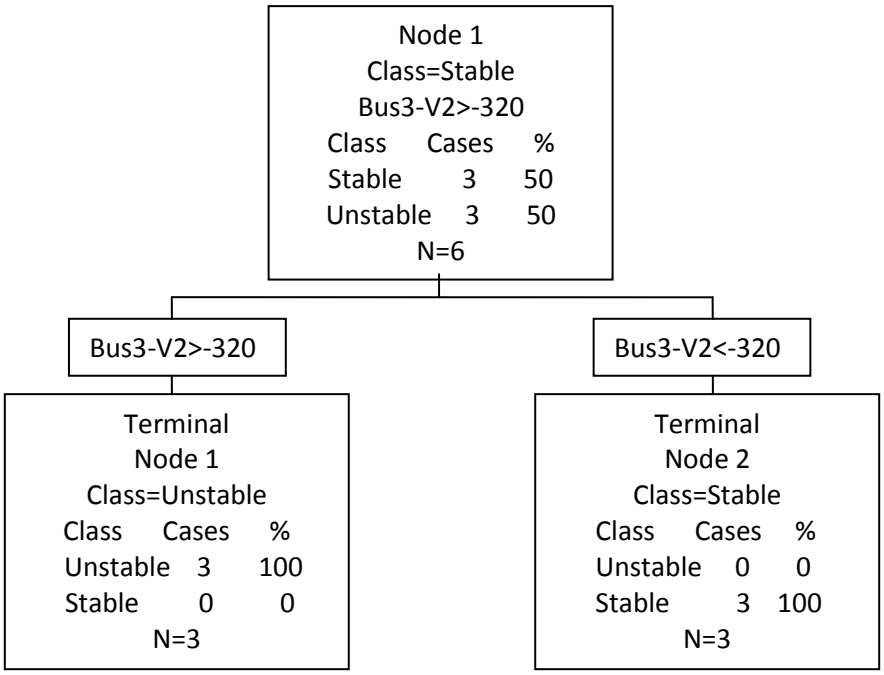

Figure 4.5: *Decision Tree for 14-busbar system.*

When the DT is built, the question regarding when to island can be decided if the CSR is violated. However, this trained DT mainly considers the loss of synchronism in the generators. Because we know that cascading outage is the main reason for blackouts, the offline trained DT could be adapted online during cascading outages. When the critical line is tripped, the DT could identify the point of no return in the system network and indicate whether the islanding scheme should be tripped before it is too late. However, this method can only be applied to particular systems in which the DT is trained based on the simulation data coming from this system. In addition, the DT has to be trained offline periodically because of the change in network topology in order to improve the robustness of DT.

4.1.5 Cascading propagation research

Because of the cascading outage, the case of the US/Canada blackout in 2003 was a typical blackout that resulted in the tripping of hundreds of transmission lines and generators during cascading outages before the blackout occurred. Therefore, one question is raised, which concerns whether the extent of this cascading propagation in real time could be estimated correctly. This cascading propagation may die out or lead to blackouts. If this information could be obtained, it would be very helpful in deciding

if and when the controlled islanding scheme should be implemented. In fact, this estimation research method was previously proposed [9][70][71] as a statistical estimator to measure the extent of propagation in cascading failures. In [70] a mathematical model of branching processes was developed to represent the behaviours of cascading failures. The parameter λ^* stands for the measured cascading propagation factor, which helps to analyse the likelihood of cascading blackouts. It was adapted into the branching processed model by using prior data on simulated blackouts. A probability density function of blackout size could then be generated from the model as well as the estimator. The estimator also represents the cascading rate of generators and transmission lines during cascade failures. The meaning of λ^* is explained in Figure 4.6:

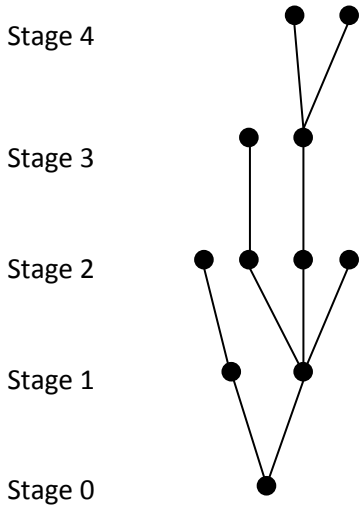

Figure 4.6: *Failures produced at stages modelled by branching processes [71].*

During the cascading process, each failure has an independent, random number of offspring; λ^* is used to represent the ratio of total number of child failures in the current stage over the total number of parent failures in a previous stage. Therefore, λ^* could determine the extent of the failure propagation. If $\lambda^*<1$, cascading failures would disappear; If $\lambda^*>1$, cascading failures would proceed to system size. This mathematically obtained signal could also be a precursor to possible imminent blackouts in the controlled islanding scheme.

The details of modelling and computation of this cascading propagation processes are described in [9][70][71]. The difference is the modelling of the chosen cascading failures, because not all elements that the affect power grid are included in each model.

Each model then predicts the behaviour of power system in cascading failures. The elements considered in each model are shown in Table 4.2:

Table 4.2: *Model details in cascading simulation [71]*

	OPA	failure	Manchester	CMU	PSA	TRELESS
overloads	X	X	X	X	X	X
generator redispatch	X	X	X		X	X
hidden failure		X		X		
protection group						X
AC network		X	X			X
generator trip						X
voltage collapse			X			X
transient stability			X			
under frequency load shed			X			X
islanding	X		X			X
operator response			X		X	X
blackout time intervals&repair					X	
load increase&grid upgrade	X					
approx. max number of buses	400	300	1000	2500	?	13000

Using probability theory, this mathematical method is based on data on previous blackouts, which are used to decide if the cascading failures will propagate. However, it is still risky in real-time operation and may lead to false dismissals or false alarms.

4.2 Where to Island?

The issue regarding where to island has been widely investigated. As mentioned in Chapter 1, several methods have been applied to answer this question, such as the ordered binary decision diagram (OBDD) method, the spectral partitioning method and the slow coherency method. These three islanding methods are explained in the following subsections.

4.2.1 OBDD methods

OBDD methods provide a splitting technique on a node-weighted graph model to decide proper islanding points (or which lines should be tripped) to form the separated islands. These islands satisfy the acceptable steady-state operating points after islanding, such as

generation/load balance and transmission line thermal limits. However, no transient dynamics exist after the system is split. In addition, this method could become a NP-hard issue in a large and complex system network. In [17], a two-phase method based on OBDD was proposed. It aimed to narrow all feasible islanding solutions. In the first phase, the power system network was transformed to a node-weighted graph model, which ignored all irrelevant power system information but kept the network topology and generators or loads. The islanding solution then was obtained by using a highly efficient OBDD-based algorithm to satisfy the power balance and synchronization constraint in the formed islands. In the second phase, a power flow analysis was conducted in the formed islands to determine whether they satisfied the transmission capacity constraints and to exclude islanding solutions that violated the constraints. However, based on this method, the formed islands could not reach the expected steady-state operating point without considering the dynamic period during islanding. In [16], another OBDD method was proposed, which adopted method in [17] to develop a three-phase based method. Compared with [17], the difference in [16] is that the proposed method simplified the original complex network to achieve a more manageable network, which could accelerate the searching process and reduce the search range for the second and third phase to continue discarding a greater number of islanding solutions that obtained in the first phase. The result of the first phase was remarkable and efficient, especially in a large power system network. The remaining two phases were the same as described in [17], which are based on the three constraints of synchronisation constraint, power balance and transmission thermal limit.

In [18], the OBDD-based method was further developed in an islanding application by considering the transient stability constraint between the steady-state operating conditions. The islands formed in [16][17] were only assumed to exist. In order to assess the transient stability during islanding, threshold value constraint (TVC) was introduced to restrict the degree of transient instability caused by islanding because islanding itself is a disturbance in the system. This TVC is set up offline based on the analysis of the power flow disruption in all feasible islanding solutions obtained in [16][17]. It excluded transiently unstable islands with power flow disruption above TVC.

In other words, transient stability assessment using the OBDD-based method is based on power flow disruption. It is chosen based on two general principles. One is that

different obtained islanding strategies could result in different power flow disruptions. The other one is that the power system's robustness could withstand small disturbances and maintain transient stability in the formed islands. However, the drawback of this approach is that the TVC selected offline can only be trained and used in a particular system rather than a general tool for every power system. In addition, it has to be updated according to changes in the power system network. In order to increase its efficiency and practicality in searching for islanding strategies, in [72] more aspects of the OBDD-based controlled islanding method were considered to affect the islanding solution and more techniques were involved. First, grid loss was taken into account to modify the method by using the zero-weight-sum graph model. The network partitioning and parallel processing were then introduced to search for feasible islanding solutions in all subnetworks. Finally, TVC was also adopted in this modified OBDD-based method.

4.2.2 Spectral partitioning methods

In [19]-[23], graph theory-based spectral partitioning was also applied to the power system islanding issue. In [19], spectral graph theory was used to identify transmission lines that result in the formation of islands, which could also deal with cascading outages. Compared with other methods, spectral graph theory requires only computation. In addition, it can be applied in a large-scale power system network. Spectral graph theory allows the deduction of the structure of a graph from its graph spectrum. The spectrum of a graph is a set of eigenvalues that are associated with a number of matrices to represent the graph. The spectrum of different matrices contain information about the power system regarding connectivity, sizing and the degree of nodes. In [19], a separator was computed from the eigenvector components to employ global information about the graph. A partitioning could be executed by consecutively obtaining the bi-sectioning of a graph. In [21], a two-stage islanding method based on spectral graph theory was proposed. The first stage aimed to find sub-networks offline based on spectral graph theory. Spectral graph partitioning was used to identify the set of edges that divided the graph into two or more pieces. The graph was broken up by the constraints based on the number of edges and weights. In the second stage, frequency-load control actions were adopted to maintain stable operating condition in each island by using under-frequency load shedding (UFLS). Whenever the frequency in the formed

islanding was below a pre-determined threshold value and maintained for a while, then UFLS was activated to bring the system back above the threshold value. In [22][23], a two-step spectral clustering islanding method was proposed based on graph partition. However, there were more dynamic assessment elements in this method because power flow disruption and generator coherency were included to modify graph weights, which narrowed down the subspace solution. Spectral clustering was then applied to find the islanding solution. The first step aimed to determine the coherency generator group. It constructed a dynamic graph with generator nodes. Normalized spectral clustering was then applied to this graph to cluster the generator nodes based on their dynamic coupling. Instead of identifying the coherency generators, the key challenge in this method was to combine and satisfy the constraints to enforce the coherent generator groups during islanding by using k-medoids in clustering the generator nodes. In the second step, minimum power flow disruption was used as the objective function to split the network while the coherent generator groups were preserved. This was done by first constructing a static graph of all nodes. Based on this two-step islanding algorithm, an optimal solution to islanding was obtained.

4.2.3 Slow coherency methods

Among these three methods, slow coherency [73]-[76] is commonly used and widely studied. The method is used to identify the coherent generator groups in the power system. The splitting boundary can then be obtained based on areas where the coherent generator groups are located. The coherent generators can be identified as follows: observation of the generator angle, phase angle measurement and model analysis. In particular, modal analysis is used in slow coherency research. The advantage of modal analysis is that the calculation results of the eigenvalue analysis can be speedily obtained. However, it can only be applied to a small disturbance in a certain power system operating condition, not to various disturbances under different load conditions. When the coherency generator groups are identified, the next step is to search for optimized cutsets to split the whole system network into several islands based on the obtained coherent generator groups. Therefore, the second step involved in the slow coherency method is an optimization problem. The objectives of determining optimized the islanding cutsets could be either the minimal generation-load imbalance or the minimal generation-load disruption. Thus, the slow coherency-based controlled

islanding scheme, which is used to decide where to island in the procedure, is described as follows:

- Step 1: Identification of coherency generator groups using modal analysis
- Step 2: Identification of splitting boundary in coherency generator areas using graph theory, such as the K-means technique, K-way partitioning and minimal cut set with minimum net flow

Slow coherency is based on the observation of the oscillations in large-scale power systems. Oscillation in power systems can be classified into two categories. One is the local mode with frequencies ranging between 1 Hz and 3 Hz. The other one is the inter-area mode with frequencies less than 1 Hz. When fast local dynamics under a disturbance finish decaying, the generators in the same area swing together again with those in the other area, so they are coherent with respect to the slow modes. Slow coherency can group generators based on their participation in the selected inter-area modes of oscillation. In [76], the dynamic reduction program (DYNRED) in the Power System Analysis Package (PSAPAC) was used to determine the slow-coherency groups of generators based on eigenvalue analysis. Therefore, this method is based on model analysis. However, there are two assumptions in using the slow coherency method, which are explained as follows:

- The slow coherency method is used to determine whether coherent groups of generators are based on a linearized model of the system network. Therefore, the formed coherent generators are independent of the fault location and disturbance severity.
- The coherency groups of generators are obtained based on classical generator modelling.

Therefore, the dynamic characteristics in the power system, especially during cascading outages, may not be considered in the islanding scheme.

4.3 Summary

This chapter reviews the previous research on the controlled islanding scheme regarding when to island and where to island. However, no previous research has conducted a dynamic analysis after islanding in each island. Regarding when to island, DT has been used in controlled islanding scheme to solve this issue. The DT technique is a computing tool that can be applied in every field. In power systems, DT is trained offline to build a database according to the requirements of a specific power system. The aim is to find all system collapse scenarios and then collect information from these blackout scenarios in order to find a rule that indicates cases that may happen again in the future. When the same case happens again in the real system, the DT matches it in the built database and compares the required data with the rule identified in training the DT in order to tell the system operator whether the system will lead to blackouts. However, the DT technique is time consuming offline because it requires a large number of offline simulations and computations under different operating condition and different disturbances, including different contingencies, contingency orders, combinations and contingency locations. In addition, it is trained for a specific system and can only be applied in that system. In a real power system, this DT might have to be updated every time the system configuration changes because the distribution generation penetrates the system. In addition to the DT method, the cascading propagation research was also reviewed to determine whether cascading outage could spread using probability analysis based on historical data, which is used to build the model. However, in real power systems, probability analysis is still quite risky in online application.

Regarding where to island, three different methods were reviewed according to their application to the controlled islanding scheme, including OBDD, spectral partitioning and slow coherency. These three methods yielded insight into the criteria that should be used to split the whole network. These criteria or constraints could be generator synchronism, transmission thermal capacity or the power balance in the formed islands. However, based on these constraints, a larger system usually is split into many pieces. Some pieces may not need to be isolated from the others. In a real power system, if faults or cascading outages happen, normally the sick area is isolated in order to prevent

the cascading outages from spreading to the healthy area. In addition, when used to find islanding strategies, these methods only consider the static system model before and after contingencies or a small-signal system model. This might lead to an invalid islanding solution if a severe disturbance happens, such as cascading outages. Based on the insights provided by the previous research regarding when to island and where to island, this thesis aims to use novel methods to improve and enhance the feasibility of the controlled islanding scheme. In the three-stage controlled islanding scheme proposed in this thesis, power flow tracing will be adopted to solve the issue of where to island, and SIME will be used to solve the issue of when to island in transient stability and assess whether the formed islands are transiently stable after islanding. The following chapters will discuss these aspects in detail.

Chapter 5:

Power Flow Tracing

Since the formation of the decentralized electricity market, generation, transmission and energy suppliers have been unbundled by suppliers, who run their own businesses in transporting electricity from generators to area suppliers. However, in this vertically integrated system, there is little incentive for each electricity sector to reduce the power losses in the network. Consequently, the cost of these losses is charged to the end users. Under these circumstances, a power flow tracing algorithm [77]-[81] was originally designed as an economic tool and used to charge energy suppliers and generators for their own contribution to the losses. For instance, if a power plant were built in a remote location, there would be large number of losses on the transmission path to the network because of the distance. Power flow tracing is proposed as an approach to clarify the contribution of losses to each electricity sector and motivate all parties to perform efficiently or be penalized. Power flow tracing was developed in [28][29]. It aims to trace the flow of electricity in the power system from the generators to all loads in order to determine the amount of power produced by each generator to each load. In this chapter, we will review the power flow tracing method, which is used in the three-stage controlled islanding scheme to decide where to island. It is also applied in the controlled islanding scheme proposed in this thesis. In this application, it mainly attempts to find the boundary around the source of the disturbance, which is weakly connected between the sick and healthy islands. Only the sick part of network is cut out, leaving the remaining healthy network running.

5.1 Proportional Sharing Principle

The main principle used in the power flow tracing method is proportional sharing in a meshed network to determine how the power flow is distributed. It is based on the fact

that the outflows from a bus share the same proportional inflows to that bus. The only requirement for the input data is that the solution of Kirchhoff's current law must be satisfied for all the nodes in the network. Kirchhoff's voltage law is taken into account because the power flows are taken from the state estimator, or they are calculated using a power flow algorithm. Figure 5.1 provides an example of how this proportional sharing principle works.

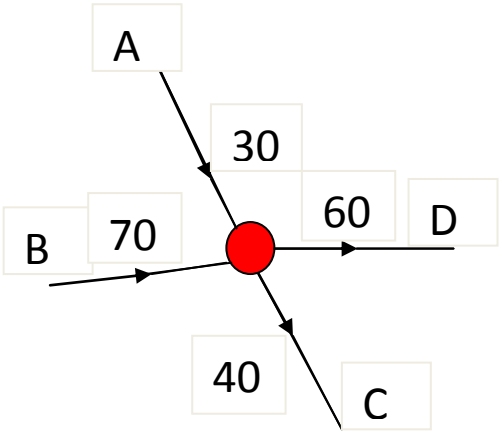

Figure 5.1: *Proportional sharing principle.*

In Figure 5.1, there are two inflows from A and B, and there are two outflows to C and D. The total inflow going to the node from A and B combined is 100 MW (30 MW + 70 MW). In the inflows coming to the bus, 30% of 100 MW comes from A and 70% of 100 MW comes from B, based on the assumption that each MW leaving the node to the outflow contains the same proportion of the inflows from the total flow into that node. Therefore, the 60 MW outflow going to D consists of 18 MW (60 MW x 30%) supplied from A and 42 MW (60 MW x 70%) supplied from B. Similarly, the 40 MW outflow going to C consists of 12 MW (40 MW x 30%) supplied from A and 28 MW (40 MW x 70%). Based on this basic proportional sharing principle, we can determine exactly how much power inflow is distributed into the outflows. However, this proportional sharing principle can neither be proved nor disproved although it can be rationalised [78]-[81]. The algorithm for power flow tracing can be divided into two categories: the downstream-looking algorithm, which looks at the nodal balance from the point of view of the outflow; the upstream-looking algorithm, which looks at nodal balance from the point of view of inflow. In the following section, these two algorithms will be explained based on a lossless network in terms of real power flow.

5.2 Tracing Methodology

5.2.1 Upstream-looking algorithm

The total inflow power P_i going through node i can be expressed as follows [78]:

$$P_i = \sum_{j \in \alpha_i^{(u)}} \left| P_{i-j} \right| + P_{Gi} \;\; ; \; i = 1, 2, \ldots, n \tag{5.1}$$

where $\alpha_i^{(u)}$ is the set of nodes supplied directly from node i via the relevant lines; P_{i-j} is the line inflow into node i in line $i-j$; and P_{Gi} is the generation at node i. Because we ignore power losses, $\left|P_{i-j}\right| = \left|P_{j-i}\right|$ can be obtained. Therefore, the line power flow in line $i-j$ can be related to nodal flow at node j by substituting $\left|P_{i-j}\right| = c_{ji} P_j$. Equation (5.1) can be derived as

$$P_i - \sum_{j \in \alpha_i^{(u)}} c_{ji} P_j = P_{Gi} \tag{5.2}$$

Where, $c_{ji} = \left|P_{j-i}\right| / P_j$. If we rearrange (5.2), then we have

$$P_i - \sum_{j \in \alpha_i^{(u)}} c_{ji} P_j = P_{Gi} \quad \text{or} \quad A_u P = P_G \tag{5.3}$$

where $\boldsymbol{A_u}$ is the (n x n) upstream distribution matrix; $\mathbf{P}$ is the vector of nodal through-flows; and $\mathbf{P_G}$ is the vector of nodal generations. The element (i, j) in matrix $\boldsymbol{A_u}$ can be shown as

$$\left[A_u\right]_{ij} = \begin{cases} 1 & for \quad i = j \\ -c_{ji} = -\left|P_{j-i}\right| / P_i & for \quad j \in \alpha_i^{(u)} \\ 0 & otherwise \end{cases} \tag{5.4}$$

$\boldsymbol{A_u}$ is sparse and nonsymmetric. If A_u^{-1} exists, then $P = A_u^{-1} P_G$ and its i th element is shown as

$$P_i = \sum_{k=1}^{n} [A_u^{-1}]_{ik} P_{Gk} \qquad for \quad i = 1, 2, \ldots, n \tag{5.5}$$

Equation (5.5) shows the power flow contribution from the *k*th system generator to the *i*th nodal power; P_i consists of two parts, one is load demand P_{Li} on node *i* and the other is the outflows in the lines leaving node *i*. Therefore, the pure line outflow in line $i-l$ from node *i* can be calculated based on the proportional sharing principle as follows:

$$\left|P_{i-l}\right| = \frac{\left|P_{i-l}\right|}{P_i} P_i = \frac{\left|P_{i-l}\right|}{P_i} \sum_{k=1}^{n} [A_u^{-1}]_{ik} P_{Gk} = \sum_{k=1}^{n} D_{i-l,k}^{G} P_{Gk} \qquad for \quad all \quad l \in \alpha_i^{(d)} \tag{5.6}$$

where $D_{i-l,k}^{G} = \left|P_{i-l}\right| [A_u^{-1}]_{ik} / P_i$ and $\alpha_i^{(d)}$ is the set of nodes supplied directly from node *i*. Similarly, the load demand P_{Li} can be calculated from P_i in (5.5) as

$$P_{Li} = \frac{P_{Li}}{P_i} P_i = \frac{P_{Li}}{P_i} \sum_{k=1}^{n} [A_u^{-1}]_{ik} P_{Gk} \qquad for \quad i = 1, 2, ..., n \tag{5.7}$$

Equation (5.7) shows the power flow contribution from the *k*th generator to the *i*th load demand. It can be used to trace the origin of the power flow of a specific load.

5.2.2 Downstream-looking algorithm

The mathematical modelling of the downstream-looking algorithm is similar to upstream-looking algorithm. The only difference is that the downstream-looking algorithm considers outflow on the nodal power, which includes load demand instead of generation, as in the upstream-looking algorithm. In the downstream-looking algorithm, the sum of outflows P_i on a node can be expressed as

$$P_i = \sum_{l \in \alpha_i^{(d)}} \left|P_{i-l}\right| + P_{Li} = \sum_{l \in \alpha_i^{(d)}} c_{li} P_l + P_{Li}; \quad i = 1, 2, \ldots, n \tag{5.8}$$

where $\alpha_i^{(d)}$ is the set of nodes supplied directly from node *i* via relevant lines, and $c_{li} = \left|P_{l-i}\right| / P_l$. Equation (5.8) can also be rewritten in terms of load demand as

$$P_i - \sum_{l \in \alpha_i^{(u)}} c_{li} P_l = P_{Li} \quad \text{or} \quad A_d P = P_L \tag{5.9}$$

where $\boldsymbol{A_d}$ is the (*n* x *n*) downstream distribution matrix, and $\boldsymbol{P_L}$ is the vector of nodal demand. The (*i*, *l*) element in $\boldsymbol{A_d}$ can be shown as

$$[A_d]_{il} = \begin{cases} 1 & for \quad i = l \\ -c_{li} = -|P_{l-i}| / P_l & for \quad l \in \alpha_i^{(d)} \\ 0 & otherwise \end{cases} \tag{5.10}$$

where $\boldsymbol{A_d}$ is like $\boldsymbol{A_u}$ and is also sparse and nonsymmetric. However, adding $\boldsymbol{A_d}$ and $\boldsymbol{A_u}$ gives a symmetric matrix. If A_d^{-1} exists, then $P = A_d^{-1} P_L$ and its *i*th element can be shown as

$$P_i = \sum_{k=1}^{n} [A_d^{-1}]_{ik} P_{Lk} \qquad for \quad i = 1, 2, ..., n \tag{5.11}$$

Equation (5.11) shows how nodal power is distributed among the loads in the system. The nodal power here contains a generation at node *i* and all the inflows in lines going to node *i* . Therefore, the inflow into node *i* on line *i*-*j* can be expressed as

$$|P_{i-j}| = \frac{|P_{i-j}|}{P_i} P_i = \frac{|P_{i-j}|}{P_i} \sum_{k=1}^{n} [A_d^{-1}]_{ik} P_{Lk} = \sum_{k=1}^{n} D_{i-j,k}^{L} P_{Lk} \qquad for \quad all \quad j \in \alpha_i^{(u)} \tag{5.12}$$

where $D_{i-j,k}^{L} = |P_{i-j}| [A_d^{-1}]_{ik} / P_l$. Similarly, the output of the *i*th generator used to supply *k* th load demand can be expressed as (5.13), which can be used to determine the direction of the power from a particular generator:

$$P_{Gi} = \frac{P_{Gi}}{P_i} P_i = \frac{P_{Gi}}{P_i} \sum_{k=1}^{n} [A_d^{-1}]_{ik} P_{Lk} \qquad for \quad i = 1, 2, ..., n \tag{5.13}$$

By comparing (5.7) and (5.13), a simple relationship between A_d^{-1} and A_u^{-1} can be obtained through the ratio of the two equations:

$$\frac{[A_u^{-1}]_{ik}}{[A_d^{-1}]_{ki}} = \frac{P_i}{P_k} \tag{5.14}$$

In a lossless network, it is enough to trace power flow among generation, load demand and transmission lines and to determine how the power flow comes and goes by using either A_d^{-1} or A_u^{-1}. Next, we will demonstrate this downstream-looking algorithm in the simple system shown in Figure 5.2:

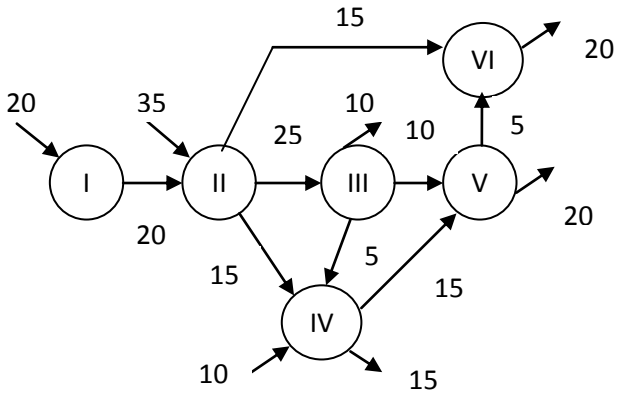

Figure 5.2: *Tracing example in a 6-busbar network [29]*.

Based on this six-bus network, (5.9) can be formed as:

$$\begin{bmatrix} 1 & -20/55 & 0 & 0 & 0 & 0 \\ 0 & 1 & -25/25 & -15/30 & 0 & -15/20 \\ 0 & 0 & 1 & -5/30 & -10/25 & 0 \\ 0 & 0 & 0 & 1 & -15/25 & 0 \\ 0 & 0 & 0 & 0 & 1 & -5/20 \\ 0 & 0 & 0 & 0 & 0 & 1 \end{bmatrix} \begin{bmatrix} P_1 \\ P_2 \\ P_3 \\ P_4 \\ P_5 \\ P_6 \end{bmatrix} = \begin{bmatrix} 0 \\ 0 \\ 10 \\ 15 \\ 20 \\ 20 \end{bmatrix}$$

Based on the above downstream distribution matrix on the left of the equation, it is easy to obtain the inversed tracing matrix A_d^{-1} as follows:

$$A_d^{-1} = \begin{bmatrix} 1 & 0.3636 & 0.3636 & 0.2424 & 0.2909 & 0.3455 \\ 0 & 1 & 1 & 0.6667 & 0.8 & 0.95 \\ 0 & 0 & 1 & 0.1667 & 0.5 & 0.125 \\ 0 & 0 & 0 & 1 & 0.6 & 0.15 \\ 0 & 0 & 0 & 0 & 1 & 0.25 \\ 0 & 0 & 0 & 0 & 0 & 1 \end{bmatrix}$$

When the tracing matrix A_d^{-1} is obtained, then based on (5.13), we can determine how much power is produced by the generator to contribute to the load demand. For example, the generation with 20 on node 1 contributes to load demand on node 3 with 3.636 (10 x 0.3636), on node 4 with 3.636 (15 x 0.2424), on node 5 with 5.818 (20 x 0.2909) and on node 6 with 6.91 (20 x 0.3455). The total amount on these nodes supplied by the

generator on node 1 is equal to the generation on node 1, which is 20 (3.636+3.636+5.818+6.91).

5.3 Application of Tracing in Controlled Islanding

This controlled islanding scheme is aimed to find the affected area boundaries that contain the disturbance, cut out the sick network and leave the remaining network running, which is demonstrated in Figure 5.3 [77]. In the tracing method, the source of disturbance is called the seed node. The disturbance in the network could be a line outage in cascading blackouts. Therefore, the seed node in this case consists of both nodes connecting the beginning and terminating point of that contingency line. The tracing method starts tracing power flow at the seed node. It tries to find weakly connected lines around the seed node where the power flow is relatively low. In other words, a relatively low power flow means a small contribution in terms of power flow between those two nodes. In the tracing method, the level of contribution is called the threshold value flow. If its contribution is less than the chosen threshold value, it is weakly connected. Hence, the tracing method provides an approach to reducing the scope of search for the islanding boundary by identifying the weakly connected lines around the seed node. Suitable measures, such as minimal power flow disruption or minimal power imbalance, will then be used to choose the best islanding strategy to use in deciding where to island.

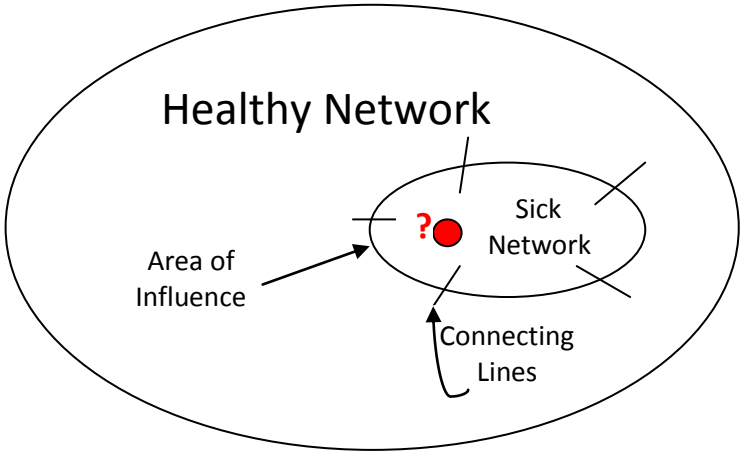

Figure 5.3: *Tracing method application in controlled islanding [77]*

In addition, in order to identify easily the weakly connected lines in tracing matrix A_d^{-1}, the unified p.u. value is required. For example, in the tracing matrix obtained in the 6-busbar system shown in Figure 5.4, the base value of each column *j* in tracing matrix A_d^{-1} is their nodal power P_j on node *j*. Therefore, we need to convert all p.u values based on the same base value. We choose 100 MW as the base value in the new p.u value system. The new converted tracing matrix T_d then can be done by first multiplying its nodal power P_j in A_d^{-1} and then dividing it by the new base value of 100 MW. Therefore, the tracing matrix T_d using the single unified base value is shown as follows:

$$T_d = \begin{bmatrix} 0.2 & 0.2 & 0.0909 & 0.0727 & 0.0727 & 0.0691 \\ 0 & 0.55 & 0.25 & 0.2 & 0.2 & 0.19 \\ 0 & 0 & 0.25 & 0.05 & 0.125 & 0.025 \\ 0 & 0 & 0 & 0.3 & 0.15 & 0.03 \\ 0 & 0 & 0 & 0 & 0.25 & 0.05 \\ 0 & 0 & 0 & 0 & 0 & 0.2 \end{bmatrix}$$

This new tracing matrix T_d will be used to find the islanding boundaries that form the islands. The objective is to let the strongly connected lines around the seed node stay in the sick island and then continue this iteration process from the identified adjacent strongly connected nodes as a new seed node until the weakly connected lines are found. These will be considered the boundaries that form the controlled islanding cutsets. The criterion used to decide if the connection is weak or strong is the threshold value. Next, we demonstrate the procedure of applying the tracing algorithm using the six-busbar system as the example. Figure 5.4 shows the tracing matrix in the first iteration of the tracing algorithm.

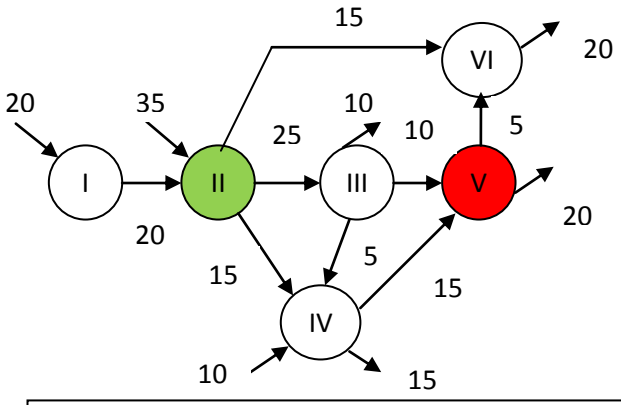

0.2	0.2	0.0909	0.0727	0.0727	0.0691
0	0.55	0.25	0.2	0.2	0.19
0	0	0.25	0.05	0.125	0.025
0	0	0	0.3	0.15	0.03
0	0	0	0	0.25	0.05
0	0	0	0	0	0.2

Figure 5.4: *Tracing method in first iteration based on seed node 5 [29]*

- Choose a seed node. In this case, it is node 5, which is shown in red in Figure 5.4.
- Set a threshold value of 0.2 p.u., which is arbitrary.
- Start from node 5 to downstream. Downstream trace the value equal to or larger than 0.2 p.u. in the tracing matrix by examining row 5 and column 5.
- One identified element of 0.2 is located in row 2 and column 5 and shown in green, which means that node 2 is strongly connected with node 5. Therefore, node 5 and node 2 should stay together in the formed islanding cut set.
- After the first iteration of the tracing algorithm, node 2 was found as the new seed node. It is shown in red in Figure 5.5.
- Start from node 2 to search for a value equal or larger than 0.2 p.u. in row 2 and column 2. Four elements in green and blue are provided in Figure 5.5.
- After the second iteration of the tracing algorithm, nodes 1, 3, 4, 5 were found to be strongly connected with node 2. The five nodes should stay in the sick island, leaving node 6 in the healthy sub-network.

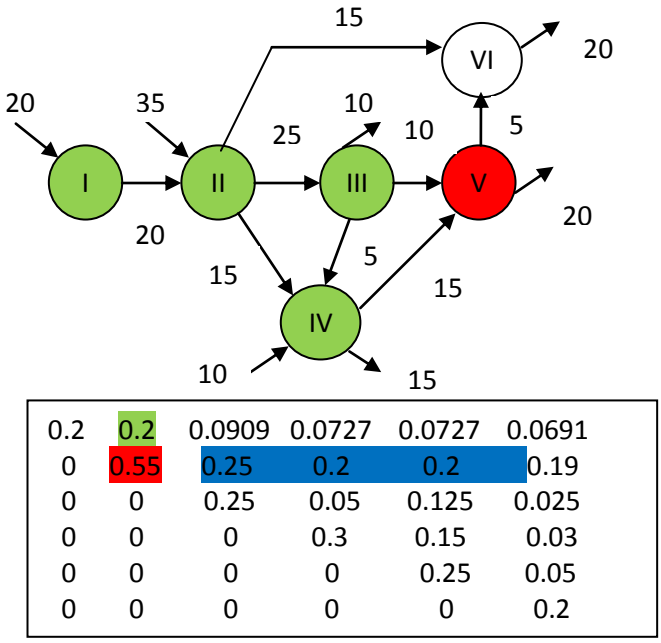

Figure 5.5: *Tracing method in second iteration based on newly identified seed node 2 [29].*

This simple 6-busbar system was used to demonstrate how the tracing method works in the application for islanding purposes. The iteration process in the tracing method should continue until no more nodes connect to the seed node, and the tracing matrix element is above the threshold value. Figure 5.6 illustrates the process of the tracing matrix algorithms which is applied in the 6-busbar system. In [25][26], it was shown that smaller threshold values increased the size of the sick island, while larger threshold values decreased the size of the sick island. Therefore, the tracing method highly depends on the selected threshold value, and different threshold values will provide different islanding cutsets. The selection of threshold values can be decided by the introduction of optimization objective for islanding scheme, which will be detailed in next section in this Chapter.

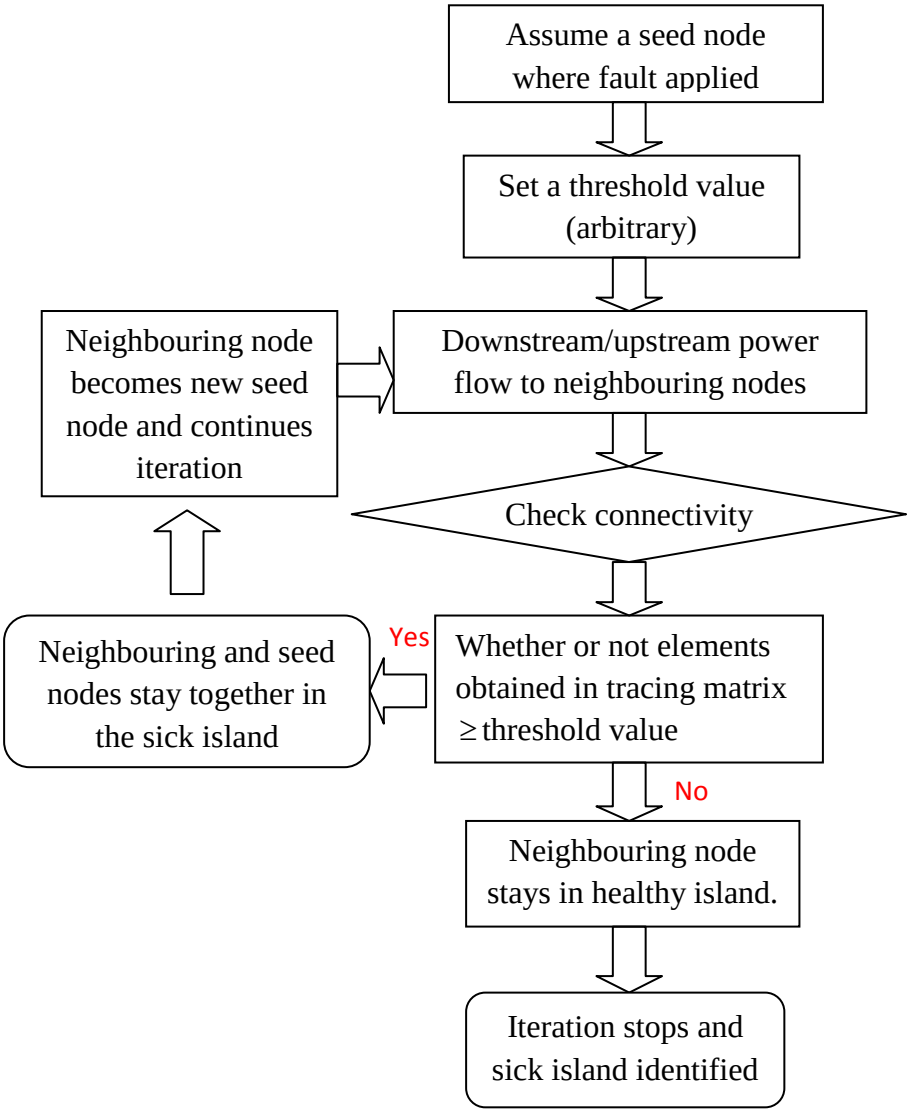

Figure 5.6: *The process of the tracing matrix algorithms which is applied in the 6-busbar system.*

Next, the IEEE 39-busbar system shown in Figure 5.7 is used to demonstrate the formation of useful islands. Power flow tracing starts from the seed node in bus 26, and a small threshold value is selected as 0.8 p.u. The tracing method continues the iteration procedure until all elements in the tracing matrix with updated seed nodes are smaller than 0.8 p.u.. Figure 5.7 shows that the identified sick island in green larger than the remaining healthy island. Because the green nodes in Figure 5.7 are strongly connected, they have to stay in the sick island to prevent the disturbance from spreading from seed node 26. This demonstrates that the smaller threshold value will isolate sick islands that are larger.

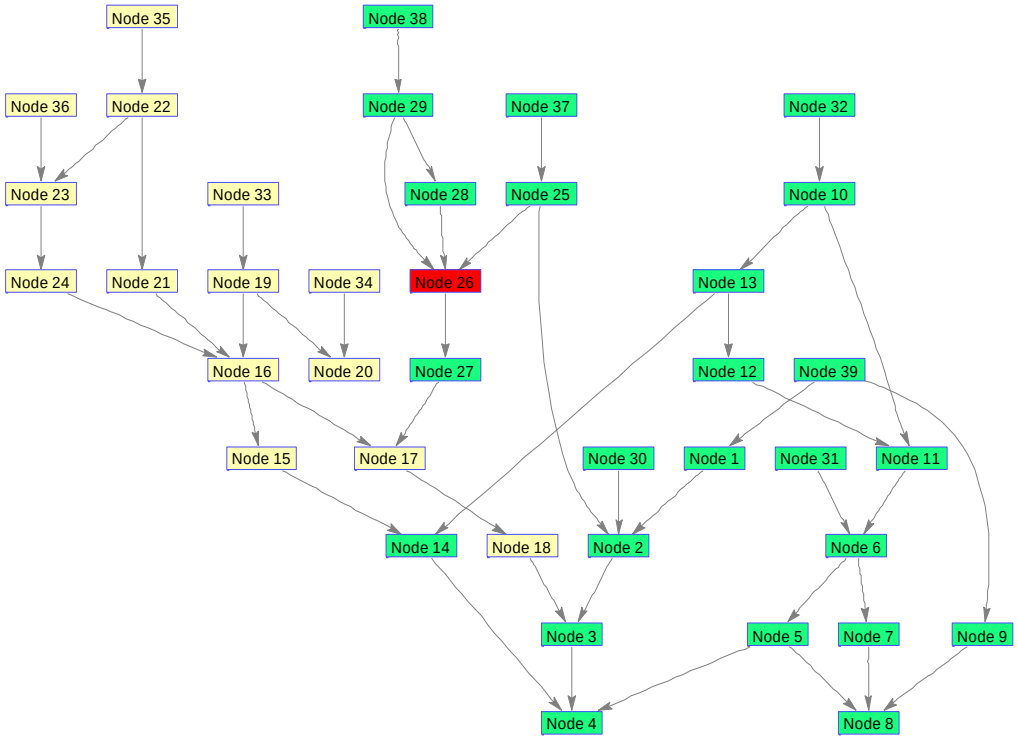

Figure 5.7: *Tracing example in 39-busbar system with seed node on bus 26 and with threshold value of 0.8 p.u. [29]*

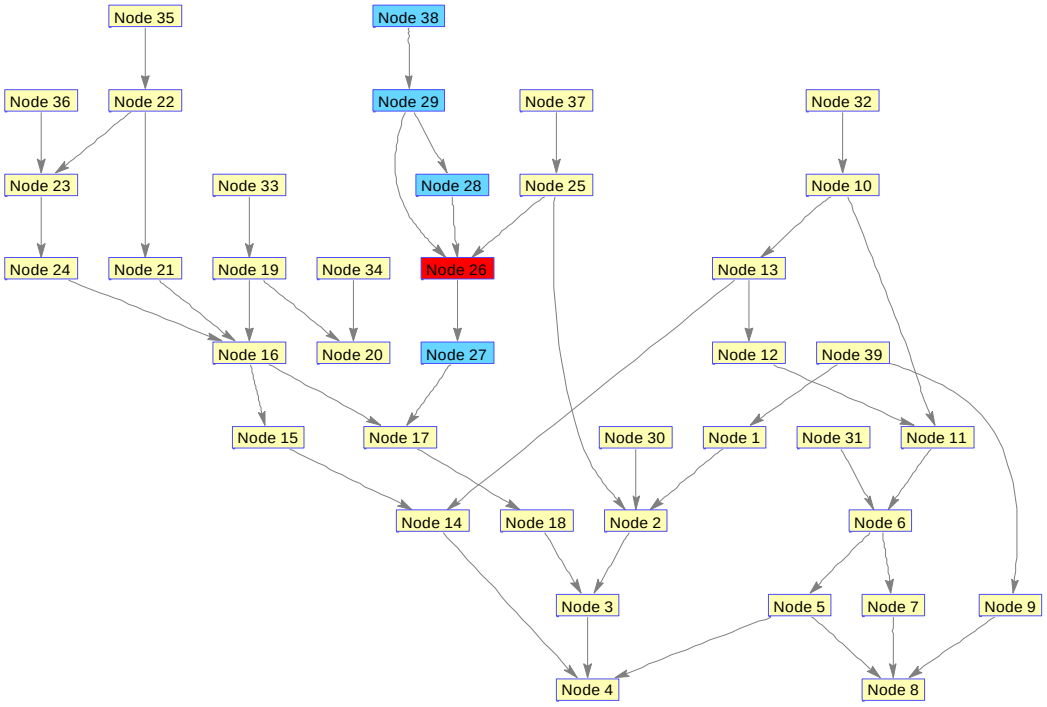

Figure 5.8: *Tracing example in 39-busbar system with seed node on bus 26 and with threshold value of 1.6 p.u. [29]*

We then chose a different threshold value of 1.6 p.u. in the 39-busbar system. The tracing method started at the same seed node as in bus 26. In Figure 5.8, the tracing results show that the sick island in blue is quite small and has a selected bigger threshold value. Therefore, another important issue concerns how we select the threshold value to obtain the best islanding solution. In order to deal with this issue, optimization in terms of power flow interruption, power flow imbalance and voltage stress are included in this tracing method for the purpose of islanding.

5.4 Optimization Objective for Islanding Scheme

In the online application of the controlled islanding scheme, the optimal solution based on the tracing method has to be provided for the use of the system operator. Therefore, the optimization objectives need to be introduced in islanding scheme in order to decide the best islanding strategy.

In order to choose the best islanding solutions by using the tracing method, three optimization objectives have to be achieved: minimise power flow disruption and minimise power imbalance.

5.4.1 Minimal power flow disruption

In [23][82], minimal power flow disruption was used to find the best islanding solution based on the slow coherency method. This could be also used in the tracing method as an objective function to identify the best islanding strategies. This objective function can be expressed as follows:

$$\min \quad F_1 = \left(\sum \left| P_{tripped\_line} \right|\right) \tag{5.15}$$

The objective function (Eq. 5.15) aims to minimize the power flow in the tripped lines that connect to the formed islands. To some extent, this objective could reduce the possible loss of transient stability in the formed island while splitting the entire network because islanding is already a huge disturbance. We have to prevent this disturbance from deteriorating the operating conditions.

5.4.2 Minimal power imbalance

The other objective function is to minimize the power imbalance in the formed islands, which can be expressed as follows in [23][82]:

$$\min \quad F_2 = \max_i \left| \sum_j P_{I_i - I_j} \right| \tag{5.16}$$

where I_i and I_j represent *i*th and *j*th formed islands; $P_{I_i - I_j}$ shows the power transfer between *i*th and *j*th islands. This objective function aims to achieve the lowest possible difference in the power imbalance in the formed island. This will decrease frequency instability or transient stability caused by the imbalance between generation and load demand.

5.4.3 Minimal voltage stress

Voltage collapse exists in some cascading blackouts that occur after a large change or incremental drop in voltages. Therefore, this objective is to minimize the voltage change in order to minimize the possibility of a local blackout collapse. In addition, because voltage relates to reactive power, the voltage stress during forming islanding cutsets can be minimised [29][77] as follows:

$$\min \quad F_3 = \max\left(abs(\Delta T_q) \right) \tag{5.17}$$

where ΔT_q is the vector of all changes in the reactive power bus throughput.

Based on any one of these three optimal objective functions, the power flow tracing-based islanding method not only determines the threshold value for the tracing method but also provides the best solution to determine where to island. Figure 5.9 represents a flow chart to illustrate the steps to find the threshold value with best islanding solutions.

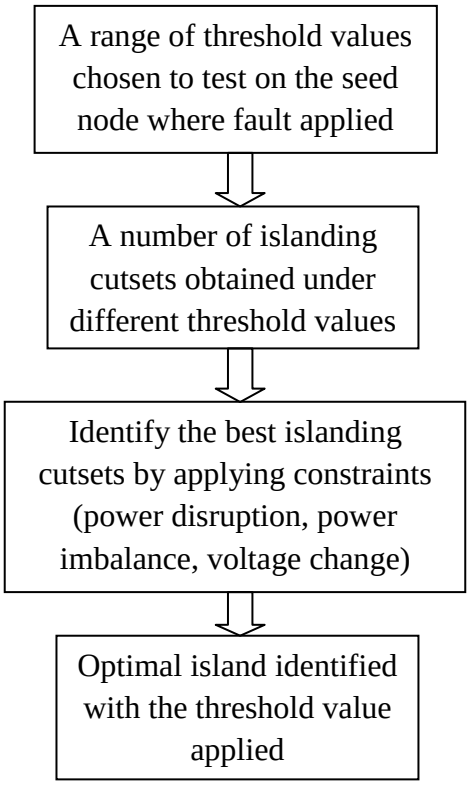

Figure 5.9: *Flow chart to illustrate the steps to find the threshold value with best islanding solutions*

5.5 Islanding Solution for Decisions

The tracing method obtained several islanding solutions. Each seed node may have different islanding strategies. Different optimization tools could be used to identify the optimal islanding solutions among the different islanding strategies. There also may be different optimal islanding strategies, which highly depends on the aspect that is focused on, such as minimal power flow disruption, minimal power imbalance or minimal voltage stress. In real power systems, if the optimal islanding strategies provided could not guarantee transient stability in an island after splitting the network, a different optimal islanding strategy would be required, which would be achieved by changing the threshold value in order to ensure that the formed islands were transiently stable.

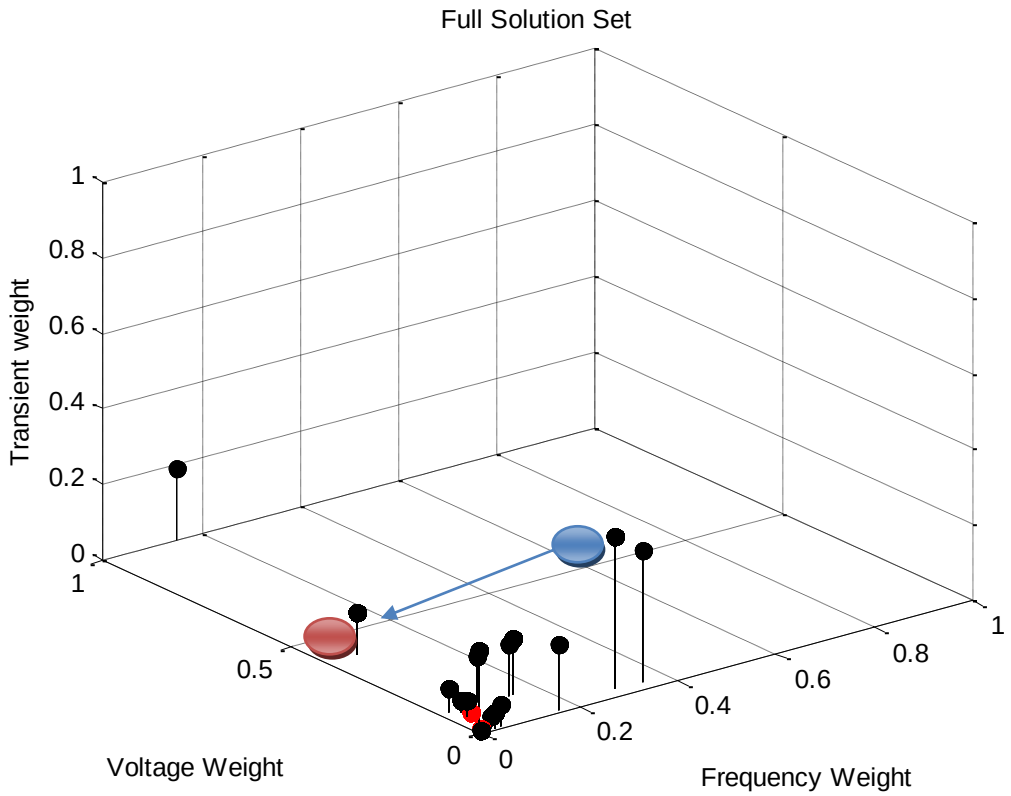

Figure 5.10: *Full solution set in 39-busbar system in terms of transient weight, voltage weight and frequency weight [29]*

Figure 5.10 shows a 3D plot of a full solution set in a 39-busbar system in terms of three indices: transient weight, voltage weight and frequency weight. Transient weight represents the transient stability margin in the formed island, which can be obtained by minimizing the power flow disruption. Voltage weight represents the voltage change during islanding, which can be gained by minimizing the voltage stress through minimizing the reactive power flow. Frequency weight represents the frequency margin, which can be derived by minimizing the power imbalance in the formed islands. In Figure 5.10, each optimal islanding strategy is represented by a black spot, which contains different information about the three indices. For example, the optimal islanding solution close to the blue spot is obtained by minimizing the voltage stress during islanding; in the example, the voltage weight is quite small. However, the transient weight is quite large, which could lead to transient instability in the formed island. Hence, this optimal islanding should be discarded, and another islanding strategy with a satisfactory transient weight should be used for islanding. When we move the

islanding solution from the blue spot to the red spot, the formed island has a lower risk of transient instability because of the lower transient weight.

5.6 Summary

The power flow tracing method is introduced in this chapter. The concept is based on the proportional sharing principle. Initially, it was used as an economic tool to solve issues in the electricity market. In this thesis, it is adopted in the three-stage controlled islanding scheme in order to determine where to island. Specifically, in order to split the entire network safely and optimally, the application of power flow tracing aims to identify the weakly connected lines between the sick island containing disturbance and the remaining healthy sub-network. In the power flow tracing method, the weakly connected line has less power flow contributed by the seed node. This is observed by obtaining the tracing matrix, which however is subject to the chosen threshold value. The appropriate threshold value must be identified, and the best islanding solution must be selected from several strategies provided by the tracing method. Optimization objectives are involved in this tracing algorithm, such as minimal power flow disruption and minimal power imbalance in formed islands. Both help to solve this problem and decide the best islanding strategy. In addition, the tracing algorithm is applied to 6-busbar system and a 39-busbar system for demonstration purposes. In real application during cascading blackouts, when the tracing methods give the islanding solution, before the order to implement the islanding strategy can be given, transient stability in each island still must be considered to avoid an unstable formed island. The assessment of transient stability should be dealt with based on the best islanding solution provided by the tracing method. However, the optimal islanding solution could be subject to different optimization indices, such as minimal power disruption, minimal power imbalance and minimal voltage stress. If the provided optimal islanding solution does not satisfy the requirement of transient stability in the formed island, another optimal islanding solution with a better transient stability should be used. This can obtained by changing the threshold value of the power flow in the tracing method.

Compared with the previous slow coherency method, power flow tracing is disturbance-dependent. The islanding solution obtained links to where the disturbance occurred. It then cuts out the sick island and prevents the spreading of disturbance to the remaining healthy sub-network, instead of creating several unnecessary islands which would complicate the re-synchronism effect required at the end. By tripping the lines, islanding is already a huge disturbance to the entire network. However, the tracing method is able to trace the power flow on each line and ensure that the power flow disruption is minimized, which results in a better transient stability safety margin in the formed islands. Therefore, in this thesis, we will adopt the tracing method in the three-stage controlled islanding scheme in order to decide where to island. The islanding cutsets provided will be assessed for transient stability status before islanding action is eventually taken.

Chapter 6:

Cascading Outage Simulation

In this chapter, the cascading outage scenarios before the imminent blackouts are simulated in order to understand dynamic behaviours in power system. Different types of modelling and protection for generators are described in Appendix A. Different devices used to protect network circuits, such as overcurrent, distance are also attached in the Appendix. Because the protections were improperly coordinated, such devices contributed significantly to the widespread cascading blackouts that have occurred during the past decade. Typically, in the US/Canada blackout (2003), at least 265 power plants with more than 508 generators shut down during the process of the cascading line tripping. It is necessary to know the protection devices that caused the generators to be tripped during cascading outages. The reasons [4] are summarized into a few categories as follows:

- Before uncontrolled islanding:

    - The generators were tripped by protective relays that responded to the overloaded transmission lines, such as the under-voltage and over-current protection relays installed in those lines to connect the generator buses.

- Uncontrolled islanding was formed not because of internal problems in the plant but because of outside conditions in the grid.

    - In some islands, generation was overwhelmed, so the generators shut down in response to the over-speed and/or over-voltage protection schemes.

    - In contrast, some islands where generation was deficient were tripped by under-frequency and/or under-voltage protection schemes.

    - The over-excitation protection scheme tripped the plant because the field

windings and coils were overheated under the effect of AVR when low voltage occurred in the generator bus.

- The under-excitation protection scheme tripped the generators because it tried to protect them from exciter component failures. This is controversial because it can operate in stable as well as transient power swings.

- Reverse power flow and loss of fuel supply

- Failure of plant control systems or actions taken to trip plants in order to protect them.

In addition, in the Italian blackout case (2003), the main causes of the tripping of the relevant thermal generating units [1] were as follows::

- Boiler failure: The power supply from the grid could not make the auxiliary equipment work properly because of the voltage collapse.

- High temperature of exhaust gas: When the frequency dropped and the generator slowed down, during dynamic periods the inadequate air mass flow in the compressor might increase the temperature of the exhaust gas, resulting in the turbine being shut down.

- Loss of excitation: Increased voltage oscillation under extended fault tripped the excitation system. Subsequently, the loss of excitation activated protection to trip the generators.

- Loss of synchronism: When power swings and oscillation occurred in the grid through weakly connected lines, some generators may have lost synchronism, and the corresponding protective relays tripped these generators.

- Under-frequency relay operation: In order to avoid the improper operation of generators and auxiliary equipment, the condition of under-frequency tripped the generator when the frequency crossed the threshold of 47.5 Hz

- Under-impedance relay operation: The under-impedance relay protects the generator against faults on the output terminals. However, increased current and decreased voltage caused by disturbance can be regarded as low impedance detected by the relay, which causes the mal-operation to trip the generator.

- Under-voltage relay operation: If the installed AVR is not sufficient to maintain the generator terminal voltage, then the low-voltage condition will trip the generator when the generator terminal voltage drops below the threshold.

- The gas turbine protection tripped the turbines.

6.1 Simulation Results for Cascading Outages

In order to create a cascading environment in which to observe the dynamic process of cascading blackouts, we apply overcurrent protection on each line in the IEEE 39-busbar system to demonstrate how current, voltage and frequency change in the cascading line trips. We also demonstrate the malfunction of distance protection. The 39-busbar system is shown in Figure 6.1. The generators used in this system are fourth-order models. A turbine governor, automatic voltage regulator and over excitation limiter are installed in each generator. The three different areas shown in Figure 6.1 define the power flow transfer in tie lines.

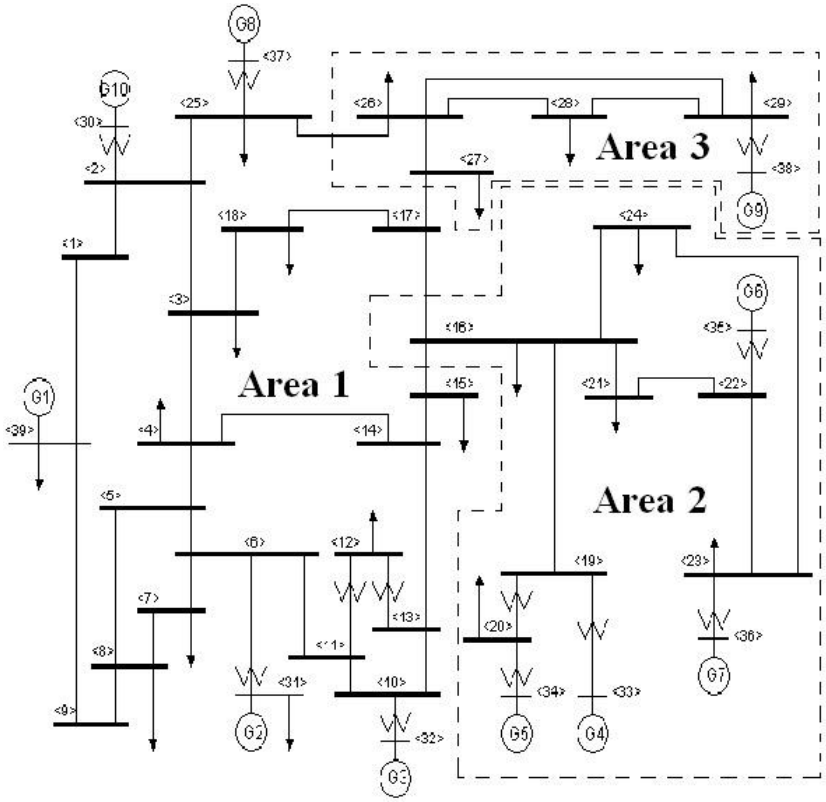

Figure 6.1: *The 39-busbar system.*

Note that in Figure 6.1, a power unbalance exists in each of the three areas. Area 1 and Area 3 have inadequate generation, so both need to import power from Area 2 by 460 MVA and 111 MVA separately through the tie lines connecting each other, as shown in Table 6.1. Therefore, these tie lines may become a cause of the system's collapse.

Table 6.1: *Power flow capacity in tie lines in the 39-bus system.*

Area Connection		Line Connection		Line Capacity (MVA)
		Bus	Bus	
Area 1	Area 3	25	26	160
		17	27	62
Area 1	Area 2	16	15	684
		16	17	458

In order to simulate cascading outages in the test network, some line contingencies are applied to make the system become stressful in a weakened condition. These lines are easily overloaded if their neighbouring lines are tripped because the power flow in the

adjacent lines has to be shared by them. This process could lead to further cascading outages until uncontrolled islands are formed. the N-1 security scan showed that the 39-busbar system satisfies the N-1 security criterion. Hence, we focus on two-line or greater simultaneous contingencies.

6.1.1 Study case A

Study case A demonstrates the frequency changes in the uncontrolled formed islands. Two tie lines (Line 15-16 and Line 16-17) connecting Area 1 and Area 2 were initially and manually tripped at 2 s. This caused Area 1 and Area 3 to be isolated from their generation import source in Area 2, and generation in Area 1 and Area 3 becomes deficient. Then Line 14-15, 9-39, 17-27 and 3-18 in Area 1 become overloaded because of the connection with the high demand areas. They are successively tripped by overcurrent protection. Because two main islands have been formed, the frequency in Area 1 and Area 3 is decreased because of the deficient generation, and the frequency level is maintained at 49.9 Hz, as shown in Figure 6.2. In contrast, the frequency in Area 2 increased at the beginning because generation was sufficient. However, Generator 4 in Area 2 exceeded the high frequency threshold value of 52 Hz at around 8 s. It was tripped by the over frequency protection installed in the generator. The generation in Area 2 also became deficient because of the loss of generator 4. The frequency in Area 2 started to decrease, and the frequency was maintained at 49.8 Hz.

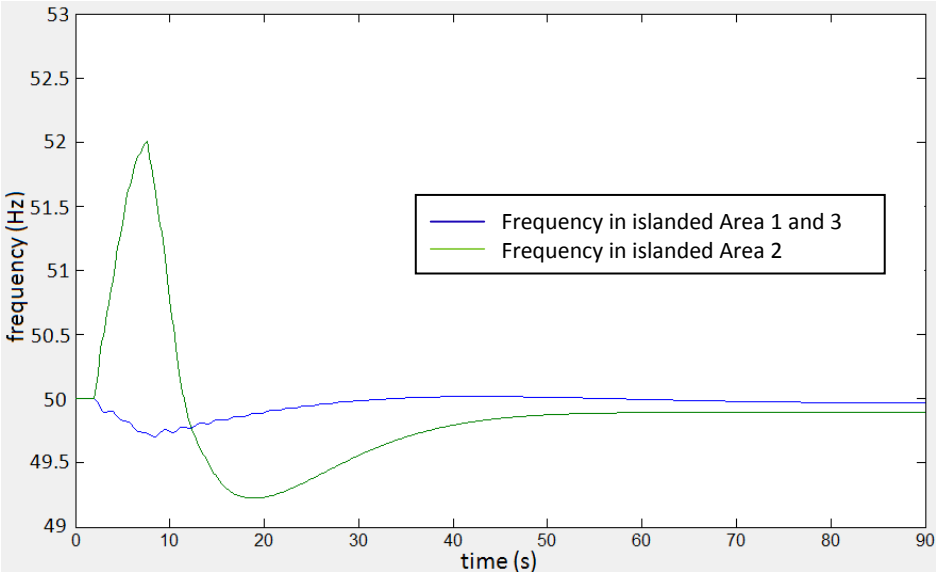

Figure 6.2: *Frequency changes in islanded Areas 1 and 3 and Area 2.*

6.1.2 Study case B

Study case B demonstrates that the tripping of the initial lines caused overloading in other parallel lines. In order to stress the system and trigger the cascading outages caused by protection, we tripped first two lines, Line 13-33 and 20-34, simultaneously at 2 s. The loss of these two lines caused the power flow to be redistributed across the network, resulting in the overloading of some lines. As shown in Figure 6.3, four neighbouring lines, Line 14-15. 17-27, 16-24 and 3-18, were overloaded immediately at the same time as the first two lines were tripped. Then at around 16 s, the overloaded Line 14-15 was tripped by the overcurrent protection, which led to further overloading on Line 17-27, 16-24 and 3-18. When the time reached 23 s, Line 17-27 was tripped after its current reached threshold value set for overcurrent protection, which led to further overloading on Line 3-18. This process continued until Line 3-18 was finally tripped because of overload, and the system collapsed in the cascading outage.

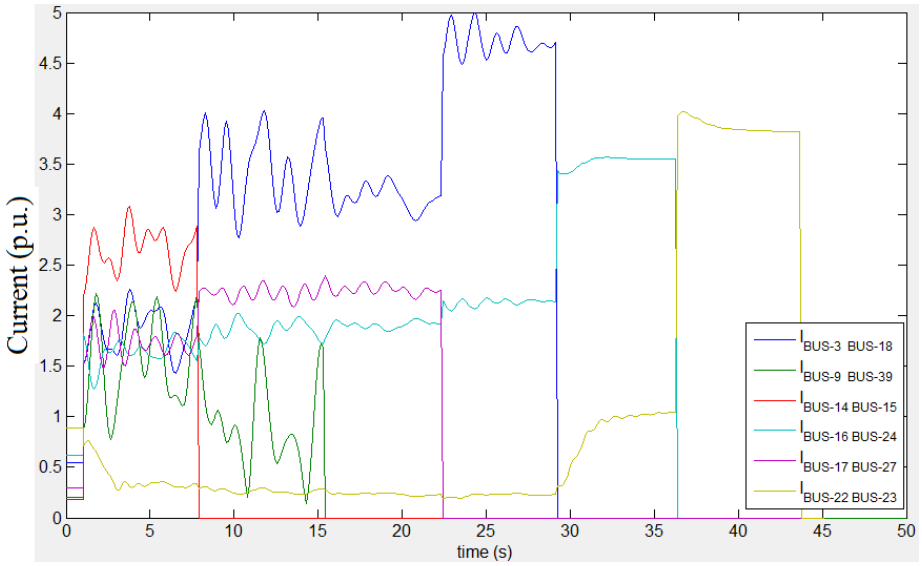

Figure 6.3: *Cascading redistribution of power flow after Line 19-33 and 20-34 were tripped*

6.1.3 Study case C

In study case C, the three lines that connect to Generator 6 and Generator 8 were manually tripped, which caused a power unbalance in the whole system. Several lines, Line 14-15, 9-39, 3-18, 17-27, 16-24, 1-2, 4-5 and 14-15, became overloaded and then

were automatically tripped by the overcurrent protection. Figure 6.4 shows the power flow redistribution during the cascading tripping, which is the same as shown in Figure 6.3. When one line was tripped, the power flow on the tripped line was shared instantaneously by the adjacent lines or the remaining network, which may have caused them to overload, thus triggering cascading outages until uncontrolled islands were formed.

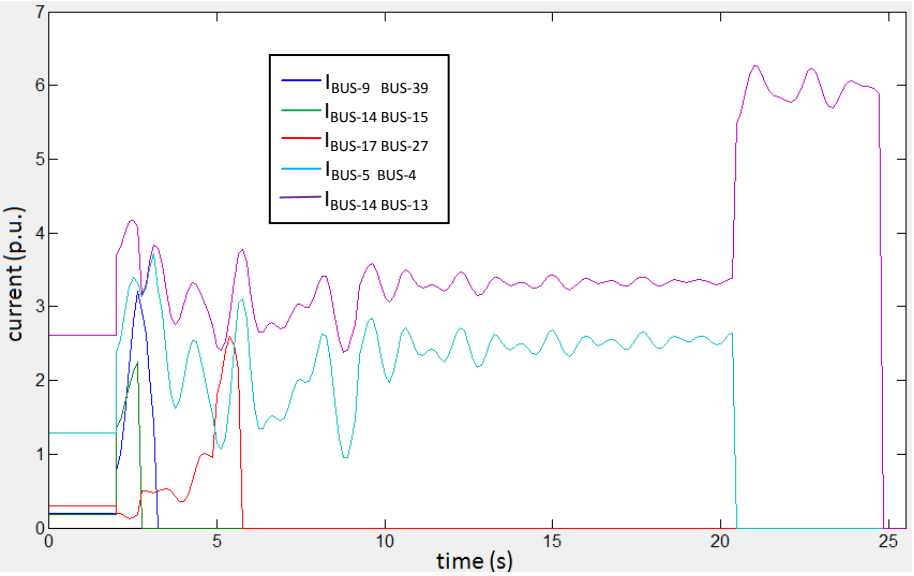

Figure 6.4: *Cascading redistribution of power flow after Line 21-22, 22-23 and 25-37 were tripped*

Figure 6.5 shows the effects of line trips on voltages. The voltages were depressed gradually with the loss of lines under continuous contingency operating conditions. The loss of transmission lines meant that relatively insufficient active power flow could not be delivered to the relatively high demand areas. Therefore, the previous stable voltage decreased and even might have crossed the critical voltage (shown in Figure 6.5) in the new contingency operating condition, causing the voltage to collapse.

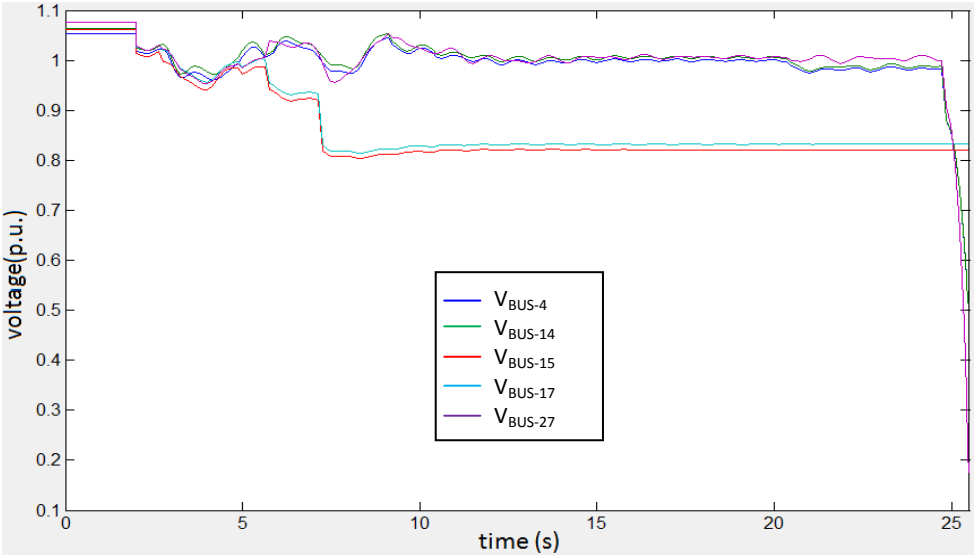

Figure 6.5: *Voltage drops and collapses during cascading tripping.*

Before the system collapsed, Lines 26-29 and 26-28 were tripped by distance protection. As shown in Figure 6.6, the significant increase in current in Line 26-29 and the decrease in voltage in bus 26 caused the distance relay installed on Line 26-29 to detect high current and low voltage. The measured apparent impedance was entered into the operating characteristic zone of the protection relays. It was not able to discriminate the changes in impedance between the faults and the power fluctuations. Therefore, Line 26-29 was tripped at 25.4 s by distance relays, which led to nine islanded networks and the collapse of the entire system. This case showed that the malfunction of distance protection also contributed to the cascading blackouts.

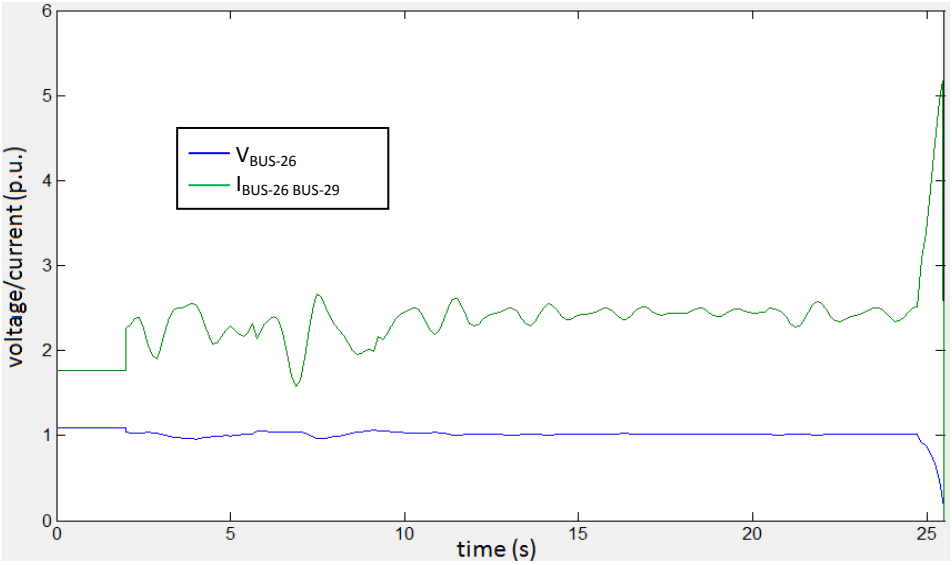

Figure 6.6: *Line 26-29 is tripped by distance protection.*

6.2 Summary

This chapter first describes the reason that generators are tripped by their relevant protection during cascading outages. The reasons for the US/Canada blackout (2003) and the Italy blackout (2003) are summarized. The associated generator models are introduced in Appendix A. The classical generator model and the fourth-order generator model are used in the case studies to simulate the dynamic process in a system under disturbance. In addition, the existing conventional protection systems for both generators and transmission lines were also described in Appendix A. They are designed to protect the system components against the occurrence of contingencies. However, the design of the protection particularly focuses on individual components. The lack of coordination and malfunction of the protection systems in severe contingency situations has contributed significantly to cascading blackouts, such as the India Blackout (2012) and US/Canada Blackout (2003). In the case studies, in order to simulate the performance of the protection devices to create cascading outages, we installed various kinds of protection in the generators, such as under/over frequency protection and under/over voltage protection. We also installed protection on the transmission lines, such as overcurrent protection and distance protection. The performance of the installed protection led to cascading outages in the 39-busbar system until the system collapsed. During the cascading outages, important scenarios were observed in the deteriorating cascading environment, such as increased overloading on adjacent lines because the neighbouring lines were tripped, the voltage drop and the malfunction of distance protection in the cascading environment.

Therefore, this chapter provides a detailed discussion of the reasons that cascading blackouts occur. The findings also help to understand the concept of cascading outage. In this thesis, this research provides the foundation on which online transient stability assessment is based. In the next chapter, we will explain the EEAC and SIME methodologies and their online application in the cascading environment.

Chapter 7:

Extended Equal Area Criterion

Chapter 7 and Chapter 8 address the question of identifying “the point of no return” by using the single machine equivalent (SIME) method when controlled islanding has to be activated. In cascading outages leading to blackouts, the point of no return is the last tripped line, which results in transient instability. SIME is applied to find an a priori transient stability indicator during cascading outages. This indicator is adapted into the controlled islanding scheme to support decision making regarding its implementation to correct transient instability. The extended equal area criterion (EEAC), on which SIME is based, is introduced first in this chapter.

7.1 Introduction of EEAC

In the cascading environment, the continuous tripping of lines and generators pushes the system towards the boundary of stability. Therefore, after each line or generator trip, the transient stability indicator should be used to analyse the signal changes in order to know in advance if the system will remain stable after the next expected overloading line is tripped. EEAC was built as a method for online transient stability assessment. It simply transforms the multi-machine system to a two-machine dynamic equivalent and then further reduces it to an OMIB system. The stability issue is then reduced to a single algebraic equation based on the well-known equal area criterion (EAC) which serves in deciding whether the system is transiently stable. The EEAC aims to enhance the advantage by obtaining the derivation of a simple analytical expression. It allows a one-shot stability analysis without any trial procedures, and it provides stability margins that can be quickly expressed analytically. In order to achieve this objective, the successful application of EEAC is subject to the following assumptions and approximation points [93]:

- Whenever the loss of synchronism in a multi-machine system occurs under critical contingencies, it is triggered by two irrevocably separated groups of generators. The angles of the two groups of generators move apart after swinging against each other.

- The modelling of the generator angles in each group is represented by their centre of angles (COA) in order to assess dynamic behaviour that is equivalent to the OMIB system.

- The angle trajectories of corresponding generator for the equivalent OMIB system and the individual generators are described by the truncated Taylor series expansion.

The principle of the EEAC method with another technique involved is implemented based on the procedures shown in Figure 7.1:

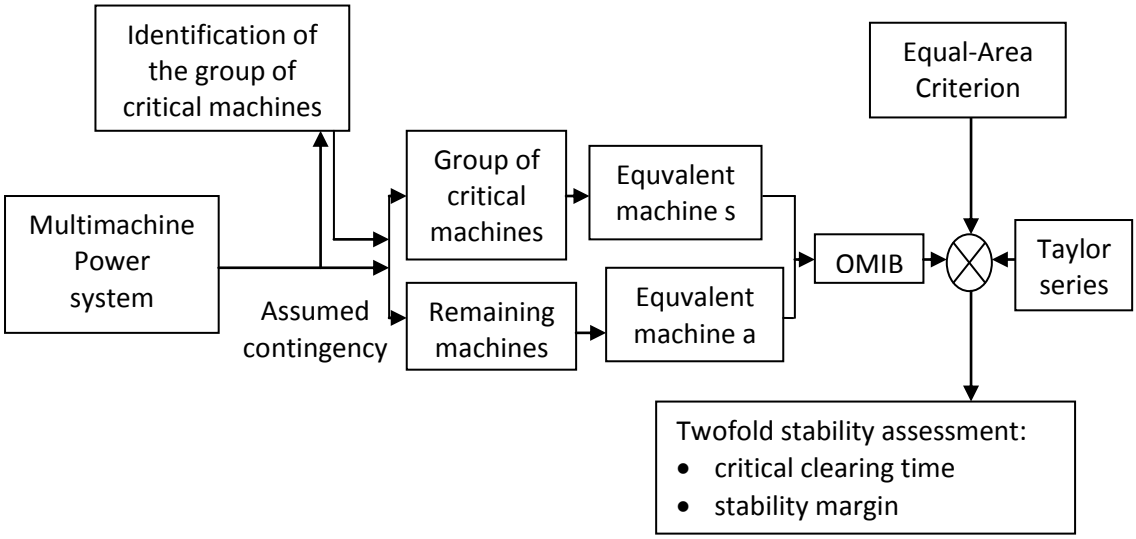

Figure 7.1: *Principle of the EEAC method [93]*.

Figure 7.1 shows that the successful application of the EEAC method relies on a two-part technique: the identification of a critical cluster of generators; and the transformation from a multi-machine system to the equivalent OMIB system. The individual generator angle trajectories must be known in advance to identify the critical cluster of generators that can be obtained through the critical machine ranking (CMR) method based on the initial measurement obtained by WAMS. When the critical cluster

of generators is found, then the successful transformation from a multi-machine system to the OMIB system can be conducted. In the static EEAC, network topology is the only variable that is sensitive to this transformation, which changes during cascading outages. Consequently, transient stability can be assessed and the stability margin can be obtained based on EAC in this equivalently transformed OMIB system.

7.1.1 General OMIB formulation

A. Multi-machine system

For each generator in an *n* machine system, the motion and electrical power of *i*-th generator are given by [94]:

$$\dot{\delta}_i = \omega_i \;\; ; \qquad M_i \dot{\omega}_i = P_{mi} - P_{ei} \qquad\qquad i = 1, 2, ..., n \tag{7.1}$$

$$P_{ei} = E_i^2 Y_{ii} \cos\theta_{ii} + \sum_{j=1, j\neq i}^{n} E_i E_j Y_{ij} \cos(\delta_i - \delta_j - \theta_{ij}) \tag{7.2}$$

and the notion used above is as follows:

δ_i: Rotor angle

M_i: Inertia coefficient

P_{mi} (P_{ei}): Mechanical input (electrical power)

E_i: Voltage behind d-axis transient reactance

Y: Reduced admittance matrix to generator nodes

$Y_{ij}\left(\theta_{ij}\right)$: Modulus (argument) of *ij*th element of Y

M_i, P_{mi} and E_i are assumed to be constant, and all loads are modelled as constant impedances.

B. Equivalent two-machine system

In the SIME method, two assumptions are made in order to transform the multi-machine system to an equivalent two-machine system. One assumption is that in a severe contingency situation, the generator angles move apart to form two groups. In a multi-machine system, transient stability is controlled by generators that are responsible for the system separation whenever the equivalent generator angle of the machines passes a corresponding unstable equilibrium point. These are called critical generators or a critical cluster; the critical generator is sometimes a single generator. The other assumption is that the COA is used to model the generator angles in each group. The two-machine system model can be given using following notions:

S : the set of machines composing the critical cluster of machines

s : the equivalent of S , aggregated machine

A : the set of all remaining machines

a : the equivalent of A , aggregated machine

In order to model the equivalent machine of *A*, COA is used. Because there are only (n-*S*) machines of *A* with machines *S* excluded, we obtain [94]:

$$M_a = \sum_{l \in A} M_l \tag{7.3}$$

$$\delta_a = M_a^{-1} \sum_{l \in A} M_l \delta_l \quad ; \quad \omega_a = \dot{\delta}_a \tag{7.4}$$

The motion of *A* is now obtained by summing the corresponding (n-*S*) equation (7.1). It then can be shown as

$$M_l \ddot{\delta}_l = P_{ml} - P_{el} \qquad \forall l \in A \tag{7.5}$$

by using the relationships in (7.3) and (7.4), we obtain

$$M_a \ddot{\delta}_a = \sum_{l \in A} \left(P_{ml} - P_{el} \right) \tag{7.6}$$

In the above equations (7.5) and (7.6), P_{el} is of the form described in (7.2). An additional simplification may be obtained by setting

$$\delta_j = \delta_a \qquad \forall j \in A \tag{7.7}$$

In this case, P_{el} is expressed by

$$P_{el} = E_l^2 Y_{ll} \cos\theta_{ll} + \sum_{j=1, j\neq i}^{n} E_l E_a Y_{la} \cos(\delta_a - \delta_s - \theta_{ls}) + ... + \sum_{j\in A, j\neq l} E_l E_j Y_{lj} \cos\theta_{lj} \tag{7.8}$$

The above assumption (7.7) is physically sound and well validated in practice. If the critical generators are a critical cluster, the modelling of the equivalent machine of *S* and its motion is the same as the modelling of *A*. If the critical generator is a single generator, the motion of machine *s* is modelled by

$$M_s \ddot{\delta}_s = P_{ms} - P_{es} \tag{7.9}$$

where P_{es} is expressed by an equation similar to (7.2), where the assumption (7.7) has been taken into account. P_{es} is expressed by

$$P_{es} = E_s^2 Y_{ss} \cos\theta_{ss} + \sum_{j\in A} E_s E_j Y_{sj} \cos(\delta_s - \delta_a - \theta_{sj}) \tag{7.10}$$

C. Equivalent OMIB System

To derive the OMIB system, we have to consider the relative rotor angle and the corresponding relative rotor acceleration between two groups of generators. They are defined by [94]

$$\delta = \delta_s - \delta_a \quad ; \quad \ddot{\delta} = \ddot{\delta}_s - \ddot{\delta}_a \tag{7.11}$$

By substituting (7.6) and (7.9) into (7.11), we obtain

$$M \ddot{\delta} = P_m - P_e \tag{7.12}$$

where

$$M = M_s M_a M_T^{-1} \quad ; \quad M_T = \sum_{i=1}^{n} M_i \tag{7.13}$$

$$P_m = (M_a P_{ms} - M_s \sum_{l \in A} P_{ml}) M_T^{-1} \tag{7.14}$$

$$P_e = (M_a P_{es} - M_s \sum_{l \in A} P_{el}) M_T^{-1} \tag{7.15}$$

Using (7.13), (7.8) and (7.10) allows the transformation of (7.12) into the familiar expression of the equivalent OMIB equation of motion:

$$M \ddot{\delta} = P_m - [P_C + P_{MAX} \sin(\delta - v)] \tag{7.16}$$

where

$$P_C = (M_a E_s^2 G_{ss} - M_s \sum_{l,j \in A} E_l E_j G_{lj}) M_T^{-1} \tag{7.17}$$

$$P_{MAX} = (C^2 + D^2)^{1/2}, \; v = \tan^{-1}(C/D) \tag{7.18}$$

$$C = (M_a - M_s) M_T^{-1} \sum_{l \in A} E_s E_l G_{sl} \tag{7.19}$$

$$D = \sum_{l \in A} E_s E_l B_{sl} \tag{7.20}$$

where B (G) stands for the susceptance and the conductance, respectively.

7.1.2 Critical machine ranking

CMR in [93]-[95] is used to identify the critical cluster of the machine(s) in order to transform a multi-machine system into the corresponding OMIB system. For any contingencies of concern in the multi-machine system, truncated Taylor series expansion in (7.21) is applied to the individual generator's angle revolution with time by choosing a large constant step size (i.e., 0.1 s) from the starting point until the oscillation ceases after the breaker operation at $t(\delta_0^+)$.

$$\delta_t = \delta_o + \gamma \frac{t^2}{2} + \gamma^{(2)} \frac{t^4}{24} + \gamma^{(4)} \frac{t^6}{720} + \ldots \tag{7.21}$$

where γ denotes the OMIB acceleration at $t = t(\delta_o^+)$:

$$\gamma = \ddot{\delta}\Big|_{t=0^+} = (\gamma_s - \gamma_a)\big|_{t=0^+} = \left[M_s^{-1} \sum_{k \in S} (P_{mk} - P_{ek}) - M_a^{-1} \sum_{j \in A} (P_{mj} - P_{ej}) \right]_{t=0^+} \tag{7.22}$$

In (5.21), δ_o represents the original steady state rotor angle. The successive derivatives $\gamma^{(2)}$ and $\gamma^{(4)}$ are obtained at $t(\delta_o^+)$. The trajectories of each individual generator angle can be plotted using the Taylor series expansion-based CMR. Critical machines are observed and identified when the predicted generator angle trajectory surpasses the unstable equilibrium point. The machines are then sorted in decreasing order of their generator angles. The candidate critical cluster is determined from the top in the list through angle clustering between the two biggest gaps in successive generator angles. Equation (7.21) is quickly calculated to give this signal for the stability margin calculation.

7.1.3 EAC in OMIB system

The reduced admittance matrix and the identification of the critical cluster of machines allow the multi-machine system to be transformed to the OMIB system. Taylor series expansion provides a rapid computation procedure that is based on the initial generator angles to determine the critical generator cluster. However, this methodology has only been used in fault cases [95]. In this research project, the transient problem is formulated in terms of line trip cases rather than fault cases in order to check in advance whether the last line trip would result in the loss of stability. An additional problem is that the initial condition in terms of generator angles will not be a steady stable equilibrium point because it is derived from the intersection of the pre-breaker power angle characteristic and mechanical power and the system will not be in equilibrium. The intersection is shown as “A” in Figure 7.2. In addition, the initial generator speed deviations will not be zero because the generator angles will be swinging.

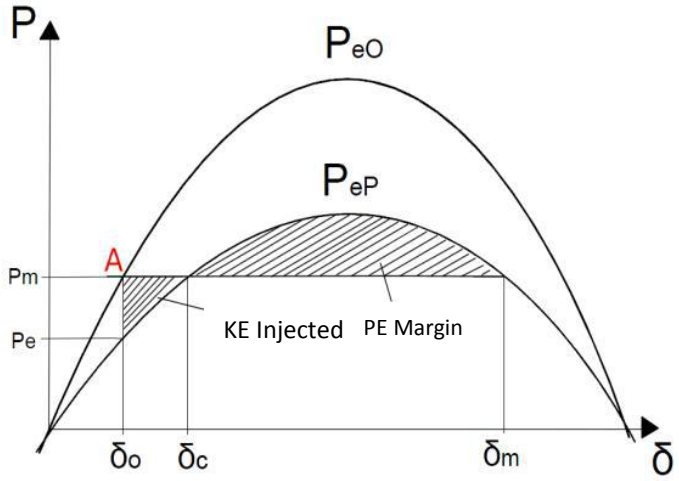

Figure 7.2: *Power angle characteristic for OMIB with breaker operation [96]*.

In the case of line tripping without the fault application in the system, only pre-breaker and post-breaker periods exist, instead of pre-fault, during-fault and post-fault periods in the fault cases used in [93]-[95], [97][98]. Therefore, it is necessary to redraw the $P-\delta$ curves under the line tripping case in the OMIB system, which is shown in Figure 7.2. P_{eO} and P_{eP} represent the pre-breaker and post-breaker $P-\delta$ curves. Because the breaker operation, or line tripping, increases the line reactance between the aggregated generator and the equivalent infinite busbar, it could decrease the peak value of electrical power in the $P-\delta$ curve and force the generator angle to move from δ_o to δ_c, resulting in increasing kinetic energy (KE) and decreasing potential energy (PE). The more lines that are tripped, the more that the gap between KE and PE will be reduced and the closer to transient instability. In addition, the existence of transmission line resistances means terms such as P_C in (7.17) and v in (7.18) are still included in the calculation of A_{acc} and A_{dec}. There is no during-fault curve in the line tripping case; therefore, the post-breaker curve in this case is equivalent to the during-fault and post-fault curves in the fault case. Accordingly, the expression of A_{acc} and A_{dec} are described as follows [94]-[102]:

$$A_{acc} = (P_m - P_{cP})(\delta_c - \delta_o) + P_{eMAX}^P \left[\cos(\delta_c - v_P) - \cos(\delta_o - v_P)\right] \tag{7.23}$$

$$A_{dec} = (P_{cP} - P_m)(\pi - 2(\delta_c - v_P)) + 2P_{eMAX}^P \cos(\delta_c - v_P) \tag{7.24}$$

7.2 Measurement Data Required in EEAC Application

In this work, the EEAC method is applied in the cascading environment. Continuous cascading line tripping will push the system further to the boundary of instability. Therefore, after each line trips, EEAC will be adapted and used to analyse and indicate the transient stability margin by comparing A_{acc} and A_{dec}. In order to obtain a stability margin in running the EEAC, some measurement data are required for calculation.

Figure 7.3 below represents a flowchart of the calculation used in EEAC. As shown in Figure 7.3, two key parts of the measurement data are involved in running the EEAC: the reduced admittance matrix and the CMR. In the cascading environment, as the network topology changes with line tripping, the reduced admittance matrix also changes. In [103] the reduced admittance matrix included three parts: the original network admittance matrix Y, the generator transient reactance x' and the load equivalent impedance (P_L, Q_L).

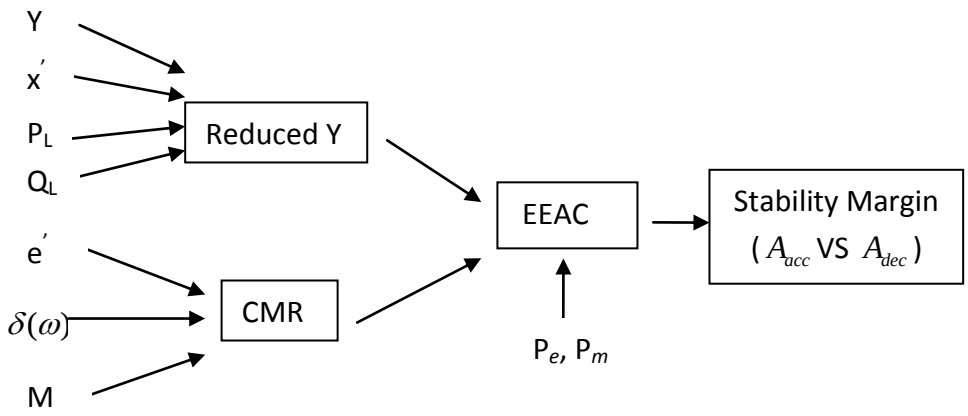

Figure 7.3: *Measurements needed for calculation in EEAC.*

In CMR, the initial generator angles are used to predict the future trajectory of the generator angle in order to identify the critical machines. Based on the identified critical generator(s), multi-machine systems are transferred to the OMIB system with a few parameters, such as generator terminal voltage, inertial, electrical power and mechanical power.

7.3 Summary

This chapter describes the methodology of EEAC, which is used online in the transient stability assessment of fault scenarios and cascading line tripping. This online application aims to support the decision to island during cascading outages to indicate transient stability. EEAC extends the well-known EAC theory applied in the single machine infinite busbar system to the application in multi-machine system. In order to achieve this goal, the transformation from a multi-machine system to a single machine infinite busbar system is required. The original network admittance matrix has to be reduced in correspondence with the equivalent infinite busbar system. The transient stability issue in the multi-machine system then becomes a single algebraic equation that it can be formulated by comparing kinetic energy and potential energy. Based on the online WAMS measurement, EEAC obtained a one-shot stability margin. However, in this online transient stability assessment, there is a trade-off between accuracy and calculation speed. Although the Computation of EEAC is very fast, it lacks the ability to update during the dynamic process after one line is tripped, which may give unreliable results. In particular, this might happen during fast dynamic oscillation immediately after line contingency although the duration time might be quite short. Compared with EEAC, SIME updates the transient stability assessment results in short time intervals based on the measurement data obtained from the online WAMS system. The calculated results of SIME are more reliable. Although the results of SIME might take longer to obtain than the one-shot results from EEAC, it is still fast enough to indicate the imminent loss of transient stability before it actually occurs. The methodology of SIME is explained in the next chapter. EEAC and SIME are based on the same fundamental principle, which is described in this chapter. Based on the same fundamental principle, the difference between SIME and EEAC in yielding accurate results will be discussed in Chapter 8.

Chapter 8:

Single Machine Equivalent and its Application for Preventive Islanding

SIME [103]-[108] is based on the same principle as the static EEAC method described in Chapter 7, that is, it is used to transform a multi-machine system to a two-machine equivalent, which is then reduced to the OMIB system. However, in the SIME method, transient stability assessment is based on the successive monitoring of generator angles according to real-time measurements taken at very short time intervals. In other words, SIME considers the dynamic changes in generator angles in certain time intervals. Because the stability margin obtained is continuously updated, the SIME method is more accurate than the static EEAC. However, it is more time-consuming than the static EEAC method. Regarding the prediction of transient stability, a trade-off exists between accuracy and computation speed. Largely, SIME satisfies both requirements in the online application to predict transient stability in a cascading environment.

8.1 Introduction of SIME

In SIME, stability assessment relies on the prediction of the OMIB's system structure and the $P-\delta$ curve. The OMIB's system structure is predicted by the identification of a critical cluster of generators using Taylor series expansion, which is the same as in the EEAC method. OMIB system's $P-\delta$ curve is predicted by using a weighted least squares (WLS) estimation, which is used to refresh the dynamic generator angles continuously during the dynamic changes after the line contingencies. It aims to correct the unstable equilibrium generator angles of OMIB in order to guarantee the accuracy of transient stability assessment. The mathematical formulation of transformation from a multi-machine system to the OMIB system is the same as in equations (7.1-7.20) in

Chapter 7. To refresh the $P-\delta$ curve in the equivalent OMIB system, the procedure in the SIME method is as follows [13]:

1) At a time t_i shortly after the line contingency occurs at t_e, three incoming data measurements of individual generator angles are obtained at three consecutive time $t_i-2\Delta t$, $t_i-\Delta t$, t_i. Then the Taylor-series-extension-based CMR is used to predict the future trajectories of individual generator angles. The machine sorts the future generator angles in decreasing order. The angles above the largest angular distance between two successive machines are considered candidate critical generators.

2) When the candidate critical machines are identified, the corresponding OMIB system can be constructed. Based on the data of the generator angles and the corresponding parameters of the individual generators, three data of the corresponding OMIB system at time $t_i-2\Delta t$, $t_i-\Delta t$, t_i are obtained and the $P_a-\delta$ curve (Figure 8.1) is approximated by solving the following quadratic function [13] to obtain the coefficients of *a, b, c*:

$$\hat{P}_a(\delta)=a\delta^2+b\delta+c \tag{8.1}$$

When these coefficients are obtained based on three sets of data measurement, the $P_a-\delta$ curve can be derived.

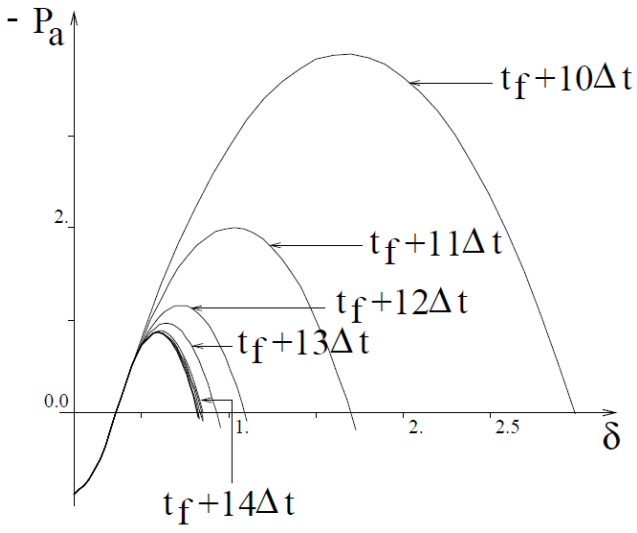

Figure 8.1: *Updating $P_a-\delta$ curves of corresponding transformed OMIB system based on updating measurements [13]*

3) When the coefficients of the quadratic function (8.1) are found, then the OMIB unstable equilibrium angle δ_u can be calculated by letting the equation be zero.

4) Based on all the required parameters calculated above, the stability margin η, which represents the subtraction of the PE from the KE, can be computed as

$$\eta = -\int_{\delta_i}^{\delta_u} P_a d\delta - \frac{1}{2} M \omega_i^2 \tag{8.2}$$

5) If η is found to be negative or close to zero, the system can be declared to be unstable and control actions are taken.

6) If the system is declared unstable, then the time to instability t_u, or the time for the OMIB to reach its unstable equilibrium angle δ_u, are computed as follows:

$$t_u = t_i + \int_{\delta_i}^{\delta_u} \frac{d\delta}{\sqrt{\frac{2}{M}\int_{\delta_i}^{\delta} -P_a d\delta + \omega_i^2}} \tag{8.3}$$

7) A new set (three data) of measurement is acquired after the next time interval Δt and continues monitoring the system for transient stability.

8.2 Application of SIME in the Preventive Islanding Scheme

8.2.1 Framework of three-stage controlled islanding

A successful controlled islanding scheme not only has to consider the dynamic state before islanding but also has to satisfy a secure state in each islanded system after splitting. Figure 8.2 shows a flowchart of the three-stage controlled islanding scheme before the islanding order is given. As shown in Figure 8.2, these three stages are closely connected, and they form the controlled islanding scheme. In order to be successful, the three stages have to co-operate in their individual performances.

The research in this project concentrates on Stages 1 and 3. Stage 2, that is, the islanding methodology, is independent of Stages 1 and 3. In this project, we use power flow tracing to identify the suitable islands. In stage 1, SIME is applied online in

cascading outages to predict transient stability to support the decision to implement the islanding strategy. In Stage 3, SIME is used to assess the dynamic stability in each island after islanding based on the formed islands produced by power flow tracing. All stages have to be implemented before the islanding strategy is actually undertaken in order to ensure that the performance of the controlled islanding scheme is satisfactory.

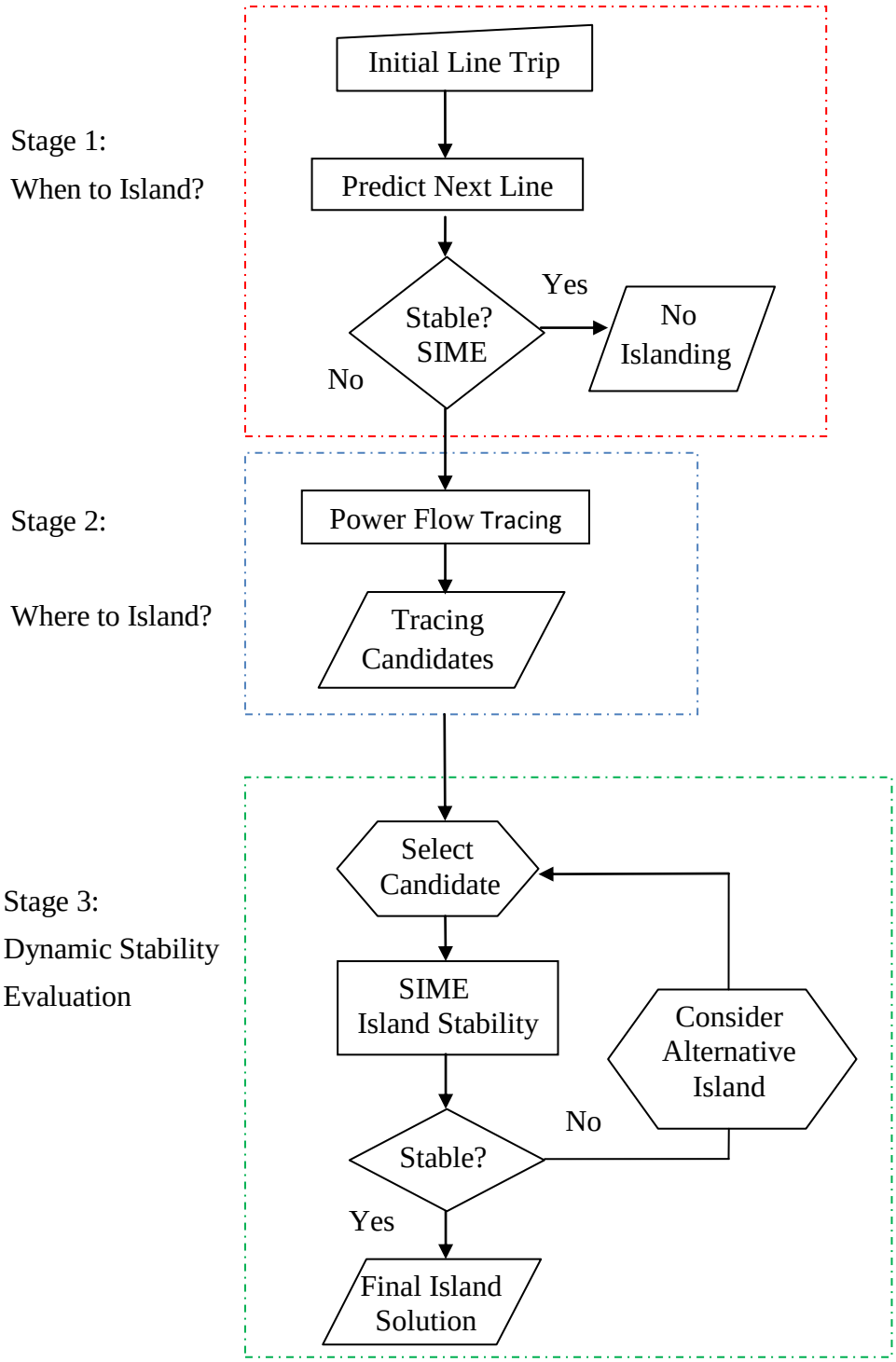

Figure 8.2: *Flowchart of three-stage strategies for controlled islanding.*

8.2.2 Stage 1: When to island

Based on the adoption of SIME, transient stability is assessed during cascading outages. Decision making also can be conducted regarding when to island before losing synchronism. Figure 8.3 shows a flowchart of the SIME application in cascading outages which is used to decide when to island.

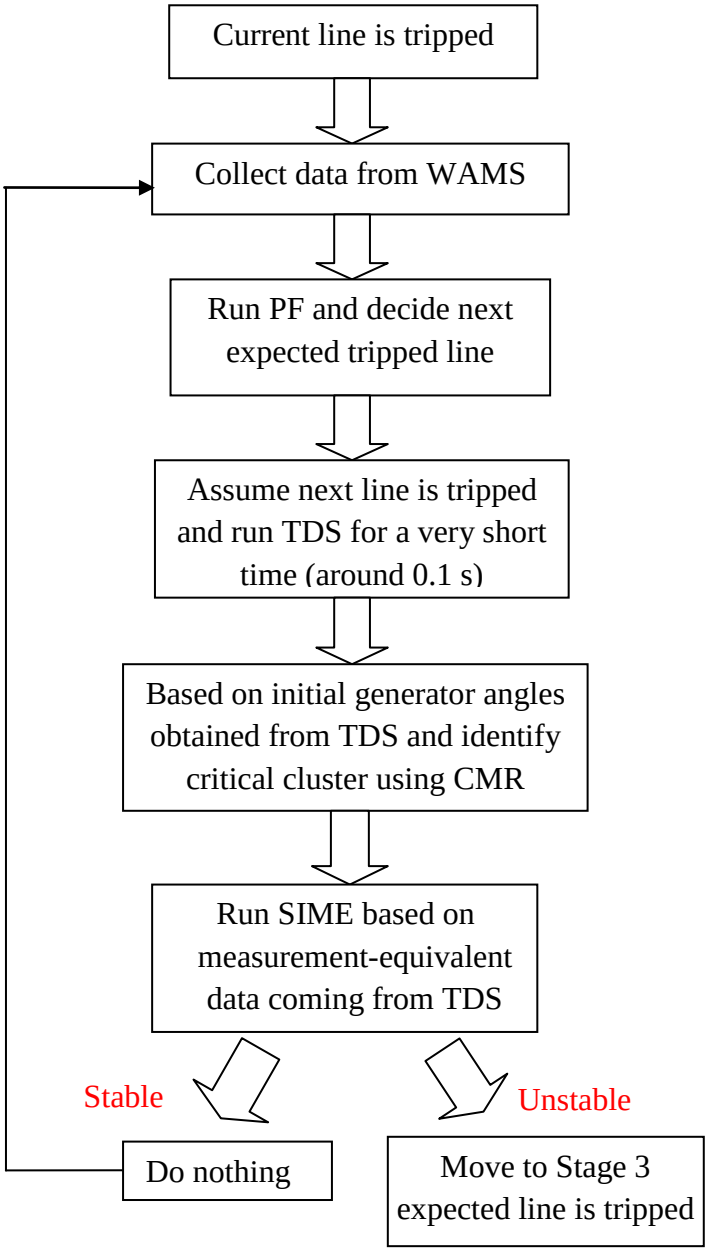

Figure 8.3: *Flowchart of online application of SIME in cascading outages for when to island*

When a line is tripped because of a fault, the online transient stability assessment begins immediately to predict the status of transient stability based on the assumption that the next expected tripped line is actually tripped. This is done in order to determine whether the next line tripping will cause transient instability and whether preparations for the preventive islanding (i.e., selecting islands and checking their stability status) should be initiated. During this period, online WAMS data are used to run the power flow (PF) and identify the next expected tripped line based on the thermal threshold of the lines and the thermal characteristics of the overcurrent protection on the lines. Assuming that the next expected tripped line does trip, then the time domain simulation (TDS) runs for a very short period (e.g., 0.1 second). This TDS allows SIME to collect the initial generator angles and the required calculation data, such as electrical power and generator angular velocity (as in (8.2)), which are used to calculate the stability margin. The delay in obtaining these required parameters (e.g., 0.1 second) is to avoid the collection of unreliable data during the fast dynamic oscillation process immediately after the line trip. Because it is also based on these initial generator angles, CMR can identify the critical cluster of a machine(s) using (7.21). If the computed stability margin is positive or indicates that the operation is stable, the diagnostic system will wait until the next expected tripped line. If the computed stability margin is negative or indicates an unstable operation, Stage 2 is activated. SIME is used to calculate the amount of time left to instability, and the scheme proceeds to Stage 2 to obtain formed islands.

Compared with the use of the conventional TDS in transient stability assessment, SIME has the advantage of detecting cascading tripping within a very short period (e.g., 0.1 s). The utilization of TDS as an initialization of computation has two points. First, the computation of SIME using the data acquisition of 0.1-second TDS is dramatically faster than the conventional TDS. Because transient instability could happen a few seconds after a severe disturbance, saving time is a priority for the system operator to respond and undertake actions based on the predicted stability. Second, the stability margin provided by SIME alerts the system operator when transient stability moves towards the instability boundary. Hence, the operator is made aware of the distance from transient instability after the next line trips.

8.2.3 Stage 2: Where to island

In Stage 2, an islanding algorithm is used to identify the islands that, when disconnected from each other, prevent transient instability. In this research, we use power flow tracing [28][29], but any other islanding scheme could be used.

Tracing is used to isolate the area in which a disturbance starts. It identifies the closely connected nodes by calculating the contributions of power flowing through a given node to all the other nodes upstream and downstream in the directed graph of flows. If the contributions are below a chosen threshold value, the nodes are deemed closely connected, and they should remain in one island. Hence, choosing a different threshold value will result in different islands, and if a particular islanding scheme is found to be transiently unstable, an alternative islanding scheme can be chosen based on a different threshold value.

The advantage of tracing-based islanding is that it attempts to find the cut set lines connecting the islands in which the power flowing through them is minimized. This has the effect of maximizing the power balance in each island and minimizing the shock to the system caused by islanding, thereby helping to maintain dynamic stability. Tracing is very fast because it is based on the simple analysis of static power flows.

8.2.4 Stage 3: Dynamic stability evaluation

In Stage 3, before islanding, another important concern is to ensure that the selected islanding candidate will be transiently stable after islanding. The selected islanding candidate will be the best islanding strategy chosen from all tracing candidates in terms of minimal power flow disruption through the optimization process. Assuming that the next expected line is tripped, if SIME indicates that all the formed islands are stable, then it confirms that the final island solution can be used. On the other hand, if SIME indicates that one or more islands are unstable, another islanding scheme has to be used. In the case of the tracing methodology we applied, finding alternative islands is made possible by changing the threshold value of the contributions or changing the weights associated with different deciding factors, as shown in Figure 5.8. SIME will then continue to assess the stability of the newly provided islands until they prove to be transiently stable. If no stable islands can be found, additional actions have to be taken,

such as generator tripping in generation-rich islands and load shedding in islands with generation deficits. SIME can also be used to identify which generation or load to shed [10]-[14].

It should be noted that time is crucial in any controlled islanding scheme; therefore, the identification of the candidate islands should be done in advance. The transient stability assessment can only be done online. The use of SIME makes it possible to execute the entire three-stage process quickly before a blackout occurs.

8.3 Summary

This chapter describes in detail the use of the SIME method for online transient stability assessment, which is based on the same fundamental principle as EEAC (Chapter 7). The difference between the two methods is that EEAC provides a one-shot transient assessment based on an online WAMS measurement, whereas SIME updates the results of the assessment of transient stability. This updating is necessary because initial fast dynamic changes after contingencies could yield unreliable results. SIME's updating results are converged to a fixed range, which is reliable in indicating whether the system is transiently stable or not. In addition, in SIME, a quadratic function is used to update the $P_a - \delta$ curves, which are used to transform a multi-machine system to a single machine infinite bus system in order to obtain the transient stability margin.

In this chapter, the framework of the three-stage controlled islanding scheme is proposed, and SIME is adapted to the first stage and the third stage in the scheme. It connects these three closely connected work packages, including when to island, where to island and the dynamic stability evaluation after islanding. Only when these three work packages are completed, online islanding is able to be ordered the implementation of the islanding scheme. In particular, the question of when to island is critical in this controlled islanding scheme because it has to be known in advance whether the system's collapse is imminent. Therefore, a flowchart of the implementation procedure use to decide when to island is also proposed. In order to predict transient stability, the next expected tripped line during a cascading outage and the post-fault initial data are

required before the line contingency actually occurs. In the proposed procedure, the thermal characteristics of the protection on the lines are used to decide the next line that will be tripped during a cascading outage. In addition, the time-domain approach is also required for a very short interval in order to obtain initial post-contingency data, which is used to calculate the stability margins in SIME. In the next chapter, SIME will be adopted for use in the controlled islanding schemes in both the 39-busbar system and the 68-busbar system.

Chapter 9:

Simulation Results of the Controlled Islanding Scheme

In this chapter, two test systems are evaluated in the case study of the online three-stage controlled islanding scheme: the 39-busbar system, which uses classical models of generators, and the 68-busbar system, which uses fourth order generator models and Type-2 standard IEEE exciter models. In the first stage of the evaluation, the dynamic characteristics will be analysed during cascading outages. Then SIME is adopted to assess the status of transient stability and decide when to island in terms of transient instability, which would lead to the system's collapse. In the second stage of the evaluation, before the order to island is given, power flow tracing provides the system operator with islanding cut sets. SIME is then used in the formed island to assess transient stability condition by assuming the islanding cut sets have been applied in the system. When transient stability can be guaranteed in the formed island, the controlled islanding order is given in islanding mode for the survival of the system in a healthy operating condition.

9.1 Case Study of a 39-busbar System

The 10-generator 39-bus New England system [109] shown in Figure 9.1 will be used to demonstrate the methodology. It includes transient stability prediction using SIME to identify the point of no return to facilitate decisions to implement islanding, and it assesses the status of transient stability in power flow tracing-based, pre-designed islanding cut sets before splitting. The IEEE 39-bus New England system with classical models of generators was modelled using the MATLAB-based Power System Stability Tool (PSAT) software. In the following case studies, the time-domain results are also shown in order to check the SIME calculation results.

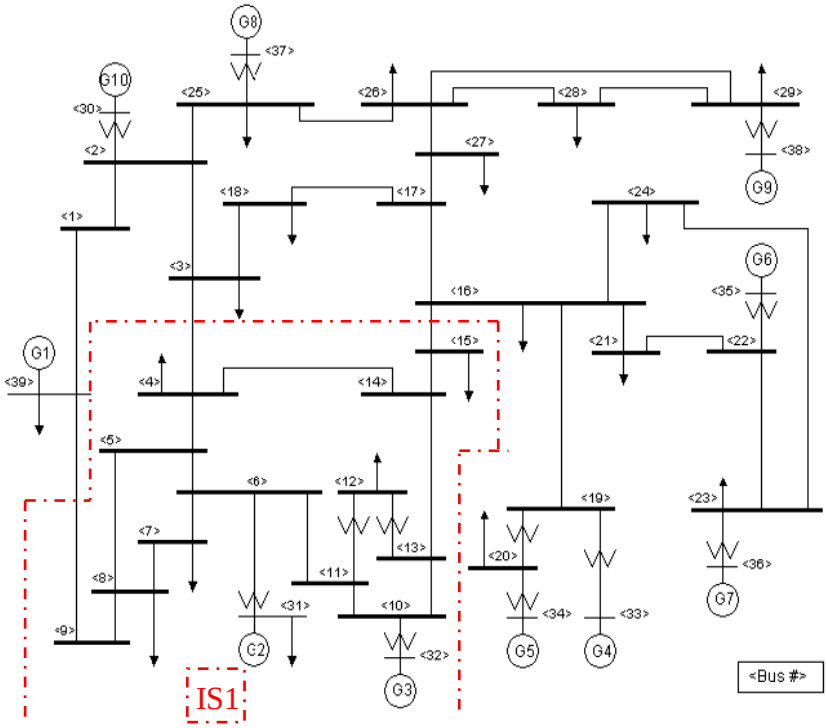

Figure 9.1: *10-generator 39-bus New England system*

In order to stress the used system model to simulate to create a cascading environment, PQ loads were increased up to 1.14 times the original level. To simulate a cascade, two neighbouring lines, 4-5 and 4-14, were tripped in 2-s intervals until transient instability occurred. The online SIME application for transient stability assessment not only relies on WAMS measurement for power flow calculation but also needs post-line-trip data to predict transient stability. These input data, such as generator angle and generator electrical power, are obtained by running a short-time TDS for 0.1 s, assuming the next expected line is actually tripped. SIME also needs data on the reduced system admittance matrix to help transform multi-machine system to OMIB system. This matrix changes as the network topology changes when the line is tripped. This reduced system admittance matrix can be obtained through calculation using network data. It is independent of both the WAMS measurement and the time-domain simulation.

9.1.1 Transient stable case for 39-busbar system

After the PQ load was increased, the power flow was redistributed, and some lines were overloaded. Assuming that Line 4-5 was the first to be tripped, the system moved to another operating condition but maintained transient stability.

After Line 4-5 was tripped, the TDS ran for 0.1 s, which is approximately equivalent to 1 s in real time. The diagnostic system started collecting data 100 ms after the line contingency in order to wait for the initial oscillation to cease. The rate of collecting data was 20 ms, and SIME started assessing the transient stability status 140 ms after the line contingency. The first set of three data was collected at 100 ms, 120 ms and 140 ms after Line 4-5 was tripped. The unstable equilibrium angle was initially estimated by SIME at 1.945 rad with a positive stability margin of 2.64 $(\text{radsec})^2$. These values were continuously updated, resulting in 1.768 rad and 2.05 $(\text{rad/s})^2$, respectively, after 740 ms. Hence, the PE was greater than the KE, and the system was still transiently stable. Table 9.1 below shows the updated predictions of transient stability using SIME after Line 4-5 was tripped. The stability margin shown in the last column is defined as the subtraction of PE from KE, and it can be calculated by using (8.2) in Chapter 8.

Table 9.1: *Transient stability indication after Line 4-5 was tripped.*

Time after Last Contingency t_i (ms)	Unstable Equilibrium Angle (rad)	Stability Margin η $(\text{rad/sec})^2$
140	1.845	2.64
220	1.829	2.55
300	1.812	2.44
380	1.797	2.33
460	1.786	2.23
540	1.778	2.15
620	1.772	2.10
700	1.769	2.06
740	1.768	2.05

During the stable scenario, critical generator(s) do not exist because generator angles are oscillating instead of splitting from each other. However, based on the oscillation groups, which are G2 and G3 in one group and the rest in the other group, the system can still be transferred to the corresponding OMIB system in order to calculate the stability margin. The calculation results were confirmed by time-domain simulations, as shown in Figure 9.2, where the calculation results regarding the stability margins obtained using SIME match the status of the system's stability.

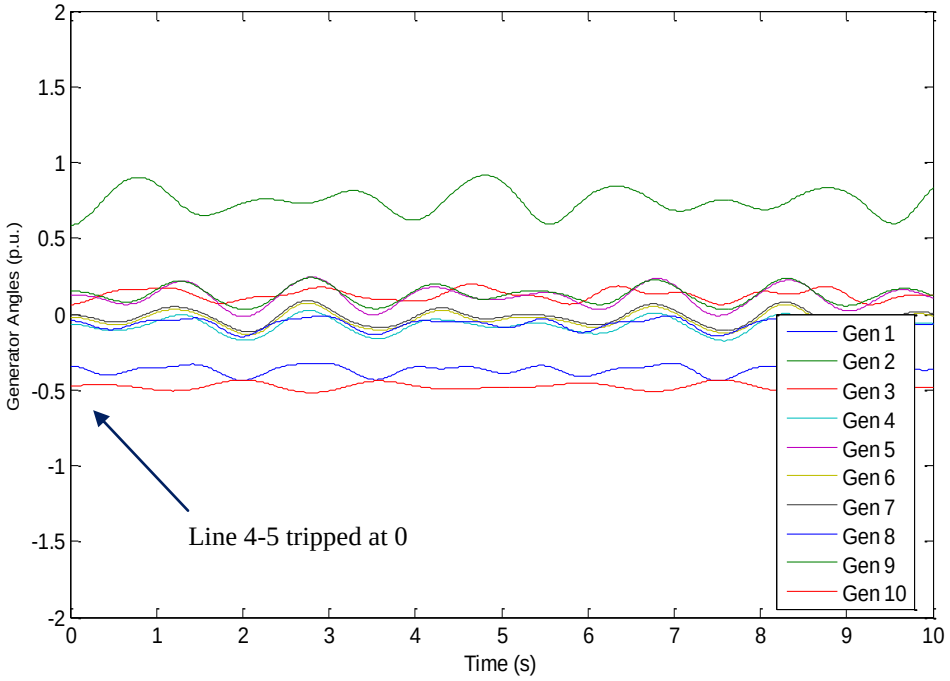

Figure 9.2: *Transiently stable case after Line 4-5 was tripped.*

9.1.2 Transient unstable case for 39-busbar system

We assumed that the neighbouring Line 4-14 was tripped by protection 2 s after Line 4-5 was tripped. Although calculations were made every 20 ms, the results in Table 9.2 are for every fourth time step.

Table 9.2: *Transient stability indication after Line 4-5 and Line 4-14 were tripped.*

Time after Last Contingency t_i (ms)	Unstable Equilibrium Angle (rad)	Time left to instability after tripping Line 4-14 t_u (ms)	Stability Margin η $(\text{rad/sec})^2$
140	1.581	406	0.19
220	1.580	475	0.17
300	1.579	540	0.14
380	1.579	601	0.10
460	1.579	657	0.06
540	1.579	707	0.01
620	1.580	747	-0.05
700	1.580	773	-0.09

Generator G2 was identified as a critical generator. Table 9.2 shows that the stability margins were initially close to zero and gradually became negative from 560 ms. When

the stability margin was negative or close to zero, the system was declared transiently unstable. The calculation results were confirmed by the time-domain simulations shown in Figure 9.3. After the second Line 4-14 was tripped at 2 s, the generator angles did not split immediately and significantly into two groups, which were observed from 1.5 s to 3.5 s. During this period, several swings might have occurred in the system until the oscillation developed to asynchronism, which could explain why initially no negative stability margins were obtained during the swing period.

Note that the third column of Table 9.2 contains an estimate of the critical islanding time (CIT), which is time remaining to execute preventive islanding to ensure that the system remains in a stable condition.

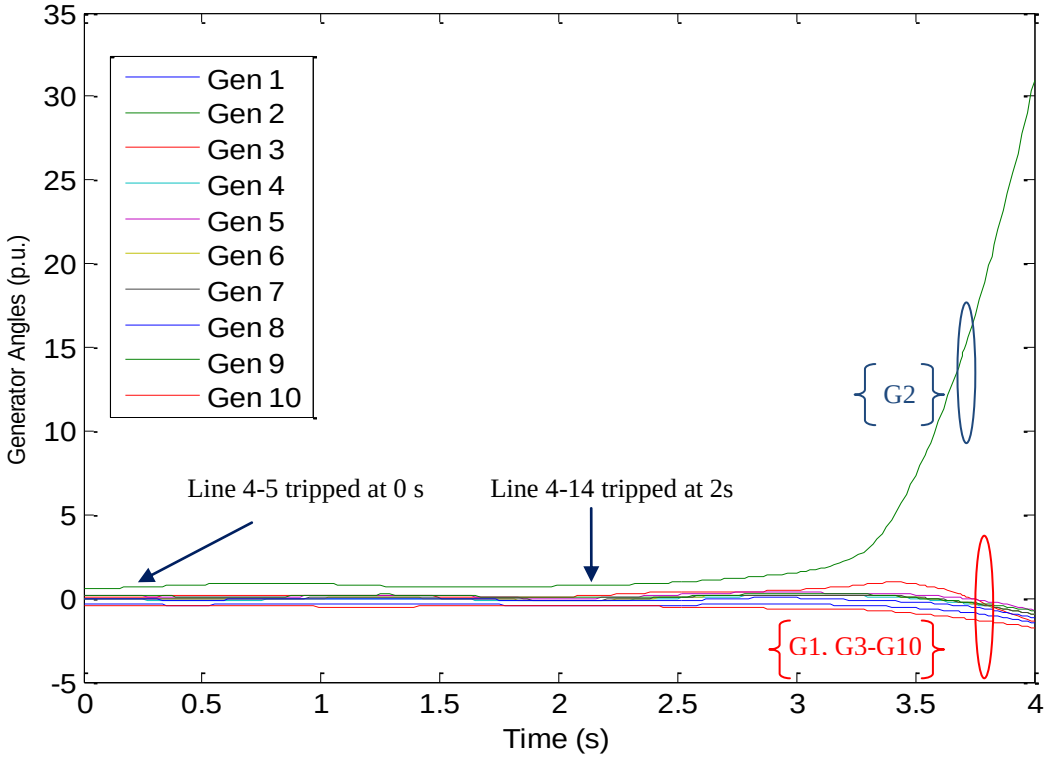

Figure 9.3: *Transiently unstable case after Lines 4-5 and 4-14 were tripped.*

9.1.3 Assessment of transient stability of the islands in a 39-busbar system

In this section, we show how SIME is used with the tracing-based islanding methodology [29] to assess the transient stability of the selected islands.

When the second Line 4-14 was tripped, and SIME indicated that the system was going

to lose synchronism, in Stage 2 of the methodology, the power flow tracing-based method was used to identify possible islands. In Figure 9.1, the dashed lines show the borders of the resulting island, denoted as IS1, and indicate that the cut set consists of lines 9-39, 3-4 and 15-16.

When an islanding scheme has been identified, SIME is used to predict whether the system will be transiently stable following islanding (Stage 3 of the methodology) assuming that islanding is executed before the critical islanding time (CIT as shown in the third column in Table 9.2). In other words, islanding is assumed to be executed in 0.77 s after Line 4-14 is tripped in order to assess the transient stability status in each island.

Table 9.3: *Optimal islanding cut sets based on power flow tracing*

Seed Nodes (buses)	Optimal Threshold for Tracing (p.u.)	Optimal Islanding Cutsets	Islanding Strategy No.
4-8, 10-11, 13-15	1.3	9-39 / 3-4 / 15-16	IS1

There are four islanding strategies (IS) and corresponding optimal cut sets that are based on different seed nodes (buses), that is, points where a disturbance started and optimal thresholds. These optimal islanding cutsets are obtained based on the pre-first contingency power flow data because the objective is to minimize the power flow disruption and after islanding returns the system to the pre-first-contingency operating condition, in which the system is stable. This also ensures that the cascading line contingencies are contained in one sick island without affecting the other healthy islands. The assumed unstable case was caused by a line contingency occurring in bus 4; therefore, the system was islanded using the IS1 strategy shown in Table 9.3.

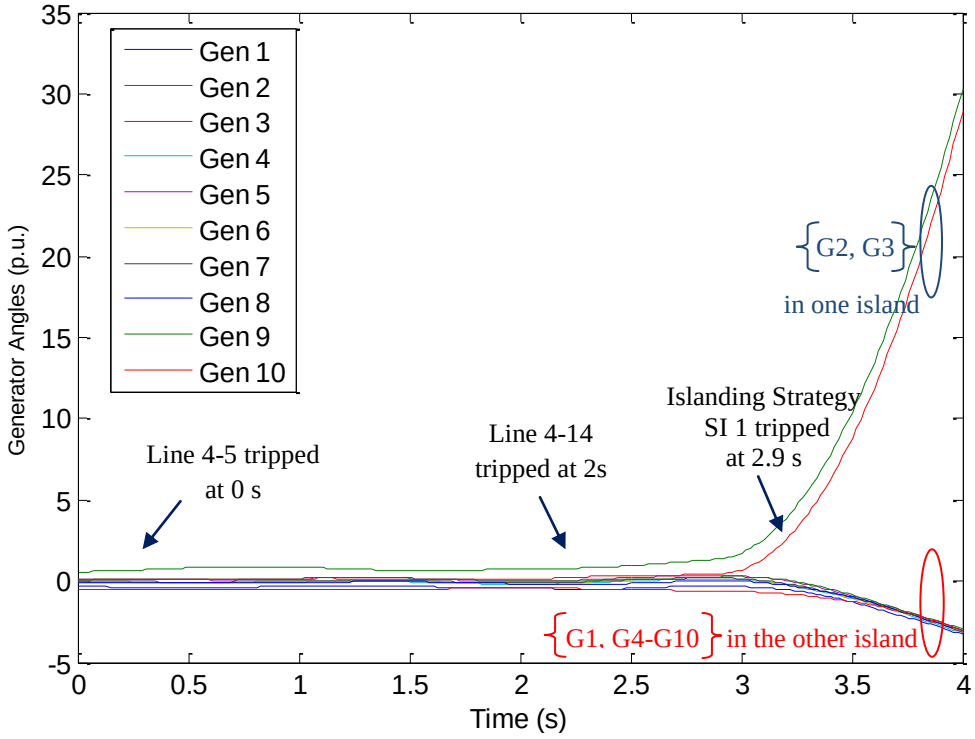

Figure 9.4: *Islanding strategy IS1 applies at critical islanding time 2.9 s*

Figure 9.4 shows the results of the time-domain simulation that confirmed the SIME predictions when islanding was executed 0.9 s after line 4-14 tripped (2.9 s after the start of simulations in Figure 9.4). After splitting the network at 2.9 s, the generator angles were separated into two groups to form two islands. One island contained two generators (G2, G3) while the other island contained the remaining generators (G1, G4, G5, G6, G7, G8, G9, G10). The two islands remained stable as the generator angles stayed close to each other in both islands although obviously both groups of angles separated following islanding.

The simulations shown in Figure 9.3 indicate that G2 separated from the other generators in the unstable case. Figure 9.4 shows that when the preventive islanding was implemented, one island consisted of G2 and G3, and the other consisted of the remaining generators. Hence, the analysis of the transient stability analysis in Stage 1 did not always correctly match the optimal split of the generators between the islands in Stage 2, which is decided by the optimal cutsets obtained by power flow tracing. It also has to satisfy power and demand balance.

The islanding time of 0.9 s was close to the maximum (critical) islanding time of 0.77 s obtained using SIME (Table 9.2). This result indicated that SIME tends to be

conservative, which is a positive feature in power system security. Being conservative is better than being overly optimistic, especially in real-time operations. Being overly optimistic could result in the occurrence of transient instability without advance notice. However, being overly conservative is not good because it could result in overly wide security margins, or islanding decisions may be taken too quickly. Therefore, conservativeness should be contained within an acceptable limit without an overly wide security margin when action is taken.

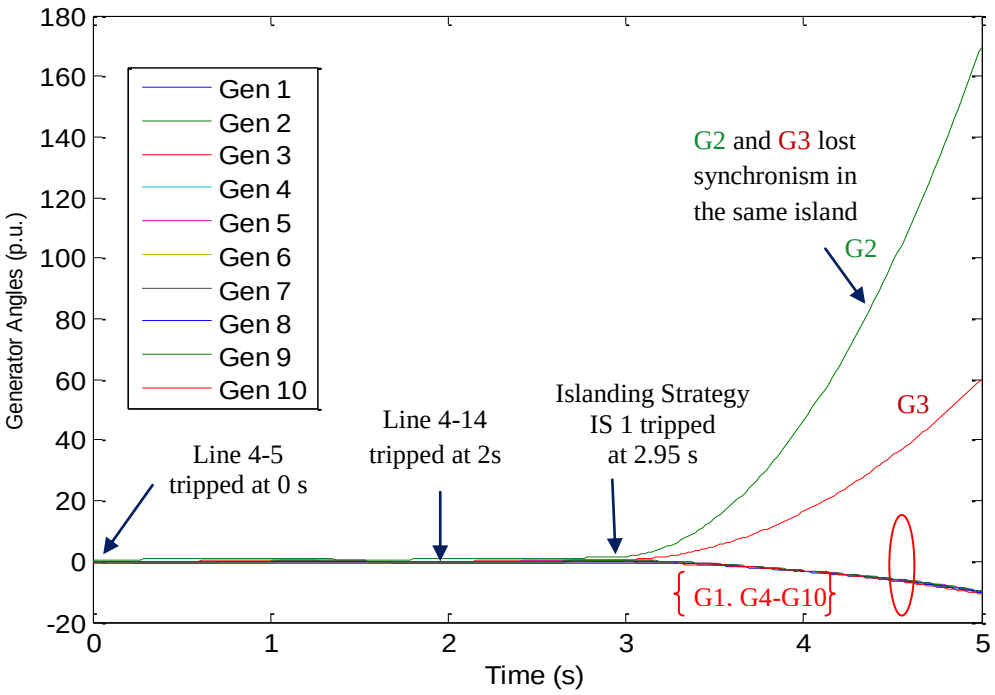

Figure 9.5: *Islanding strategy IS1 applied beyond critical islanding time at 2.95 s.*

Figure 9.5 illustrates the results of the time-domain simulations when the islanding strategy IS1 was used to split the network into two islands at 2.95 s, that is, 0.95 sec after line 4-14 was tripped. Consequently, G2 and G3 lost synchronism because the islanding was undertaken too late. The loss of stability was predicted using SIME, as shown in Table 9.4, which shows that the calculated stability margins were first close to zero and then became negative from the fourth updating.

Table 9.4: *Transiently stable indication in the island containing G2 and G3 after islanding strategy IS1 undertaken.*

Time after Last Contingency t_i (ms)	Unstable Equilibrium Angle (rad)	Time left to instability after islanding IS1 t_u (ms)	Stability Margin η (rad/sec)^2
140	2.959	1121	2.67
200	2.996	1172	-1.02
280	3.101	1226	-3.68
360	6.286	------	-12.9
440	6.316	1391	-3.74
520	9.253	1494	-0.24
620	12.49	------	-9.12
660	12.60	1609	-3.74
740	15.65	1693	-3.70

9.1.4 Stability evaluation of each island in a 39-busbar system

When SIME predicts that the system is transiently unstable, and the power flow tracing also provides pre-designed islanding cut sets, the controlled islanding scheme enters Stage 3. Before the controlled islanding scheme is activated, the status of transient stability in each island has to be assessed. Assuming that the optimal islanding cut sets were tripped before CIT, the measurement data collected from the 0.1 s TDS were used to assess the transient stability in each island. The stability margin in the first (sick) island was initially (140 ms after islanding) 7.01 (rad/sec)^2 and reduced to 2.59 (rad/sec)^2 after 740 ms. The unstable equilibrium angle was initially 3.099 rad, which reduced to 2.995 after 740 ms. The second larger island was found to be very stable. The stability margin increased from 14 (rad/sec)^2 to 160 (rad/sec)^2 after 740 ms.

The first island contained two generators (G2 and G3). Table 9.5 shows the transient stability in the first island after islanding. The stability margins obtained were continuously positive and then decreased to converge to the value of 2.6. The stable indication also matched the time-domain simulation shown in Figure 9.6. In Figure 9.6, G3 is the reference angle, and G2 and G3 are coherent and slightly oscillating.

Table 9.5: *Transiently stable indication in the first island after islanding*

Time after Last Contingency t_i (ms)	Unstable Equilibrium Angle (rad)	Stability Margin η (rad/sec)^2
140	3.099	7.01
220	3.031	5.85
300	2.989	4.84
380	2.967	4.03
460	2.957	3.42
540	2.954	2.98
620	2.954	2.76
700	2.954	2.61
740	2.955	2.59

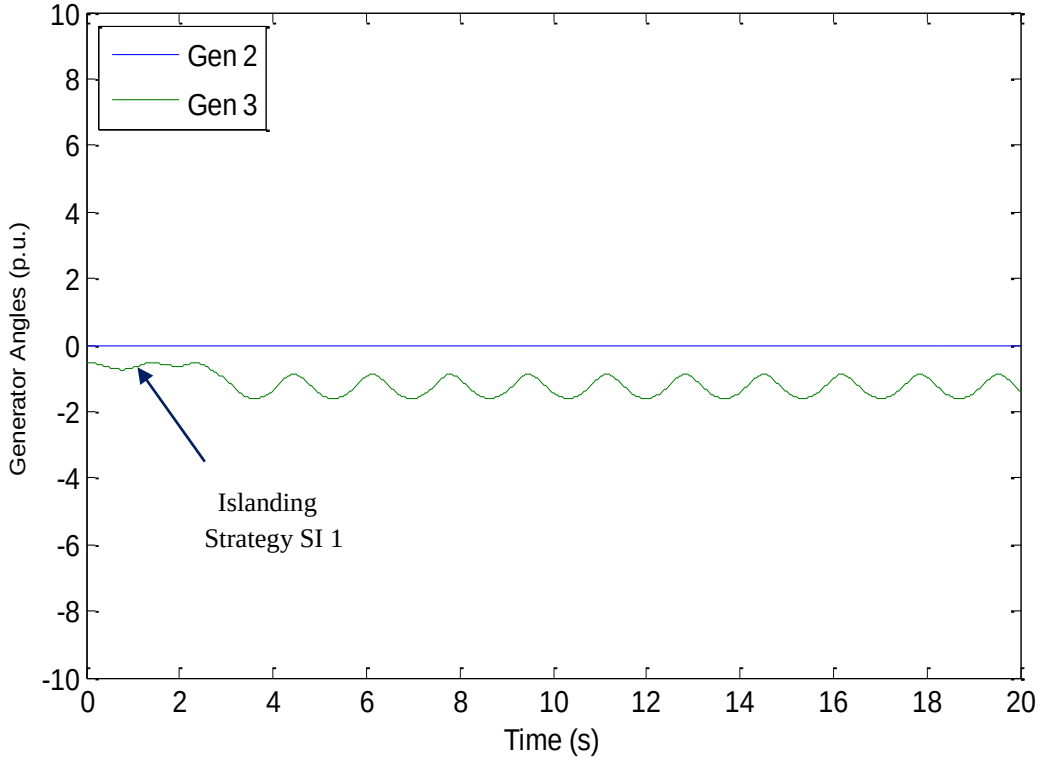

Figure 9.6: *Transient stability status in the first island after controlled islanding scheme is assumed to happen.*

The second island contained the remaining generators (G1, G4, G5, G6, G7, G8, G9, G10). Similarly, Table 9.6 and Figure 9.7 show the status of transient stability in the second island. The stability margins obtained using SIME are shown in Table 9.6. They were constantly positive and indicated that the system was stable. Figure 9.7 also shows the status of stability. The entire group of generators were coherent. and G10 oscillated with the remaining generators.

Table 9.6: *Transiently stable indication in the second island after islanding*

Time after Last Contingency t_i (ms)	Unstable Equilibrium Angle (rad)	Stability Margin η (rad/sec)^2
140	3.051	14.0
220	3.110	14.8
300	3.229	16.4
380	3.441	19.1
460	3.808	24.0
540	4.446	33.6
620	5.592	54.6
700	7.750	108
740	9.542	166

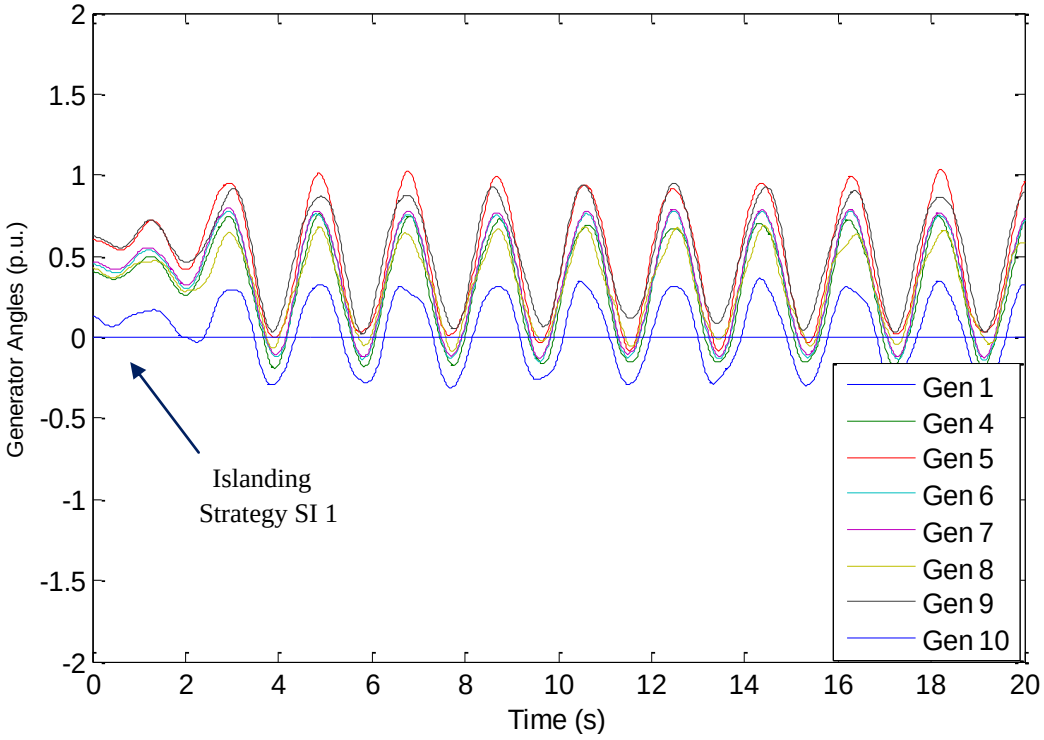

Figure 9.7: *Transient stability status in the second island after controlled islanding scheme is assumed to happen.*

9.2 Case Study of a 68-busbar System

The 68-busbar system shown in Figure 9.8 is based on the 39-busbar New-England system. It was extended to a much larger system that includes 16 generators and 68 transmission lines. In this system model, fourth-order generator models with dynamic

details were used to assess the performance of the three-stage controlled islanding scheme. In addition, Type-2 exciters (standard IEEE model 1) [83][84] were installed in each generator. The same procedure was followed as in the case study on the 39-busbar system. The time-domain simulation was used to test the SIME calculation results in Stage 1 and Stage 3. Figure 9.8 also shows the islanding cut set provided by the power flow tracing method based on the disturbance location, which was required in Stage 2. The transient stability issue was further assessed by using SIME in Stage 3, which aimed to satisfy the post-island stability requirements of the sub-systems.

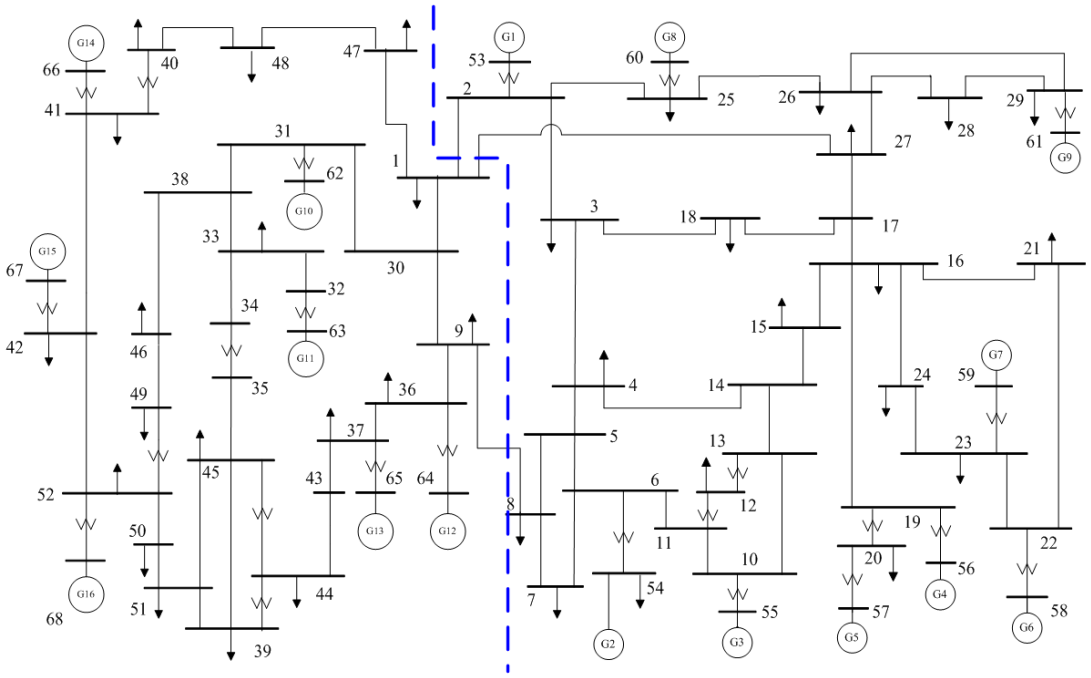

Figure 9.8: *16-generator and 68-busbar system.*

To create a cascading environment in the 68-busbar system (similar to that in the 39-busbar system) several neighbouring lines had to be tripped after the initial line was tripped, which resulted in a transiently unstable scenario. In real time, the application of this controlled islanding scheme was based on the flowchart shown in Figure 8.2. After one line was tripped, the power flow calculation was conducted based on the measurement obtained by WAMS. In the case study, we used time-domain simulation data to represent the WAMS measurement. Assuming that the next expected tripped line was actually tripped, the post-contingency data was collected from the time-domain simulation, which was run for 0.1 s in order to transform the multi-machine system to OMIB system. SIME was used to calculate the stability margin. The entire procedure in

the transient stable case and the unstable case during cascading line outages will be demonstrated.

9.2.1 Transient stable case in a 68-busbar system

In this transient stable case, initially Line 2-3 was tripped at 1 s. The neighbouring lines were assumed to be tripping continuously in order to push the system to the boundary of transient instability. After Line 2-3 was tripped at 1 s, Line 2-4 was tripped at 2 s, Line 3-18 was tripped at 3 s, and Line 4-5 was tripped at 4s. Until the fourth line 4-5 was tripped at 4 s, the system was still transiently stable. However, it was approaching transient instability because the stability margin calculated by SIME was positive but close to zero. Table 9.7 shows the updating transient stability indications using SIME after Line 4-5 was tripped at 4 s. The transient stability assessment started at 140 ms after Line 4-5 was tripped. It used the first set of three data collected at 100 ms, 120 ms and 140 ms after Line 4-5 was tripped at 4 s. The updating SIME calculation results gave the unstable equilibrium angle of 0.191 rad and a positive but close-to-zero stability margin of 0.27 $(\text{radsec})^2$. These results showed that the potential energy obtained by the generator was greater than the kinetic energy. When the oscillation of the generator angle is nearly ceased, another operating condition is gained.

Table 9.7: *Transient stability indication after Line 2-3, 2-4, 3-18 and 4-5 were tripped*

Time after Last Contingency t_i (ms)	Unstable Equilibrium Angle (rad)	Stability Margin η $(\text{rad/sec})^2$
140	0.822	0.57
220	0.719	0.62
300	0.544	0.61
380	0.296	0.43
460	0.075	0.14
540	0.011	0.03
620	0.191	0.27

Although the system was still transiently stable with oscillation and the two groups of generator angles did not split, a critical cluster of generators was identified based on the

oscillation group, which transformed the multi-machine system into the OMIB system. In this test case, the oscillation groups were classified as G1, G2, G3, G4, G5, G6, G7, G8, G9, G10, G11, G12, G13, G14, G15 and G16, which started oscillating at 4 s, as shown in Figure 9.9. Figure 9.9 shows that the time-domain simulation matched the transient induction, which was calculated using SIME.

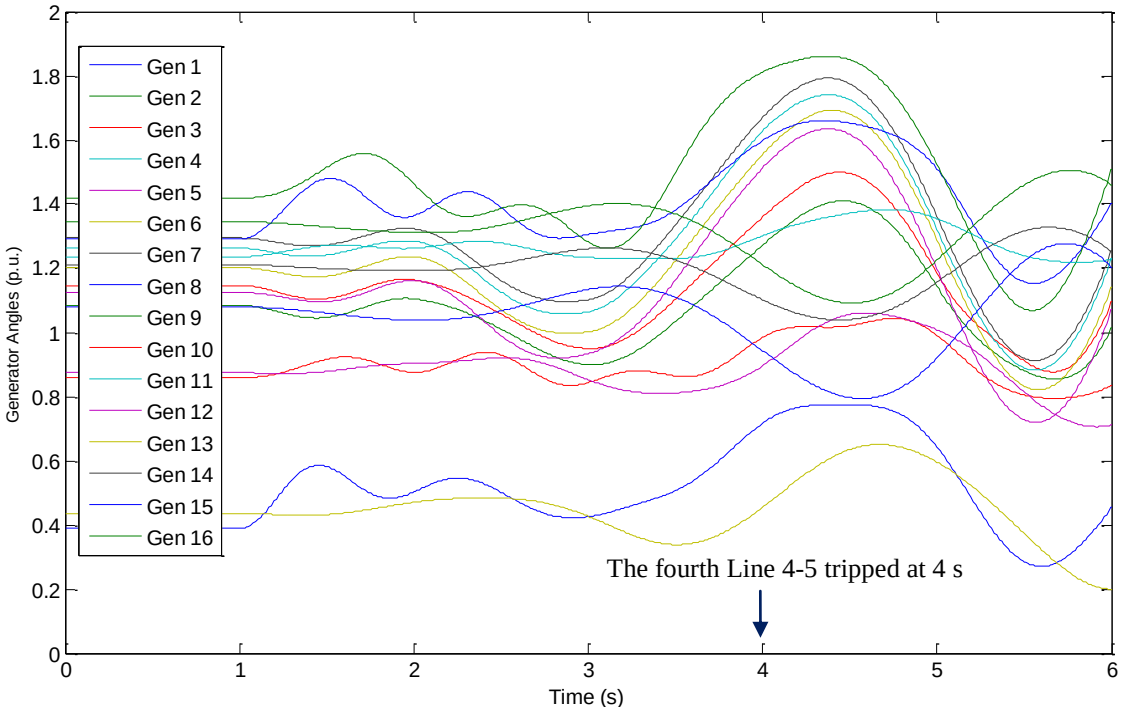

Figure 9.9: *Transiently stable case after Lines 2-3, 2-4, 3-18 and 4-5 were tripped*

9.2.2 Transient Unstable Case for 68-busbar system

Because the system was still transiently stable after four lines were tripped, the next neighbouring Line 4-14 was assumed to be tripped at 5 s in order to push the system to the boundary of transient stability. The first set of three data with a time interval of 0.2 s was collected from the time-domain simulation 0.7 s after Line 4-14 was tripped at 5 s in order to avoid an initial, fast dynamic oscillation. The results of the SIME calculation are shown in Table 9.8.

Table 9.8: *Transient stability indication after Line 2-3, 2-4, 3-18, 4-5 and 4-14 were tripped*

Time after Last Contingency t_i (ms)	Unstable Equilibrium Angle (rad)	Time left to instability after tripping Line 4-14 t_u (ms)	Stability Margin η (rad/sec)^2
700	0.742	1140	-6.0
760	0.734	1200	-3.0
800	0.731	1240	-1.0
860	0.729	1304	-1.0
900	0.729	1339	-1.0
960	0.729	1400	-3.0
1000	0.730	1440	-7.0
1060	0.724	1500	-9.0
1100	0.725	1540	-9.0
1160	0.746	1600	-9.0
1200	0.781	1640	-10.0

In this case, nine generators (G1, G2, G3, G4, G5, G6, G7, G8, G9) were chosen as the critical generators, which is shown Figure 9.10. The results of the updating SIME calculation shown in Table 9.8 indicate that 1.2 s after Line 4-14 was tripped, SIME obtained the unstable equilibrium angle of 0.781 rand and converged the stability margin of -10.0 (rad/s)^2. Because the stability margin obtained was negative, the system was declared transiently unstable. The SIME calculation results indicating the system's transient status also matched the time-domain simulation, as shown in Figure 9.10. After the fifth Line 4-14 was tripped at 5 s, nine critical generators were not easily recognized until 5.7 s because 0.7 s after Line 4-14 was tripped, the critical generators started accelerating against the decelerated generators. As shown in Figure 9.10, at 5.7 s, the generator angles of the critical generator started to increase. The generator angles of the critical generators started increasing from 5.7 s and the first-swing instability further developed into asynchronism. This also explains why SIME obtained a negative stability margin directly from the transient stability assessment at 5.7 s.

In Table 9.8, the third column shows the time remaining to instability after Line 4-14 was tripped. As shown in Table 9.8, the final updating calculated time was 1.64 s, which indicated the critical islanding time. If the islanding scheme was implemented within

this time, the system might survived through controlled islanding. Otherwise, the system would lose its synchronism with no point of return even when controlled islanding was executed.

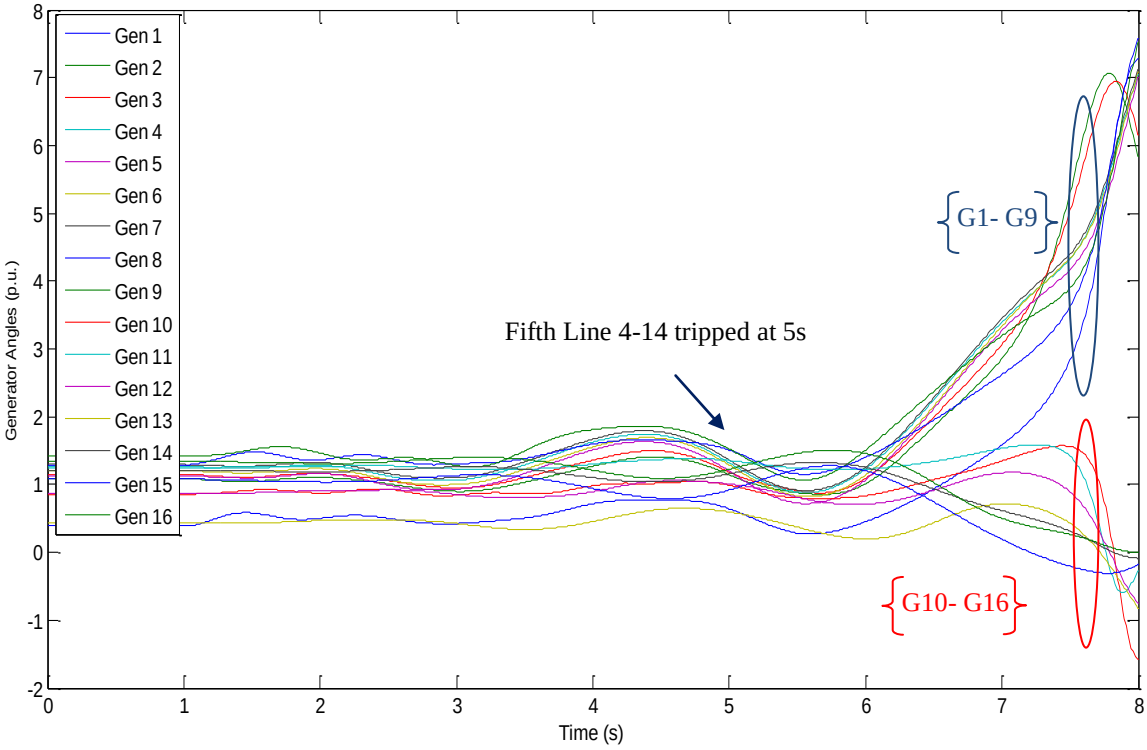

Figure 9.10: *Transiently unstable case after Line 2-3, 2-4, 3-18, 4-5 and 4-14 were tripped.*

9.2.3 Assessment of the transient stability of islands in a 68-busbar system

It was assumed that when Line 4-14 was tripped, the system would lose transient stability. The controlled islanding scheme then entered Stage 2, in which the best islanding cutsets using power flow tracing method were identified. The sick island was used to contain the cascading and identify the weakly connected boundary lines with the remaining healthy island. The blue dashed line in Figure 9.8 represents the cutting boundary. The cut set lines include three lines 1-2, 1-27 and 8-9, which were also identified as weakly connected lines with less power flow. The disruption of power flow by cutting the boundary lines also indicated that the system would be less effected by transient instability.

In Stage 3, SIME was used to assess the transient stability in each island when the islanding cut sets were identified in Stage 2. The assessment was conducted by assuming that the islanding scheme was implemented and that both islands were formed. However, the islanding scheme had to be implemented within the critical islanding time of 1.64 s after the fifth Line 4-14 was tripped. Otherwise, the system or the islands formed after islanding would lose transient stability anyway.

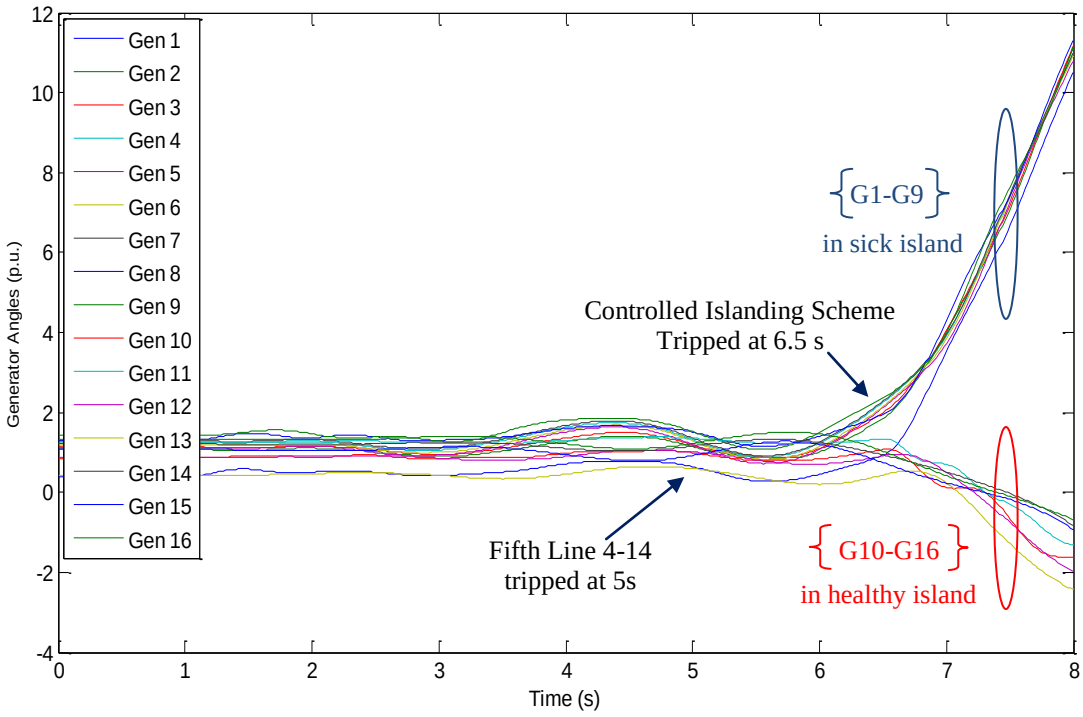

Figure 9.11: *Islanding scheme applies within critical islanding time at 6.5 s.*

Figure 9.11 shows the time-domain simulation results when islanding scheme was implemented 1.5 s after the fifth Line 4-14 was tripped. Figure 9.11 shows that two islands were formed with two separated groups of generators. The sick island contained nine generators (G1, G2, G3, G4, G5, G6, G7, G8, G9). The healthy island contained the remaining seven generators (G10, G11, G12, G13, G14, G15, G16). Each cluster of generators in both islands was coherent without moving apart, which indicates that the formed islands did not lose transient stability in their sub-systems because of the disturbance of the controlled islanding. In addition, the results of the time-domain simulation results (Figure 9.11) confirmed the SIME predictions in Stage 1 regarding the calculated critical islanding time before transient instability occurred. The system was split 1.5 s after the last tripped line of no return, which was within the critical

islanding time of 1.62 s obtained in SIME, the formed islands were still transiently stable. However, if the controlled islanding were implemented beyond critical islanding time, then the formed islands, especially sick island, might not be transiently stable. In this test case, we used a step-by-step trial in the time-domain simulation to determine that the actual critical islanding time was 2.5 s. Compared with the 1.62 s obtained by SIME, the results of the SIME calculation were relatively conservative.

In this case, the islands consisted of the same generators that were previously shown to remain coherent when the transient stability was analysed in Stage 1 (see Figure 9.10). However, this may not always the case, as shown in the results of simulations in the 39-bus system.

Figure 9.12 shows the results of the time-domain simulation of the generator angle trajectories when the controlled islanding scheme was implemented 2.8 s after the fifth Line 4-14 was tripped at 5 s, which is beyond the determined critical islanding time. Hence, it was too late to conduct the controlled islanding scheme because, as shown in Figure 9.12, generator G9 lost synchronism with the remaining generator cluster (G1, G2, G3, G4, G5, G6, G7, G8) in the sick island, whereas the healthy island maintained transient stability after splitting. This result is shown in Figure 9.13.

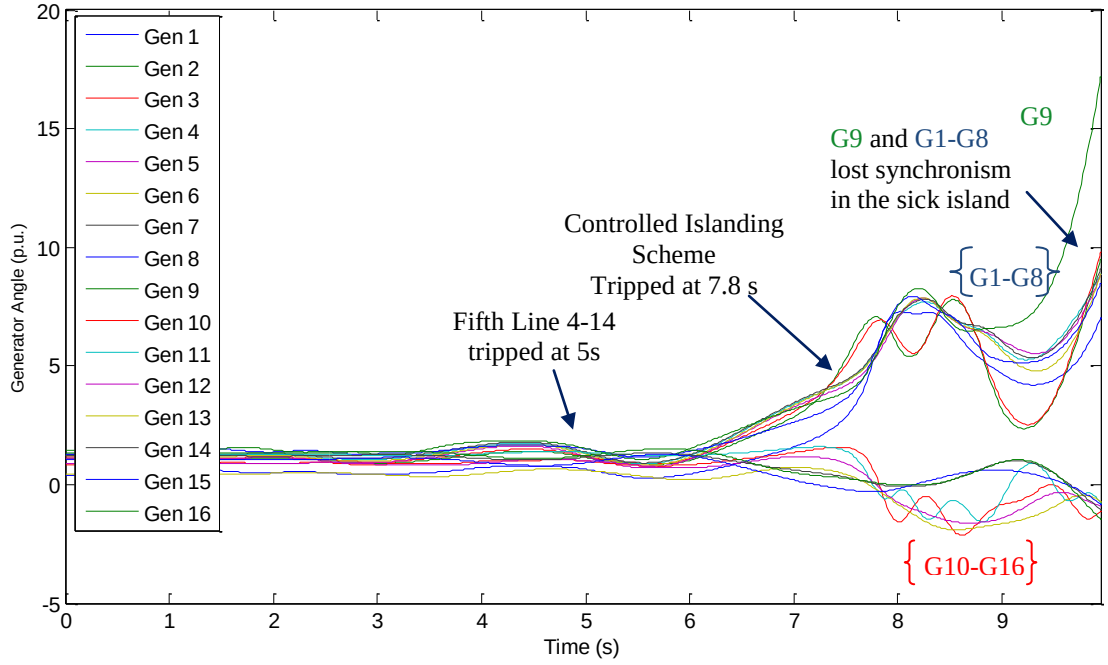

Figure 9.12: *Controlled islanding scheme applied beyond critical islanding time at 7.8 s*

9.2.4 Stability evaluation in each island in the 68-busbar system

SIME was used in real time to assess the status of transient stability in each island after islanding was implemented. Assuming that the islands were formed using the islanding cut sets provided by the power flow tracing method in Stage 2, the measurement data obtained by the 0.1 s TDS were used to run SIME to calculate the stability margin. If the islanding scheme were conducted beyond the critical islanding time, SIME would assess transient stability before it actually happened. For example, the calculation results are shown as follows. The sick island contains two groups of generators: G9 and the larger group (G1, G2, G3, G4, G5, G6, G7, G8). Table 9.9 presents the updating results of the SIME calculation, which indicate that the transient stability status in the sick island after the fifth Line 4-14 was tripped beyond the critical islanding time. The calculation was started 1 s after the fifth Line 4-14 was tripped in order to wait for the oscillation to cease and identify the critical cluster of generator, which was G9 in this case. The stability margin obtained for the sick island converged at -1.0 $(\text{rad/sec})^2$ after 1,400 ms. The unstable equilibrium angle of 3.849 rad was obtained after 1,400 ms.

Table 9.9: *Transient stability indication in the sick island after the fifth line 4-14 was tripped beyond critical islanding time.*

Time after Last Contingency t_i (ms)	Unstable Equilibrium Angle (rad)	Time left to instability after tripping Line 4-14 t_u (ms)	Stability Margin η $(\text{rad/sec})^2$
1000	3.864	1224	-6.0
1060	3.150	1264	-1.0
1100	3.105	1300	-1.0
1160	3.223	1357	-1.0
1200	3.419	1407	-1.0
1260	2.972	1369	-1.0
1300	4.169	1493	-2.0
1360	4.039	1534	-1.0
1400	3.849	1526	-1.0

Figure 9.13 shows the results of the time-domain simulation of the generator angle trajectory in the sick island. The generator angle of G 6 was chosen as the reference angle. Figure 9.13 shows that G9 lost synchronism with the other cluster of generators

in the sick island shortly after the controlled islanding scheme was implemented at 7.8 s. This time-domain simulation also matched the SIME indication result if the islanding scheme was implemented beyond the critical islanding time.

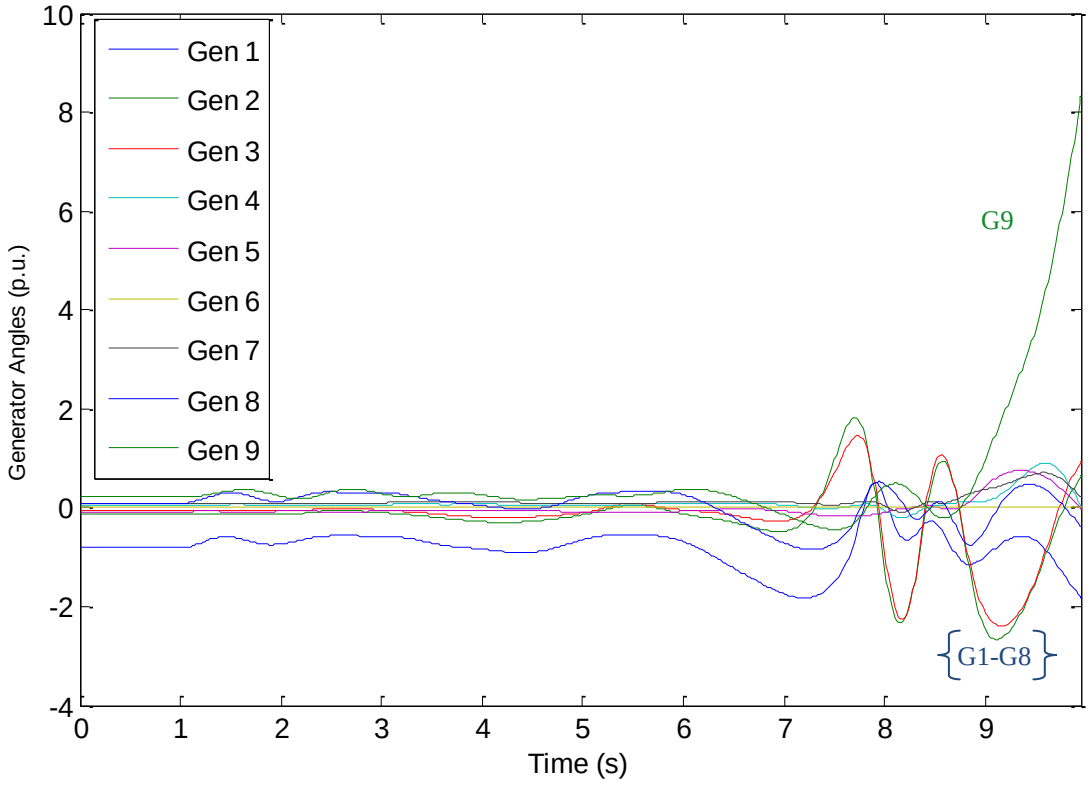

Figure 9.13: *Transient stability status in the sick island after controlled islanding scheme is assumed to happen beyond critical islanding time.*

The healthy island contained the remaining generators (G10, G11, G12, G13, G14, G15, G16). Table 9.10 shows the results of the updating calculation by SIME 0.4 s after islanding was implemented at 7.8 s. The obtained stability margin was found to be 1.69 $(rad/sec)^2$, which indicates a transiently stable status in the healthy island. The unstable equilibrium angle was calculated as 2.381 rad. The transient stability assessment using SIME also matched the results of the time-domain simulation, which are shown in Figure 9.14. As shown in Figure 9.14, the generator angle of G11 was chosen as the reference angle. Although it oscillated with the remaining generators in the healthy island, it maintained its transient stable status.

Table 9.10: *Transiently stable indication in the healthy island after controlled islanding scheme was implemented beyond critical islanding time.*

Time after Last Contingency t_i (ms)	Unstable Equilibrium Angle (rad)	Stability Margin η (rad/sec)^2
400	2.250	6.44
460	2.225	0.84
500	2.222	1.14
560	2.220	2.45
600	2.214	4.33
660	2.285	9.28
700	2.319	5.57
760	2.381	1.69

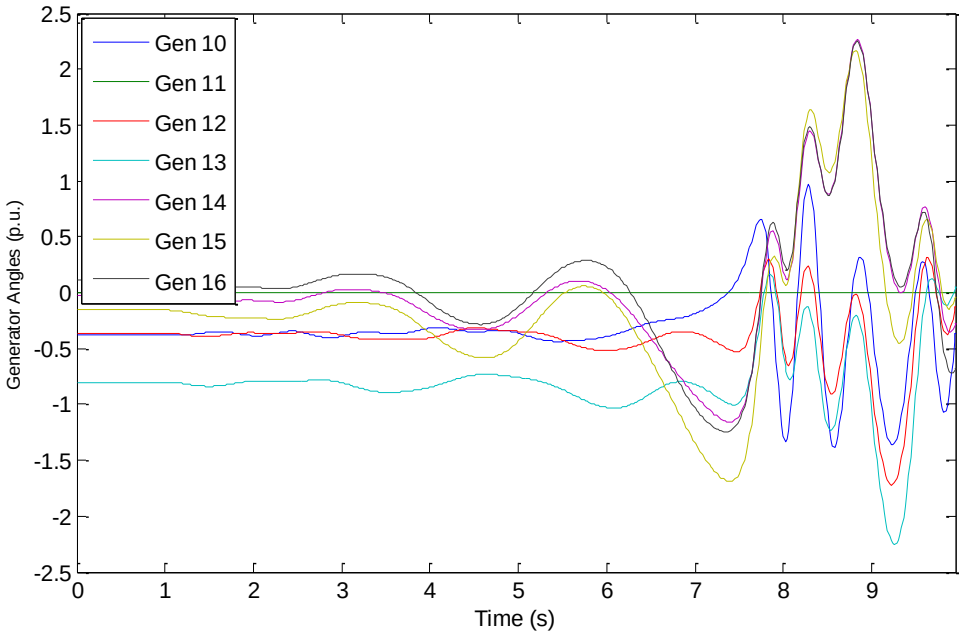

Figure 9.14: *Transient stability status in the healthy island after controlled islanding scheme is assumed to happen beyond critical islanding time.*

9.3 How Long Does It Take to Execute the Three-Stage Procedure?

The analysis and calculation in the proposed three-stage procedure must be conducted as quickly as possible in order to leave enough time for the islanding process. Therefore,

SIME was used because it calculates only the stability margin based on the transformed OMIB system. In the case study on the 39-busbar system, using an Intel Core 2.93 GHz processor with 4 GB of RAM, the time consumed by using SIME in both Stage 1 and Stage 3 to predict transient stability was 0.33 s. This included running the power flow (0.03 s) to identify the next expected tripped line, the short-time TDS (0.1 sec) assuming the next line was tripped, and running the SIME codes (0.2 sec) to obtain the stability margin. In addition, 0.03 s were required to obtain the islanding cut sets, which included finding the islanding candidates based on tracing and identifying the best islanding solution through optimization in terms of minimal power flow disruption. Thus, the total amount of time consumed in the three-stage controlled islanding scheme was 0.36 s, which is less than the 0.9 s identified as the time margin, that is, as CIT.

In the case study on the 68-busbar system, the total time used to predict transient stability was 0.98 s in the three-stage controlled islanding scheme. This included the power flow calculation (0.04 s), the short-time TDS (0.1 s), running the SIME codes (0.8 s) and identifying the islanding cut sets (0.04 s). This total amount of time consumed was 0.98 s, which was less than that identified by CIT, which was 1.62 s. Therefore, in this controlled islanding scheme, the amount of time used to predict increased with the size and complexity of the system. Moreover, even if SIME was run after the last expected tripped line was actually tripped, the time used by SIME to indicate transient instability was still less than that identified by CIT. In the proposed controlled islanding scheme, SIME runs by assuming that the identified last expected tripped line is tripped, which to some extent gives enough time to run the SIME before it actually tripped at some point.

9.4 Summary

This chapter proposes a framework for the adaptive three-stage controlled islanding scheme used as a last resort action to prevent widespread blackouts. The framework includes when to island, where to island and the evaluation of dynamic stability. The SIME method is used in this controlled islanding scheme to predict transient stability status in order to determine when to island. In addition, SIME is used to evaluate the

dynamic stability in each island that is identified by the controlled islanding scheme, which uses the power flow tracing method. Power flow tracing provides islanding cut sets that are used in SIME to assess issues in stability. The framework using SIME in an online application with measurement data from SCADA is also demonstrated. The IEEE 10-generator 39-bus system with classical generator models and 16-generator 68-bus system with fourth-order generator models and Type-2 exciter installed are used to test the three-stage controlled islanding scheme during cascading line outages. The results of the calculation of transient stability using SIME in the two test systems demonstrated that they matched the time-domain simulation. Regarding calculation speed, the total amount of time used in the three stages in the controlled islanding scheme was less than critical islanding time. In other words, when the stability margin was identified, there was time remaining before system lost synchronism between the generator groups. Regarding accuracy, SIME was relatively conservative in a small number of cases when the cascading lines were tripped. When the second from the last line was tripped, SIME showed instability before the last line was actually tripped. However, in most cases, SIME gave accurate results that aligned with those obtained in the time-domain simulation when the last line was tripped in both case studies.

Chapter 10:

Conclusion and Future Work

In this thesis, the controlled islanding scheme was investigated as a last resort action to prevent blackouts. The idea for this research arose from recent events in which the usual control methods failed and blackouts occurred around the world, such as the India blackout in 2011 and the US/Canada blackout in 2003. The controlled islanding scheme consists of a framework of three closely connected work packages: when to island, where to island and the dynamic evaluation of each formed island. This thesis contributes to the analysis of the dynamic characteristics of cascading outages. The SIME method was used online to predict the system's collapse in terms of transient instability, giving time to respond and support decisions to implement controlled islanding scheme as a last resort when system collapse or blackout is imminent. In addition, the power flow tracing method was adopted to determine the islanding cutsets. The power flow tracing method was used to isolate the sick islands and prevent the disturbance from spreading to the remaining healthy network. In this method, power flow tracing divides the entire network into two parts through the cut lines. The cut lines are identified as weakly connected lines in which the power flows are relatively low. When the islands were identified, SIME was adopted to assess the transient stability of both the sick island and the healthy island to ensure that they were stable before the islanding scheme was implemented. Because islanding is a disturbance, it might cause subsequent instability in the formed islands.

10.1 Conclusion

Chapter 1 introduced the research background and objectives. Because blackouts have occurred in recent decades although control methods were used, environmentally controlled islanding methods were proposed as a last-resort action. A framework of controlled islanding was proposed, including when to island, where to island and the evaluation of dynamic stability in each island after islanding. The previous research on

this topic was briefly described. Our contribution to knowledge was compared with the previous research on the controlled islanding scheme.

Chapter 2 begins by describing blackouts that happened in recent decades, including the India blackout (2011), the California blackout (2011), the Brazil blackout (2009), the US/Canada blackout (2003), the Denmark/Sweden blackout (2003), the Italy blackout (2003) and the UCTE disturbance (2003). This thesis focused on dynamic stability during cascading outage. In addition, conventional prevention methods in the three-defence lines scheme were also described, particularly when the usual means failed in the relevant cases of blackouts.

Chapter 3 focused on the assessment of power system security. It began with factors that affect system security assessment and then introduced online dynamic security assessment. It reviewed the previous research on the development of direct methods to assess transient stability in order to get rid of the time-consuming numerical integration approach. The criteria for the security of the power system and the classification of power system's stability were explained. The well-known swing equations of generators and equal area criterion in power-angle curve were presented. This is the fundamental principle of the methodologies of EEAC and SIME, which are explained in Chapter 7 and Chapter 8.

Chapter 4 reviewed the previous islanding methods in terms of when to island and where to island. Regarding when to island, the decision tree was proposed previously. It was built offline using offline simulation data on a system's collapse. A case study of 14-busbar system was used to demonstrate training a decision tree offline for online application. However, decision tree based methods are too inflexible for use in power systems with continuously updating system topology. In addition, regarding where to island, the OBDD, spectral graph theory and slow coherency-based methods were reviewed.

Chapter 5 proposed the novel approach of power flow tracing. This method is practical because it isolates the sick island, leaving the remaining healthy island intact without any further splitting and unnecessary disruption. It also identifies the cut lines with the least power flow, causing the least impact on the system. In terms of transient stability in the formed islands, power flow tracing-based methods identify reliable islanding

cutsets. Specific details regarding the power flow tracing method and its application in 39-busbar system are explained. In addition, islanding solutions using different indices are also discussed, such as different transient weight, voltage weight and frequency weight.

Chapter 6 summarizes the reasons that the generators in the US/Canada blackout (2003) and the Italy blackout (2003) were tripped. The protections for the generators are specified as well as protection used on the lines. Different generator models are introduced. The case study of a 39-busbar system is conducted to simulate a cascading line trip environment, in which important scenarios are observed, such as increased overloading on adjacent lines caused by the tripping of neighbouring lines, voltage drop and the malfunction in distance protection in the cascading environment.

In Chapter 7 and Chapter 8, the methodology of EEAC and SIME are described in detail. They are based on the same fundamental principle to transform a multi-machine system to a single-machine-infinite-busbar system. The final proposed approach using SIME was applied in the three-stage controlled islanding scheme to support decisions about when to island. The novel contribution of this research is that it uses SIME to formulate and assess transient stability during cascading line trips instead of the conventional fault applied on a line. In addition, this thesis proposes a framework for three-stage controlled islanding. In deciding when to island, the framework used SIME online to predict transient stability. In the case study, the cascading line trip environment is simulated. Assuming that the next expected tripped line is known, SIME was used online to predict transient stability status and decide whether the next expected line was at the "point of no return". If so, SIME was used to assess the transient stability status in each island after the islanding cut sets were provided by the power tracing method. If not, SIME continued monitoring the system's transient stability status after each line was tripped.

Chapter 9 presents the results of the case studies of the 39-busbar system and the 68-busbar system. Both sets of results showed that SIME matched the time-domain simulation. In addition, the time left to instability was obtained by SIME when the last line of "point of no return" was assumed to be tripped. The time left to instability was the critical islanding time that remained to respond and take islanding actions, which

also matched time left to instability in the time-domain simulation in the study case. The critical islanding time was obtained before the next expected line was tripped. However, it was subject to the cascading speed.

10.2 Future Work

In this thesis, the online application of SIME used to decide when to island was based on certain assumptions. The online transient stability assessment in the predictive mode was based on the assumption that the next expected tripped line could be predicted in advance. In some low-voltage-rating transmission networks, this could be obtained based on the thermal characteristics of the overcurrent protection installed in each line. In control rooms, N-1 contingency analysis is implemented every ten minutes, so the system operators know which line will overload if a particular fault happens, and the relevant line is assumed to be tripped. However, in high-voltage-rating transmission networks, distance protection is normally installed in each line. Therefore, it is difficult to know in advance. In addition, the network configuration in the transmission network is not radial; instead, it is a complicated meshed power network. The back-up Zone 3 distance protection, which is a two-line distance away from the faulted line, may operate because of the inappropriate integration of distance relays in a meshed power system, especially across the borders between two areas or two countries. This could accelerate the speed of cascading outages. Future research should investigate how distance protections are affected by cascading line outages.

Voltage stability is another issue for future research. It is well known that voltage collapse leads to the collapse of local systems. However, this thesis mainly focused on online transient stability assessment during cascading outages, which could result in global system collapse. Currently, voltage stability assessment is based on small-signal stability analysis. However, during the dynamic process the operating condition keeps varying, so small-signal stability analysis would not satisfy the accuracy of voltage stability assessment. Online dynamic voltage stability assessment is still being investigated for its online application. Future research should investigate online voltage stability assessment during cascading outages to check the voltage cross the threshold

value or assess the distance from the monitored voltage to the threshold value. The more online assessment tools that we have, the more reliable and supportive information we can gain about the operation of systems and the better we will be able to implement the controlled islanding scheme in a reliable manner.

Appendix A:

Modelling and Protection

A.1 Generator Modelling

Power system generators play a significant role in dynamic change under a contingency situation. Any dynamic behaviour in the power system is linked to generator modelling, particularly any oscillation occurs in variables in the network is caused by the oscillation of the generator angle. Therefore, different generator models have different effects on the system's dynamic behaviour under disturbance. The generator models in a power network within the scope of this research. They will be used to test the methodology implemented to achieve the research objective. Some generator models are listed in the following section, including classic second-order, fourth-order and sixth-order generator modelling. Different orders of generator models represent different numbers of state variables that are used to describe the generator's dynamic behaviour. These three generator models are described as follows:

➢ Second-order generator model

In the second-order model, the state variables used to describe the generator's dynamic behaviour are generator angle δ and angular speed ω. In [83][84], the two state variables were described by two differential equations as follows:

$$\dot{\delta} = \Omega_b (\omega - 1) \tag{A.1}$$

$$\dot{\omega} = \left(P_m - P_e - D(\omega - 1)\right) / M \tag{A.2}$$

where, Ω_b is the angular speed coefficient; D is the damping coefficient; M is the mechanical starting time; P_m is the mechanical power; P_e is the electrical power; and P_e is defined as follows:

$$P_e = \left(v_q + r_a i_q\right) i_q + \left(v_d + r_a i_d\right) i_d \tag{A.3}$$

where v_q and i_q are q-axis voltage and current; v_d and i_d are d-axis voltage and current; and r_a is armature resistance. The generator terminal voltage and current relationship is described as

$$0 = v_q + r_a i_q - e_q^{'} + \left(x_d^{'} - x_l\right) i_d \tag{A.4}$$

$$0 = v_d + r_a i_d - \left(x_d^{'} - x_l\right) i_q \tag{A.5}$$

where x_l is leakage reactance; $x_d^{'}$ is d-axis transient reactance; $e_q^{'}$ is q-axis transient voltage, which is constant because in the classic generator model, no field current is introduced into the modelling, which helps adjust the generator terminal voltage.

➢ Fourth-order generator model

In the fourth-order generator model, there are four state variables, which are expected to change during the transient process. In addition to the generator angle and angular speed, the q-axis transient voltage $e_q^{'}$ and d-axis transient voltage $e_d^{'}$ are introduced into the generator modelling, which are used to form q-axis and d-axis inductances because of the field winding effect. In [83][84] the four variables were described by the four following differential equations:

$$\dot{\delta} = \Omega_b \left(\omega - 1\right) \tag{A.6}$$

$$\dot{\omega} = \left(P_m - P_e - D\left(\omega - 1\right)\right) / M \tag{A.7}$$

$$\dot{e}_q^{'} = (-f_s(e_q^{'}) - (x_d - x_d^{'}) i_d + v_f^{*}) / T_{d0}^{'} \tag{A.8}$$

$$\dot{e}_d^{'} = (-e_d^{'} + (x_q - x_q^{'}) i_q) / T_{q0}^{'} \tag{A.9}$$

where x_d and $x_d^{'}$ are d-axis synchronous reactance and transient reactance; x_q and $x_q^{'}$ are q-axis synchronous reactance and transient reactance; $T_{d0}^{'}$ and $T_{q0}^{'}$ are d-axis and q-axis open circuit transient time constant; and v_f^{*} is the field current, which is controlled by the AVR to adjust generator voltage. The remaining variables are the same as those in the second-order generator model. The generator terminal voltage and current relationship with the introduced transient components can be expressed as follows:

$$0 = v_q + r_a i_q - e_q^{'} + \left(x_d^{'} - x_l\right) i_d \tag{A.10}$$

$$0 = v_d + r_a i_d - e_d^{'} - \left(x_q^{'} - x_l\right) i_q \tag{A.11}$$

➢ Sixth-order generator model

Compared with the fourth-order model, the sixth-order model is more accurate and it introduces extra sub-transient components, which link to the effect of damper winding. It introduces more sub-transient inductance into the d-axis and the q-axis of the circuit, which can be presented by the d-axis and q-axis sub-transient voltage $e_d^{"}$ and $e_q^{"}$. Therefore, the six state variables can be expressed as follows [83][84]:

$$\dot{\delta} = \Omega_b \left(\omega - 1\right) \tag{A.12}$$

$$\dot{\omega} = \left(P_m - P_e - D\left(\omega - 1\right)\right) / M \tag{A.13}$$

$$\dot{e}_q^{'} = (-f_s(e_q^{'}) - (x_d - x_d^{'} - \frac{T_{d0}^{"}}{T_{d0}^{'}} \frac{x_d^{"}}{x_d^{'}} (x_d^{'} - x_d^{"}))i_d + (1 - \frac{T_{AA}}{T_{d0}^{'}})v_f^{*}) / T_{d0}^{'} \tag{A.14}$$

$$\dot{e}_d^{'} = (-e_d^{'} + (x_q - x_q^{'} - \frac{T_{q0}^{"}}{T_{q0}^{'}} \frac{x_q^{"}}{x_q^{'}} (x_q - x_q^{'}))i_q) / T_{q0}^{'} \tag{A.15}$$

$$\dot{e}_q^{"} = (-e_q^{"} + e_q^{'} - (x_d^{'} - x_d^{"} + \frac{T_{d0}^{"}}{T_{d0}^{'}} \frac{x_d^{"}}{x_d^{'}} (x_d - x_d^{'}))i_d + \frac{T_{AA}}{T_{d0}^{'}} v_f^{*}) / T_{d0}^{"} \tag{A.16}$$

$$\dot{e}_d^{"} = (-e_d^{"} + e_d^{'} + (x_q^{'} - x_q^{"} + \frac{T_{q0}^{"}}{T_{q0}^{'}} \frac{x_q^{"}}{x_q^{'}} (x_q - x_q^{'}))i_q) / T_{q0}^{"} \tag{A.17}$$

where $x_d^{"}$ and $x_q^{"}$ are the d-axis and q-axis sub-transient reactance; $T_{d0}^{"}$ and $T_{q0}^{"}$ are d-axis and q-axis open circuit sub-transient time constant. The remaining state variables are the same as those in the fourth-order generator model. The generator terminal voltage and the current relationship with both transient and sub-transient components introduced can be expressed as follows:

$$0 = v_q + r_a i_q - e_q^{"} + \left(x_d^{"} - x_l\right) i_d \tag{A.18}$$

$$0 = v_d + r_a i_d - e_d^{"} - \left(x_q^{"} - x_l\right) i_q \tag{A.19}$$

A.2 Generator Protection

The safe operation of the generator cannot be guaranteed without the installation of corresponding protection. The most widely used devices used to protect generators are as follows:

- Under-voltage protection: Under-voltage protection is used as low voltage protection at the generator terminal in case of the failure of the AVR. The setting of under-voltage relays in [87] could be either inverse time characteristics when the voltage drops to 90% of the rated voltage after a 9-s delay, or it could respond instantaneously when the voltage decreases to 80% of the rated voltage.

- Over-voltage protection: Normally, over-voltage protection is provided for hydro generating units and combustion turbine units. When no AVR or backup protection is required, overvoltage relays are used. The setting of overvoltage relays [62] could either have a pickup of value at above 110% of rated voltage with a time delay of about 5-10 s based on inverse time characteristics or respond instantaneously performance when the voltage exceeds the value of 130%-150% of the voltage rating.

- Under-frequency protection: In order to achieve a power balance in system, under-frequency load shedding will take action before the frequency reaches 47.7 Hz [1]. When the frequency drops to 47.5 Hz, which is the minimum frequency setting for under-frequency protection, the latter intervenes and trips the generators.

- Over-speed (over-frequency) protection: Normally, the detection of high frequency can be an indication of unintended island operation, in which the generation is more than the demand. This may cause additional mechanical stresses or even damage to the rotor. Hence, the installed over-frequency relay aims to protect and trip the generator. Normally, the threshold is set at +2 Hz of the nominal frequency [1].

- Loss-of-field protection and overloading field protection: In the excitation system of generators, the OEL is generally sleeping unless the field current is required to increase and exceeds its thermal limit. The limiter is then activated, and it sends a signal to the reference voltage of AVR to prevent it from trying to provide more field current.

Meanwhile, the field current is maintained at its maximum value without violating the threshold.

A.3 Transmission Network Protection

➢ Overcurrent Protection

In the network, the fundamental and most often used type of protection is the overcurrent relay. The settings of overcurrent relays have to coordinate with the other relays located in the network so that under fault conditions, the relays that are required to be tripped actually trip. At present, most overcurrent relays are inverse time overcurrent relays, which are advantageous in adapting to the increasing size and complexity of power systems.

In addition, overcurrent relays monitor the primary current in a network by monitoring the secondary current obtained via the current transformer (CT) whose primary winding is connected in high-voltage distribution lines. Typically, the secondary current is rated at either 1A or 5A, which can also be adjusted by the plug scale multiplier (PSM) to match the rated primary current of CT the current setting of the relays. IEC 60255 defined standard characteristics of IDMT relays that have different time/current tripping characteristics. These are according to the following defined standard equations shown in Table A.1.

Table A.1: *Relay characteristics and corresponding equations [89]*.

Relay Characteristic	Equation (IEC60255)
Standard Inverse (SI)	$t = TMS \times 0.14 / I_r^{0.02} - 1$
Very Inverse (VI)	$t = TMS \times 13.5 / I_r - 1$
Extremely Inverse (EI)	$t = TMS \times 80 / I_r^2 - 1$
Long time standard earth fault	$t = TMS \times 120 / I_r - 1$

where, $I_r = \dfrac{I}{PSM \cdot I_N}$, I is the faulted current monitored by the relay; I_N is the nominal current of the relay; PSM is the plug scale multiplier, which is used to adjust the setting of the relay current. Normally, in order to achieve both sensitivity and operation reliability, it is usual to set the pickup current (which is equal to $PSM \cdot I_N$) well above twice the maximum of the load current expected in the network and below half the minimum fault current, which also can be shown as $I_{pickup} > 2 \times I_{load-\max}$, $I_{pickup} < \dfrac{1}{2} \times I_{fault-\min}$. In Table A.1. TMS is the time multiplier setting, which is used to obtain time discrimination between the main relay located near the fault area and the back-up relays on the same line in order to achieve better selectivity.

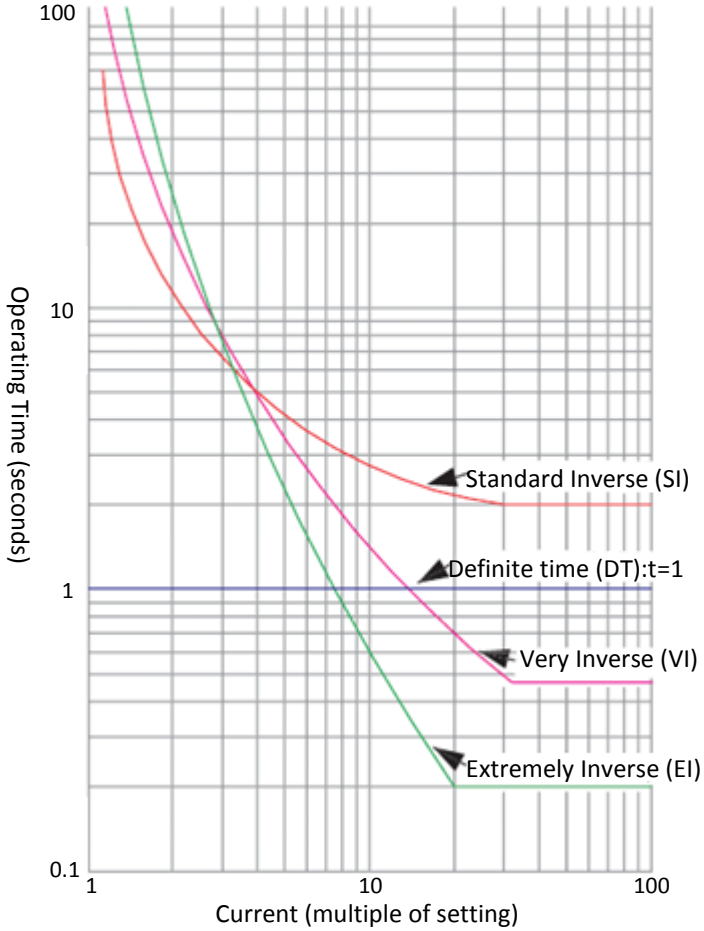

Figure A.1: *Characteristics of different type of IDMT overcurrent relays [89].*

In Figure A.1, the relay characteristics are inverse ratio curves. The larger the overcurrent is, the less time the circuit breaker needs to clear the faulted line.

➢ Distance Protection

The primary advantages of overcurrent protection are simplicity, reliability and low cost. However, in complicated high-voltage transmission, the sensitivity, rapidity and selectivity of overcurrent protection cannot be guaranteed. Under this circumstance, distance protection is used in transmission networks. It determined the location where faults occur, and it is not susceptible to operation status and network topology [15]. Figure A.2 shows three zones of distance protection in transmission lines.

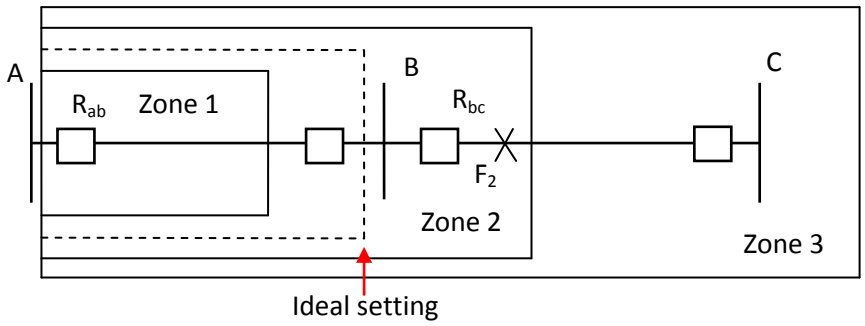

Figure A.2: *Stepped distance protection [15]*.

In Figure A.2 the under reaching Zone-1 is set between 80% and 90% of the first line length. The distance relay (DR) in this zone operates instantaneously. The overreaching Zone-2 is set at 120%-150% of the first line length AB as the back-up operation, which is beyond the remote terminal of the first line. The DR operates after a coordination time delay of 0.3 seconds. Zone-3 is set at 120%-180% of the second line BC as the back-up protection for the entire line BC. Similarly, the DR has a delayed tripping time of 1 s.

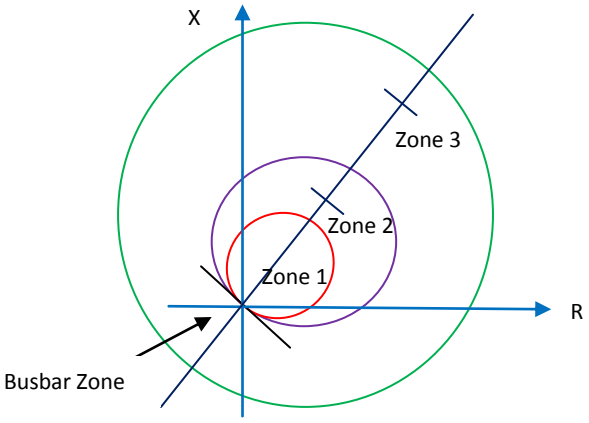

Figure A.3: *Complex R-X diagram for characteristics of DR [87].*

Figure A.3 shows a complex R-X diagram using the impedance characteristics of DR, which is a circle with a circumference that passes through the origin of coordinates. This indicates that the impedance element is directional. The DR only operates for the faults in the forward direction on the straight line, not in the reverse direction. In addition, the impedance characteristic can be adjusted by setting the impedance, which is the diameter of the circle, to finish the reach control. When a fault occurs and the value of the fault impedance is a characteristic, the DR will operate. The characteristic equation of the DR is as follows:

$$\left| Z_{measure} - \frac{1}{2} Z_{set} \right| \leq \left| \frac{1}{2} Z_{set} \right| \tag{20}$$

Appendix B:

System data for simulated network

Appendix B consists of the system data used for 39-busbar and 68-busbar systems' simulation in Chapter 9. The date are represented in MATLAB-based PSAT fomat [83]-[84], including all of components and devices, such as busbar, line, slack bus, PQ bus, PV bus, synchronous generator, excitor and governor.

B.1 39-bus system

```
Bus.con = [ ...
  1   1.00  1.048    -0.1646   1 1;
  2   1.00  1.0505   -0.1203   1 1;
  3   1.00  1.0341   -0.1698   1 1;
  4   1.00  1.0116   -0.1838   1 1;
  5   1.00  1.0165   -0.1637   1 1;
  6   1.00  1.0172   -0.1515   1 1;
  7   1.00  1.0067   -0.1892   1 1;
  8   1.00  1.0057   -0.1979   1 1;
  9   1.00  1.0322   -0.1946   1 1;
 10   1.00  1.0235   -0.1101   1 1;
 11   1.00  1.0201   -0.1243   1 1;
 12   1.00  1.0072   -0.1246   2 1;
 13   1.00  1.0207   -0.1225   3 1;
 14   1.00  1.0181   -0.1511   4 1;
 15   1.00  1.0194   -0.1581   5 1;
 16   1.00  1.0346   -0.1337   6 1;
 17   1.00  1.0365   -0.1510   7 1;
 18   1.00  1.0343   -0.1656   8 1;
 19   1.00  1.0509   -0.0531   9 1;
 20   1.00  0.9914   -0.0777   1 1;
 21   1.00  1.0337   -0.0918   1 1;
 22   1.00  1.0509   -0.0143   2 1;
 23   1.00  1.0459   -0.0178   3 1;
 24   1.00  1.0399   -0.1316   4 1;
 25   1.00  1.0587   -0.0962   5 1;
 26   1.00  1.0536   -0.1182   6 1;
 27   1.00  1.0399   -0.1532   7 1;
 28   1.00  1.0509   -0.0571   8 1;
 29   1.00  1.0505   -0.0089   9 1;
```

```
 30   1.00  1.0475  -0.0780   1 1;
 31   1.00  0.9820  -0.0308   1 1;
 32   1.00  0.9831   0.0284   2 1;
 33   1.00  0.9972   0.0380   3 1;
 34   1.00  1.0123   0.0129   4 1;
 35   1.00  1.0493   0.0723   5 1;
 36   1.00  1.0635   0.1192   6 1;
 37   1.00  1.0278   0.0220   7 1;
 38   1.00  1.0265   0.1143   8 1;
 39   1.00  1.0300  -0         9 1;];

Line.con = [ ...
1   2   100.00   1.00 60 0  0  0.00350  0.04110  0.69870  1.00000  0  0   0  0  1;
1   39 100.00   1.00 60 0  0  0.00100  0.02500  0.75000  1.00000  0  0   0  0  1;
2   3   100.00   1.00 60 0  0  0.00130  0.01510  0.25720  1.00000  0  0   0  0  1;
2   25 100.00   1.00 60 0  0  0.00700  0.00860  0.14600  1.00000  0  0   0  0  1;
2   30 100.00   1.00 60 0  1.025   0    0.01810  0.00000  1.02500  0  0   0  0  1;
3   18 100.00   1.00 60 0  0  0.00110  0.01330  0.21380  1.00000  0  0   0  0  1;
4   5   100.00   1.00 60 0  0  0.00080  0.01280  0.13420  1.00000  0  0   0  0  1;
4   14 100.00   1.00 60 0  0  0.00080  0.01290  0.13820  1.00000  0  0   0  0  1;
5   8   100.00   1.00 60 0  0  0.00080  0.01120  0.14760  1.00000  0  0   0  0  1;
6   5   100.00   1.00 60 0  0  0.00020  0.00260  0.04340  1.00000  0  0   0  0  1;
6   7   100.00   1.00 60 0  0  0.00060  0.00920  0.11300  1.00000  0  0   0  0  1;
6   11 100.00   1.00 60 0  0  0.00070  0.00820  0.13890  1.00000  0  0   0  0  1;
7   8   100.00   1.00 60 0  0  0.00040  0.00460  0.07800  1.00000  0  0   0  0  1;
8   9   100.00   1.00 60 0  0  0.00230  0.03630  0.38040  1.00000  0  0   0  0  1;
9   39 100.00   1.00 60 0  0  0.00100  0.02500  1.20000  1.00000  0  0   0  0  1;
10  11 100.00   1.00 60 0  0  0.00040  0.00430  0.07290  1.00000  0  0   0  0  1;
10  13 100.00   1.00 60 0  0  0.00040  0.00430  0.07290  1.00000  0  0   0  0  1;
10  32 100.00   1.00 60 0  1.07  0      0.02000  0.00000  1.07000  0  0   0  0  1;
12  11 100.00   1.00 60 0  1.006  0.00160  0.04350   0    1.00600  0  0   0  0  1;
12  13 100.00   1.00 60 0  1.006  0.00160  0.04350   0    1.00600  0  0   0  0  1;
13  14 100.00   1.00 60 0  0  0.00090  0.01010  0.17230  1.00000  0  0   0  0  1;
14  15 100.00   1.00 60 0  0  0.00180  0.02170  0.36600  1.00000  0  0   0  0  1;
15  16 100.00   1.00 60 0  0  0.00090  0.00940  0.17100  1.00000  0  0   0  0  1;
16  17 100.00   1.00 60 0  0  0.00070  0.00890  0.13420  1.00000  0  0   0  0  1;
16  19 100.00   1.00 60 0  0  0.00160  0.01950  0.30400  1.00000  0  0   0  0  1;
16  21 100.00   1.00 60 0  0  0.00080  0.01350  0.25480  1.00000  0  0   0  0  1;
16  24 100.00   1.00 60 0  0  0.00030  0.00590  0.06800  1.00000  0  0   0  0  1;
17  18 100.00   1.00 60 0  0  0.00070  0.00820  0.13190  1.00000  0  0   0  0  1;
17  27 100.00   1.00 60 0  0  0.00130  0.01730  0.32160  1.00000  0  0   0  0  1;
19  33 100.00   1.00 60 0  1.07  0.00070  0.01420   0    1.07000  0  0   0  0  1;
19  20 100.00   1.00 60 0  1.06  0.00070  0.01380   0    1.06000  0  0   0  0  1;
20  34 100.00   1.00 60 0  1.009 0.00090  0.01800   0    1.00900  0  0   0  0  1;
21  22 100.00   1.00 60 0  0  0.00080  0.01400  0.25650  1.00000  0  0   0  0  1;
22  23 100.00   1.00 60 0  0  0.00060  0.00960  0.18460  1.00000  0  0   0  0  1;
22  35 100.00   1.00 60 0  1.025  0    0.01430       0    1.02500  0  0   0  0  1;
23  24 100.00   1.00 60 0  0  0.00220  0.03500  0.36100  1.00000  0  0   0  0  1;
23  36 100.00   1.00 60 0  1  0.00050  0.02720       0    1.00000  0  0   0  0  1;
```

```
25  26 100.00   1.00 60 0  0  0.00320  0.03230  0.51300  1.00000  0  0   0  0  1;
25  37 100.00   1.00 60 0  1.025 0.00060  0.02320   0      1.02500  0  0   0  0  1;
26  27 100.00   1.00 60 0  0  0.00140  0.01470  0.23960  1.00000  0  0   0  0  1;
26  28 100.00   1.00 60 0  0  0.00430  0.04740  0.78020  1.00000  0  0   0  0  1;
26  29 100.00   1.00 60 0  0  0.00570  0.06250  1.02900  1.00000  0  0   0  0  1;
28  29 100.00   1.00 60 0  0  0.00140  0.01510  0.24900  1.00000  0  0   0  0  1;
29  38 100.00   1.00 60 0  1.025 0.00080  0.01560   0      1.02500  0  0   0  0  1;
6   31 100.00   1.00 60 0  1.07     0     0.02500         0      1.07000  0  0   0  0  1;
3   4   100.00   1.00 60 0  0  0.00130  0.02130  0.22140  1.00000  0  0   0  0  1; ];

SW.con = [ ...
 39 100.0   1.00  1.0300    0    15   -10     1.1 0.9  10 1;];


PQ.con = [ ...
   1  100.0   1.00  0.0000   0.0000  1.1  0.9 1;
   2  100.0   1.00  0.0000   0.0000  1.1  0.9 1;
   3  100.0   1.00  3.2200   0.0240  1.1  0.9 1;
   4  100.0   1.00  5.0000   1.8400  1.1  0.9 1;
   5  100.0   1.00  0.0000   0.0000  1.1  0.9 1;
   6  100.0   1.00  0.0000   0.0000  1.1  0.9 1;
   7  100.0   1.00  2.3380   0.8400  1.1  0.9 1;
   8  100.0   1.00  5.2200   1.7600  1.1  0.9 1;
   9  100.0   1.00  0.0000   0.0000  1.1  0.9 1;
  10 100.0   1.00  0.0000   0.0000  1.1  0.9 1;
  11 100.0   1.00  0.0000   0.0000  1.1  0.9 1;
  12 100.0   1.00  0.0850   0.8800  1.1  0.9 1;
  13 100.0   1.00  0.0000   0.0000  1.1  0.9 1;
  14 100.0   1.00  0.0000   0.0000  1.1  0.9 1;
  15 100.0   1.00  3.2000   1.5300  1.1  0.9 1;
  16 100.0   1.00  3.2900   0.3230  1.1  0.9 1;
  17 100.0   1.00  0.0000   0.0000  1.1  0.9 1;
  18 100.0   1.00  1.5800   0.3000  1.1  0.9 1;
  19 100.0   1.00  0.0000   0.0000  1.1  0.9 1;
  20 100.0   1.00  6.2800   1.0300  1.1  0.9 1;
  21 100.0   1.00  2.7400   1.1500  1.1  0.9 1;
  22 100.0   1.00  0.0000   0.0000  1.1  0.9 1;
  23 100.0   1.00  2.4750   0.8460  1.1  0.9 1;
  24 100.0   1.00  3.0860   -0.922   1.1  0.9 1;
  25 100.0   1.00  2.2400   0.4720  1.1  0.9 1;
  26 100.0   1.00  1.3900   0.1700  1.1  0.9 1;
  27 100.0   1.00  2.8100   0.7550  1.1  0.9 1;
  28 100.0   1.00  2.0600   0.2760  1.1  0.9 1;
  29 100.0   1.00  2.8350   0.2690  1.1  0.9 1;
  39 100.0   1.00  11.040   2.5000  1.1  0.9 1;];

PV.con = [ ...
  30 100.0   1.00  2.5000   1.0475  8    -5    1.1 0.9 1;
  31 100.0   1.00  2.0000   0.985    8    -5    1.1 0.9 1;
  32 100.0   1.00  6.5000   0.9831  8    -5    1.1 0.9 1;
```

```
 33 100.0   1.00  6.3200   0.9972  8    -5    1.1 0.9 1;
 34 100.0   1.00  5.0800   1.0123  4    -3    1.1 0.9 1;
 35 100.0   1.00  6.5000   1.0493  8    -5    1.1 0.9 1;
 36 100.0   1.00  5.6000   1.0635  8    -5    1.1 0.9 1;
 37 100.0   1.00  5.4000   1.0278  8    -5    1.1 0.9 1;
 38 100.0   1.00  8.3000   1.0265  8    -5    1.1 0.9 1;];

Syn.con = [ ...
30  100.0  1.0  60  5  0.0125  0.00014  0.1000  0.0310   0    10.20  0    0.0690  0.0310  0
1.500  0    84.000     0  0  0  1  1  0.002;
31  100.0  1.0  60  5  0.035   0.00270  0.2950  0.0697   0    6.560  0    0.2820  0.170   0
1.500  0    60.600     0  0  0  1  1  0.002;
32  100.0  1.0  60  5  0.0304  0.000386 0.2495  0.0531   0    5.700  0    0.2370  0.0531  0
1.500  0    70.600     0  0  0  1  1  0.002;
33  100.0  1.0  60  5  0.0295  0.000222 0.2620  0.0436   0    5.690  0    0.2580  0.0436  0
1.500  0    57.200     0  0  0  1  1  0.002;
34  100.0  1.0  60  5  0.0540  0.00014  0.6700  0.1320   0    5.400  0    0.6200  0.1320  0
0.440  0    52.000     0  0  0  1  1  0.002;
35  100.0  1.0  60  5  0.0224  0.00615  0.2540  0.0500   0    7.300  0    0.2410  0.0500  0
0.400  0    69.600     0  0  0  1  1  0.002;
36  100.0  1.0  60  5  0.0322  0.000268 0.2950  0.0490   0    5.660  0    0.2920  0.0490  0
1.500  0    52.800     0  0  0  1  1  0.002;
37  100.0  1.0  60  5  0.0280  0.000686 0.2900  0.0570   0    6.700  0    0.2800  0.0570  0
0.410  0    48.600     0  0  0  1  1  0.002;
38  100.0  1.0  60  5  0.0298  0.00030  0.2106  0.0570   0    4.790  0    0.2050  0.0570  0
1.960  0    69.000     0  0  0  1  1  0.002;
39  100.0  1.0  60  5  0.0030  0.00010  0.0200  0.0060   0    7.000  0    0.019   0.008   0
0.700  0    1000.0     0  0  0  1  1  0.002;];
```

B.2 68-bus system

```
Bus.con = [ ...
  1      1      1          0;
  2      1      1          0;
  3      1      1          0;
  4      1      1          0;
  5      1      1          0;
  6      1      1          0;
  7      1      1          0;
  8      1      1          0;
  9      1      1          0;
 10      1      1          0;
 11      1      1          0;
 12      1      1          0;
 13      1      1          0;
 14      1      1          0;
 15      1      1          0;
```

16	1	1	0;
17	1	1	0;
18	1	1	0;
19	1	1	0;
20	1	1	0;
21	1	1	0;
22	1	1	0;
23	1	1	0;
24	1	1	0;
25	1	1	0;
26	1	1	0;
27	1	1	0;
28	1	1	0;
29	1	1	0;
30	1	1	0;
31	1	1	0;
32	1	1	0;
33	1	1	0;
34	1	1	0;
35	1	1	0;
36	1	1	0;
37	1	1	0;
38	1	1	0;
39	1	1	0;
40	1	1	0;
41	1	1	0;
42	1	1	0;
43	1	1	0;
44	1	1	0;
45	1	1	0;
46	1	1	0;
47	1	1	0;
48	1	1	0;
49	1	1	0;
50	1	1	0;
51	1	1	0;
52	1	1	0;
53	13.8	1.045	0;
54	13.8	0.98	0;
55	13.8	0.983	0;
56	13.8	0.997	0;
57	13.8	1.011	0;
58	13.8	1.05	0;
59	13.8	1.063	0;
60	13.8	1.03	0;
61	13.8	1.025	0;
62	13.8	1.01	0;
63	13.8	1	0;
64	13.8	1.016	0;

```
 65      13.8   1.011      0;
 66      13.8      1       0;
 67      13.8      1       0;
 68      13.8      1       0];

Line.con = [ ...
1   2  100    1  60  0   0   0.0035    0.0411    0.6987    0     0   0;
1   30 100    1  60  0   0   0.0008    0.0074    0.48      0     0   0;
2   3  100    1  60  0   0   0.0013    0.0151    0.2572    0     0   0;
2   25 100    1  60  0   0   0.007     0.0086    0.146     0     0   0;
2   53 100    1  60  0   10  0         0.0181    0         1.025 0   0;
3   4  100    1  60  0   0   0.0013    0.0213    0.2214    0     0   0;
3   18 100    1  60  0   0   0.0011    0.0133    0.2138    0     0   0;
4   5  100    1  60  0   0   0.0008    0.0128    0.1342    0     0   0;
4   14 100    1  60  0   0   0.0008    0.0129    0.1382    0     0   0;
5   6  100    1  60  0   0   0.0002    0.0026    0.0434    0     0   0;
5   8  100    1  60  0   0   0.0008    0.0112    0.1476    0     0   0;
6   7  100    1  60  0   0   0.0006    0.0092    0.113     0     0   0;
6   11 100    1  60  0   0   0.0007    0.0082    0.1389    0     0   0;
6   54 100    1  60  0   10  0         0.025     0         1.07  0   0;
7   8  100    1  60  0   0   0.0004    0.0046    0.078     0     0   0;
8   9  100    1  60  0   0   0.0023    0.0363    0.3804    0     0   0;
10  11 100    1  60  0   0   0.0004    0.0043    0.0729    0     0   0;
10  13 100    1  60  0   0   0.0004    0.0043    0.0729    0     0   0;
10  55 100    1  60  0   10  0         0.02      0         1.07  0   0;
12  11 100    1  60  0   0   0.0016    0.0435    0         1.06  0   0;
12  13 100    1  60  0   0   0.0016    0.0435    0         1.06  0   0;
13  14 100    1  60  0   0   0.0009    0.0101    0.1723    0     0   0;
14  15 100    1  60  0   0   0.0018    0.0217    0.366     0     0   0;
15  16 100    1  60  0   0   0.0009    0.0094    0.171     0     0   0;
16  17 100    1  60  0   0   0.0007    0.0089    0.1342    0     0   0;
16  19 100    1  60  0   0   0.0016    0.0195    0.304     0     0   0;
16  21 100    1  60  0   0   0.0008    0.0135    0.2548    0     0   0;
16  24 100    1  60  0   0   0.0003    0.0059    0.068     0     0   0;
17  18 100    1  60  0   0   0.0007    0.0082    0.1319    0     0   0;
17  27 100    1  60  0   0   0.0013    0.0173    0.3216    0     0   0;
19  20 100    1  60  0   0   0.0007    0.0138    0         1.06  0   0;
19  56 100    1  60  0   10  0.0007    0.0142    0         1.07  0   0;
20  57 100    1  60  0   10  0.0009    0.018     0         1.009 0   0;
21  22 100    1  60  0   0   0.0008    0.014     0.2565    0     0   0;
22  23 100    1  60  0   0   0.0006    0.0096    0.1846    0     0   0;
22  58 100    1  60  0   10  0         0.0143    0         1.025 0   0;
23  24 100    1  60  0   0   0.0022    0.035     0.361     0     0   0;
23  59 100    1  60  0   10  0.0005    0.0272    0         0     0   0;
25  26 100    1  60  0   0   0.0032    0.0323    0.531     0     0   0;
25  60 100    1  60  0   10  0.0006    0.0232    0         1.025 0   0;
26  27 100    1  60  0   0   0.0014    0.0147    0.2396    0     0   0;
26  28 100    1  60  0   0   0.0043    0.0474    0.7802    0     0   0;
26  29 100    1  60  0   0   0.0057    0.0625    1.029     0     0   0;
```

```
28  29  100    1   60   0   0   0.0014    0.0151    0.249    0       0    0;
29  61  100    1   60   0  10   0.0008    0.0156    0        1.025   0    0;
 9  30  100    1   60   0   0   0.00095   0.00915   0.145    0       0    0;
 9  36  100    1   60   0   0   0.0011    0.0098    0.17     0       0    0;
36  37  100    1   60   0   0   0.0005    0.0045    0.32     0       0    0;
34  36  100    1   60   0   0   0.0033    0.0111    1.45     0       0    0;
35  34  100    1   60   0   0   0.0001    0.0074    0        0.946   0    0;
33  34  100    1   60   0   0   0.0011    0.0157    0.202    0       0    0;
32  33  100    1   60   0   0   0.0008    0.0099    0.168    0       0    0;
30  31  100    1   60   0   0   0.0013    0.0187    0.333    0       0    0;
30  32  100    1   60   0   0   0.0024    0.0288    0.488    0       0    0;
 1  31  100    1   60   0   0   0.0016    0.0163    0.25     0       0    0;
31  38  100    1   60   0   0   0.0011    0.0147    0.247    0       0    0;
33  38  100    1   60   0   0   0.0036    0.0444    0.693    0       0    0;
38  46  100    1   60   0   0   0.0022    0.0284    0.43     0       0    0;
46  49  100    1   60   0   0   0.0018    0.0274    0.27     0       0    0;
 1  47  100    1   60   0   0   0.0013    0.0188    1.31     0       0    0;
47  48  100    1   60   0   0   0.00125   0.0134    0.2      0       0    0;
48  40  100    1   60   0   0   0.002     0.022     1.28     0       0    0;
35  45  100    1   60   0   0   0.0007    0.0175    1.39     0       0    0;
37  43  100    1   60   0   0   0.0005    0.0276    0        0       0    0;
43  44  100    1   60   0   0   0.0001    0.0011    0        0       0    0;
44  45  100    1   60   0   0   0.0025    0.073     0        0       0    0;
39  44  100    1   60   0   0   0         0.0411    0        0       0    0;
39  45  100    1   60   0   0   0         0.0839    0        0       0    0;
45  51  100    1   60   0   0   0.0002    0.0052    0.72     0       0    0;
50  52  100    1   60   0   0   0.0012    0.0288    2.06     0       0    0;
50  51  100    1   60   0   0   0.0009    0.0221    1.62     0       0    0;
49  52  100    1   60   0   0   0.0076    0.1141    1.16     0       0    0;
52  42  100    1   60   0   0   0.004     0.06      2.25     0       0    0;
42  41  100    1   60   0   0   0.004     0.06      2.25     0       0    0;
41  40  100    1   60   0   0   0.006     0.084     3.15     0       0    0;
31  62  100    1   60   0  10   0         0.026     0        1.04    0    0;
32  63  100    1   60   0  10   0         0.013     0        1.04    0    0;
36  64  100    1   60   0  10   0         0.0075    0        1.04    0    0;
37  65  100    1   60   0  10   0         0.0033    0        1.04    0    0;
41  66  100    1   60   0  10   0         0.0015    0        1       0    0;
42  67  100    1   60   0  10   0         0.015     0        1       0    0;
52  68  100    1   60   0  10   0         0.003     0        1       0    0;
 1  27  100    1   60   0   0   0.032     0.32      0.41     1       0    0];

SW.con = [ ...
 65   100   13.8   1.011   0   999   -999   1.5   0.5   35.91   1];

PV.con = [ ...
 53   100   13.8   2.5    1.045   999   -999   1.2   0.8   1;
 54   100   13.8   5.45   0.98    999   -999   1.2   0.8   1;
 55   100   13.8   6.5    0.983   999   -999   1.2   0.8   1;
 56   100   13.8   6.32   0.997   999   -999   1.2   0.8   1;
```

```
57    100    13.8    5.052    1.011    999    -999    1.2    0.8  1;
58    100    13.8      7      1.05     999    -999    1.2    0.8  1;
59    100    13.8    5.6      1.063    999    -999    1.2    0.8  1;
60    100    13.8    5.4      1.03     999    -999    1.2    0.8  1;
61    100    13.8      8      1.025    999    -999    1.2    0.8  1;
62    100    13.8      5      1.01     999    -999    1.2    0.8  1;
63    100    13.8     10      1        999    -999    1.2    0.8  1;
64    100    13.8    13.5     1.016    999    -999    1.2    0.8  1;
66    100    13.8    17.85    1        999    -999    1.2    0.8  1;
67    100    13.8    10       1        999    -999    1.2    0.8  1;
68    100    13.8    40       1        999    -999    1.2    0.8  1];

PQ.con = [ ...
 1    100    1    2.527     1.186     1.2    0.8  0;
 3    100    1    3.22      0.02      1.2    0.8  0;
 4    100    1    5         1.84      1.2    0.8  0;
 7    100    1    2.34      0.84      1.2    0.8  0;
 8    100    1    5.22      1.77      1.2    0.8  0;
 9    100    1    1.04      1.25      1.2    0.8  0;
12    100    1    0.09      0.88      1.2    0.8  0;
15    100    1    3.2       1.53      1.2    0.8  0;
16    100    1    3.29      0.32      1.2    0.8  0;
18    100    1    1.58      0.3       1.2    0.8  0;
20    100    1    6.8       1.03      1.2    0.8  0;
21    100    1    2.74      1.15      1.2    0.8  0;
23    100    1    2.48      0.85      1.2    0.8  0;
24    100    1    3.09     -0.92      1.2    0.8  0;
25    100    1    2.24      0.47      1.2    0.8  0;
26    100    1    1.39      0.17      1.2    0.8  0;
27    100    1    2.81      0.76      1.2    0.8  0;
28    100    1    2.06      0.28      1.2    0.8  0;
29    100    1    2.84      0.27      1.2    0.8  0;
33    100    1    1.12      0         1.2    0.8  0;
36    100    1    1.02     -0.1946    1.2    0.8  0;
37    100    1    60        3         1.2    0.8  0;
39    100    1    2.67      0.126     1.2    0.8  0;
40    100    1    0.6563    0.2353    1.2    0.8  0;
41    100    1    10        2.5       1.2    0.8  0;
42    100    1    11.5      2.5       1.2    0.8  0;
44    100    1    2.676     0.0484    1.2    0.8  0;
45    100    1    2.08      0.21      1.2    0.8  0;
46    100    1    1.507     0.285     1.2    0.8  0;
47    100    1    2.031     0.3259    1.2    0.8  0;
48    100    1    2.412     0.022     1.2    0.8  0;
49    100    1    1.64      0.29      1.2    0.8  0;
50    100    1    1        -1.47      1.2    0.8  0;
51    100    1    3.37     -1.22      1.2    0.8  0;
52    100    1    24.7      1.23      1.2    0.8  0;];
```

Syn.con=[...

53 100 13.8 60 4 0.01 0 0.1 0.031 0.03 10.2 0.05 0.07 0.03 0.03
1.5 0.04 84 4 0 0 1 1 1 0;
54 100 13.8 60 4 0.04 0 0.3 0.07 0.05 6.56 0.05 0.28 0.06 0.05
1.5 0.04 60.4 9.8 0 0 1 1 1 0;
55 100 13.8 60 4 0.03 0 0.25 0.053 0.05 5.7 0.05 0.24 0.05 0.05
1.5 0.04 71.6 10 0 0 1 1 1 0;
56 100 13.8 60 4 0.03 0 0.26 0.044 0.04 5.69 0.05 0.26 0.04 0.04
1.5 0.04 57.2 10 0 0 1 1 1 0;
57 100 13.8 60 4 0.03 0 0.33 0.066 0.05 5.4 0.05 0.31 0.06 0.05
0.44 0.04 52 3 0 0 1 1 1 0;
58 100 13.8 60 4 0.02 0 0.25 0.05 0.04 7.3 0.05 0.24 0.05 0.04
0.4 0.04 69.6 10 0 0 1 1 1 0;
59 100 13.8 60 4 0.03 0 0.3 0.049 0.04 5.66 0.05 0.29 0.05 0.04
1.5 0.04 52.8 8 0 0 1 1 1 0;
60 100 13.8 60 4 0.03 0 0.29 0.057 0.05 6.7 0.05 0.28 0.05 0.05
0.41 0.04 48.6 9 0 0 1 1 1 0;
61 100 13.8 60 4 0.03 0 0.21 0.057 0.05 4.79 0.05 0.21 0.05 0.05
1.96 0.04 69 14 0 0 1 1 1 0;
62 100 13.8 60 4 0.02 0 0.17 0.046 0.04 9.37 0.05 0.12 0.05 0.04
1.5 0.04 62 5.6 0 0 1 1 1 0;
63 100 13.8 60 4 0.01 0 0.13 0.018 0.01 4.1 0.05 0.12 0.02 0.01
1.5 0.04 56.4 13.6 0 0 1 1 1 0;
64 100 13.8 60 4 0.02 0 0.1 0.031 0.03 7.4 0.05 0.1 0.03 0.03
1.5 0.04 184.6 13.5 0 0 1 1 1 0;
65 200 13.8 60 4 0.01 0 0.03 0.006 0 5.9 0.05 0.03 0.01 0
1.5 0.04 496 33 0 0 1 1 1 0;
66 100 13.8 60 4 0.03 0 0.02 0.003 0 4.1 0.05 0.02 0.01 0
1.5 0.04 600 100 0 0 1 1 1 0;
67 100 13.8 60 4 0.02 0 0.02 0.003 0 4.1 0.05 0.02 0.01 0
1.5 0.04 600 100 0 0 1 1 1 0;
68 200 13.8 60 4 0.01 0 0.04 0.007 0.01 7.8 0.05 0.03 0.01 0.01
1.5 0.04 450 50 0 0 1 1 1 0];

Exc.con=[...
1 2 10 -10 30 0.02 0 1 0.1 0.785 0.001 0 0.9
2 2 10 -10 30 0.02 0 1 0.1 0.785 0.001 0 0.9
3 2 10 -10 30 0.02 0 1 0.1 0.785 0.001 0 0.9
4 2 10 -10 30 0.02 0 1 0.1 0.785 0.001 0 0.9
5 2 10 -10 30 0.02 0 1 0.1 0.785 0.001 0 0.9
6 2 10 -10 30 0.02 0 1 0.1 0.785 0.001 0 0.9
7 2 10 -10 30 0.02 0 1 0.1 0.785 0.001 0 0.9
8 2 10 -10 30 0.02 0 1 0.1 0.785 0.001 0 0.9
9 2 10 -10 30 0.02 0 1 0.1 0.785 0.001 0 0.9
10 2 10 -10 30 0.02 0 1 0.1 0.785 0.001 0 0.9
11 2 10 -10 30 0.02 0 1 0.1 0.785 0.001 0 0.9

```
12  2  10  -10  30  0.02  0     1     0.1   0.785  0.001  0     0.9
13  2  10  -10  30  0.02  0     1     0.1   0.785  0.001  0     0.9
14  2  10  -10  30  0.02  0     1     0.1   0.785  0.001  0     0.9
15  2  10  -10  30  0.02  0     1     0.1   0.785  0.001  0     0.9
16  2  10  -10  30  0.02  0     1     0.1   0.785  0.001  0     0.9;];

Tg.con = [ ...
1   2  1  0.02  12  0.3   10  1  0  12  50  1;
2   2  1  0.02  12  0.3   10  1  0  12  50  1;
3   2  1  0.01  12  0.3   10  1  0  12  50  1;
4   2  1  0.02  12  0.3   10  1  0  12  50  1;
5   2  1  0.02  12  0.3   10  1  0  12  50  1;
6   2  1  0.02  12  0.3   10  1  0  12  50  1;
7   2  1  0.01  12  0.3   10  1  0  12  50  1;
8   2  1  0.02  12  0.3   10  1  0  12  50  1;
9   2  1  0.02  12  0.3   10  1  0  12  50  1;
10  2  1  0.02  12  0.3   10  1  0  12  50  1;
11  2  1  0.02  20  0.3   10  1  0  12  50  1;
12  2  1  0.02  40  0.3   10  1  0  12  50  1;
13  2  1  0.02  50  0.1   10  1  0  12  50  1;
14  2  1  0.01  50  0.1   10  1  0  12  50  1;
15  2  1  0.02  50  0.05  10  1  0  12  50  1;
16  2  1  0.02  50  0.3   10  1  0  12  50  1;];
```

References:

[1] UCTE. Final report of the investigation committee on the 28 September 2003 blackout in Italy.

[2] Ministry of power, G.o.I., Report on the grid disturbance on 30th July 2012 and grid disturbance on 31st July 2012, 2012.

[3] Ministry of power, G.o.I., Report of the Enquiry Committee on Grid Disturbance in Northern Region on 30th July 2012 and in Northern, Eastern & North-Eastern Region on 31st July 2012, 2012.

[4] U.S.-Canada power system outage task force. Final report on the August 14, 2003 blackout in the United States and Canada: Causes and Recommendations. Apr. 2004.

[5] Y. Xue, "Towards space-time cooperative defence framework against blackouts in China," *Power Engineering Society General Meeting, IEEE,* Tampa, FL, Jun. 2007.

[6] N. Senroy and G.T. Heydt, "A conceptual framework for the controlled islanding of interconnected power systems," IEEE Trans. On Power Systems, vol. 2, pp. 1005-1006, May. 2006.

[7] N. Senroy, G.T. Heydt and V. Vittal, "Decision tree assisted controlled islanding," IEEE Trans. On Power Systems, vol. 4, pp. 1790-1797, Nov. 2006.

[8] K. Mei and S.M. Rovnyak, "Response-based decision trees to trigger one-shot stabilizing control," *IEEE Trans. Power Systems,* vol. 19, pp. 531-537, Feb. 2004.

[9] I. Dobson, K.R. Wierzbicki, B.A. Carreras, V.E. Lynch and D.E. Newman, "An estimator of propagation of cascading failure," *Thirty-ninth Hawaii International Conference on System Science,* Hawaii, University of Wisconsin, Jan. 2006.

[10] M. Glavic, D. Ernst, D. Ruiz-Vega, L. Wehenkel and M. Pavella, "E-SIME- A Method for Transient Stability Closed-Loop Emergency Control: Achievements and Prospects," *Bulk Power System Dynamics and Control-VII*, Charleston, South Carolina, USA, Aug. 2007.

[11] A.L. Bettiol, L. Wehenkel and M. Pavella, "Transient Stability-constrained Maximum Allowable Transfer," *IEEE Trans. Power Systems*, Vol. 14, No. 2, May 1999.

[12] A.L. Bettiol, Y. Zhang, L. Wehenkel and M. Pavella, "Transient Stability Investigations on A Brazilian Network by SIME," *4th International Conference on*

Advances in Power System Control, Operation and Management, APSCOM-97, Hong Kong, Nov. 1997.

[13] M. Pavella, D. Ernst and D. Ruiz-Vega, *Transient Stability of Power Systems: A Unified Approach to Assessment and Control*, Kluwer Academic Publishers, 2000.

[14] D. Ernst, D. Ruiz-Vega, M. Pavella, P. M. Hirsch and D. Sobajic, "A Unified Approach to Transient Stability Contingency Filtering, Ranking and Assessment," *IEEE Trans. Power Systems*, vol. 16, no. 3, pp. 435-443, Aug. 2001.

[15] H. Shao and J.W. Bialek, "When to island in the controlled islanding scheme to prevent imminent wide-area blackouts," *47th International Universities' Power Engineering Conference*, London, UK. Sep. 2012.

[16] K. Sun, D. Zheng, and Q. Lu. "Splitting Strategies for Islanding Operation of Large-scale Power Systems Using OBDD-based Methods," *IEEE Trans. Power Systems*, vol.18, pp. 912-923, May 2003.

[17] Q. Zhao, K. Sun, D. Zheng, J. Ma, and Q. Lu, "A study of system splitting strategies for island operation of power system: a two-phase method based on OBDDs," *IEEE Trans. Power Systems*, vol.18, pp.1556-1565, Nov. 2003.

[18] K. Sun, D. Zheng, Q. Lu, "A Simulation Study of OBDD-based Proper Splitting Strategies for Power Systems under Consideration of Transient Stability," *IEEE Trans. Power Systems*, vol.20, pp.389-399, Feb. 2005.

[19] R. Moreno and A. Torres, "Security of the power system based on the separation into island," *IEEE PES Conference on Innovative Smart Grid Technologies (ISGT Latin America)*, 2011.

[20] J. Cheeger, A Lower Bound for the Smallest Eigenvalue of the Laplacian. Princeton Univ. Press, Problems in Analysis (R. C Gunning, ed.), 1970: p. 195-199.

[21] R. Moreno, Mario A. Ríos and Á , Torres, "Security schemes of power systems against blackouts in Bulk Power System Dynamics and Control (iREP) - VIII (iREP), " *iREP Symposium*, Rio de Janeiro, 2010.

[22] L. Ding, P. Wall amd V. Terzija, "A novel controlled islanding algorithm based on constrained spectral clustering," International Conference in Advanced Power System Automation and Protection (APAP), Beijing, 2011.

[23] L. Ding, F. M. Gonzalez-Longatt, P. Wall and V. Terzija, "Two-Step Spectral Clustering Controlled Islanding Algorithm," IEEE Transactions on Power Systems, vol.28, no.1, pp.75-84, 2003.

[24] H. You, V. Vittal and X. M. Wang, "Slow coherency-based islanding," *IEEE Trans. Power Systems*, vol.18, no.1, pp.483-491, 2004.

[25] B. Yang, V. Vittal and G. T. Heydt, "Slow-Coherency-Based Controlled Islanding ─ A Demonstration of the Approach on the August 14, 2003 Blackout Scenario," *IEEE Trans. Power Systems*, vol.21, no.4, pp.1840-1847, 2006.

[26] G. Y. Xu and V. Vittal, "Slow Coherency Based Cutset Determination Algorithm for Large Power Systems," *IEEE Trans. Power Systems*, vol.25, no.2, pp.877-884, 2010.

[27] M. Jin, T.S. Sidhu and K. Sun, "A New System Splitting Scheme Based on the Unified Stability Control Framework," *IEEE Trans. Power Systems*, vol.22, no.1, pp.433-441, 2007.

[28] S. Norris, S. Guo and J. Bialek, "Tracing of power flows applied to islanding," in Proc. 2012 IEEE Power and Energy Society General Meeting, pp. 1-8.

[29] S. Norris: "Preventing wide area blackouts in transmission systems: a new approach of controlled islanding using power flow tracing", PhD Dissertation, Durham University, 2014.

[30] Federal Energy Regulatory Commission, N.A.E.R.C., Arizona-Southern California Outages on September 8, 2011 – Causes and Recommendations, 2012.

[31] Jorge Miguel Ordacgi Filho, ONS. Brazilian Blackout 2009: Blackout Watch.National Grid, Updates from the November 2009 Brazilian Blackout - A simplified account based on public documents, 2010.

[32] J.D. McCalley. Transmission security: rules, risks and blackouts. Midwest ISO's System Operator Training Short Course. Iowa State University, Apr. 2006.

[33] Final reports on the blackout in southern Sweden and eastern Denmark, Sep. 23, 2003. www.svk.se

[34] Union for the co-ordination of transmission of electricity (UCTE). Final report: system disturbance on 4 November 2006.

[35] J. Bialek, “Why has it happened again? Comparison between the UCTE blackout in 2006 and the blackouts of 2003,” IEEE PowerTech Conference, Lausanne, Switzerland. Jul. 2007.

[36] J. Bialek, “Blackouts in the US/Canada and continental Europe in 2003: Is liberalisation to blame?” IEEE PowerTech Conference, St. Petersburg, Russia. Jun. 2005.

[37] D. S. Kirschen, “Do investment prevent blackouts?” Power Engineering Society General Meeting, IEEE. Tampa, FL, Jun. 2007.

[38] F. Bouffard. Power system security, lecture notes, 2010.

[39] Task force on understanding, prediction, mitigation and restoration of cascading failures. Vulnerability assessment for cascading failures in electric power systems, IEEE Power and Energy Society Power Systems Conference and Exposition, Seattle, WA, 2009.

[40] C.D. Vournas, “Technical Summary on the Athens and Southern Greece Blackout of July 12, 2004,” Aug. 2004.

[41] C.D. Vournas, V.C. Nikolaidis and A. Tassoulis, “Experience from the Athens blackout of July 12, 2004” IEEE PowerTech Conference, St. Petersburg, Russia. Jun. 2005.

[42] J. Mutale. Generation control and frequency regulation. lecture notes, 2010.

[43] P. Kundur, J. Paserba, V. Ajjarapu, G. Andersson, A. Bose, C. Canizares, N. Hatziargyriou, D. Hill, A. Stankovic, C. Taylor, T. Van Cutsem and V. Vittal, “Definition and classification of power system stability IEEE/CIGRE joint task force on stability terms and definitions,” *IEEE Trans. Power Systems*, Vol.19, pp.1387 – 1401, 2004.

[44] K. Morison, L. Wang and P. Kundur, “Power system security assessment,” *IEEE Power and Energy Magazine*, 2004.

[45] H. D. Chiang, C. C. Chu and G. Cauley, "Direct stability analysis of electric power systems using energy functions: Theory, applications and perspectives" *Proc. of the IEEE*, vol. 38, n. 11, pp. 1497-1529, Nov 1995.

[46] H. D. Chiang, F. F. Wu and P. P. Varaya, "Foundations of direct methods for power system transient stability analysis" *IEEE Trans. on Circuit and Systems*, vol. CAS-34, n.2, Feb 1987.

[47] H. D. Chiang. *Direct methods for stability analysis of electrical power systeml*. John Wiley & Sons, 2011.

[48] C. C. Chu and H. D. Chiang, "Boundary properties of the BCU method for power system transient stability," Proc. of *IEEE International Symposium on Circuit and System*, May 2010.

[49] C. C. Chu and H. D. Chiang, "Constructing analytical energy functions for lossless network-reduction power system models: Framework and new developments" *Circuits, Systems, and Signal Processing*, 18, pp. 1-16, 1999

[50] H. D. Chiang, "A theory-based controlling UEP method for direct analysis of power system transient stability," *IEEE International Symposium on Circuit and Systems*, May, 1989.

[51] Y. Zou, M. Yin, and H. D. Chiang, "Theoretical Foundation of Controlling UEP Method for Direct Transient Stability Analysis of Network-Preserving Power System Models" *IEEE Transactions on Circuits and Systems I: Fundamental Theory and Applications*, 50, 2003.

[52] J. P. LaSalle, "Some extensions of Liapunov's second method", *IRE Thns. on Circuit Theory*, vol. CT-7, 1960 pp.520-527.

[53] J. P. LaSalle, "Generalized invariance principles and the theory of stability", Centre for Dynamical Systems, Division of Applied Mathematics, Brown University, 1970.

[54] A. H. El-Abiad, K. Nagappan, "Transient stability regions of multimachine power systems", *IEEE Transaction on Power Apparatus and Systems*, vol.85, no. 2, Feb 1966 pp.169-178.

[55] N. Kakimoto, Y. Oshawa, M. Hayashi, " Transient stability analysis of elctrical power system via Lure-type Lyapunov function, part I and 11", *IEE of Japan*, vol.98 no. 5 and 6, May/June 1978.

[56] H. D. Chiang, F. F. Wu, P. P. Varaiya, "Foundations of PEBS method for power system transient stability analysis", *IEEE Bans. on Circuits and Systems*, vol. CAS-35 n.6,1988.

[57] H. D. Chiang, F. F. Wu, P. P. Varaiya, "A BCU method for direct analysis of power system transient stability", *IEEE Thns. on Power Systems*, 1994 pp.1194-1208.

[58] L.F.C Alberto, F.H.J.R Silva, N.G. Bretas, "Direct methods for transient stability analysis in power systems: state of art and future perspectives," *2001 IEEE Porto Power Tech Conference,* September, Porto, Portugal

[59] M. Pavella, "Bansient Stability of MultimachinePower Systems by Lyapunov's Direct Method," Paper 71-CP17-PWR, *IEEE Winter Power Meeting,* New York, Jan. 1971.

[60] C. K. Pang, F. S. Prabhakara, A. H. El-Abiad, A. J. Koivo, "Security evaluation in power systems using pattern recognition," *IEEE Transaction on Power Apparatus and Systems*, vol.93, pp.969-976, May 1974.

[61] P. Hou: "Power system security analysis: Applications for wind power allocations and smart islanding," Chalmers university of technology, MSc thesis, 2010.

[62] J. Machowski, J.W. Bialek and J.R. Bumby. *Power system dynamics: stability and control*. Oxford: J. Wiley&Sons, 2008.

[63] J.V. Milanovic. Modelling of synchronous machines, angular and voltage stability. Lecture notes, 2010.

[64] P. Kundur. Power system stability and control. New York: McGrawHill, 1994.

[65] G. O. A. Kalcon, G. P. Adam, O. Anaya-Lara, G. Burt and K. Lo, "Potential benefits of decoupling the Scotland-England network using VSC-HVDC," In *Proceedings of the 9th IET International Conference on AC and DC Power Transmission 2010.*

[66] R. Tumilty, C. G. Bright, G. M. Burt, O. Anaya-Lara and J. R. McDonald, "Applying series braking resistors to improve the stability of low inertia synchronous generators," *CIRED 2007,* Vienna, Austria.

[67] O. Anaya-Lara, F. M. Hughes, N. Jenkins and G. Strbac, "Influence of wind farms on power system dynamic and transient stability," *Wind Engineering*, *30*(2), 107-127.

[68] V. Vittal, R. Diao, S. Likhate, K. Sun and G. Xue. Arizona State University. Detection, prevention and mitigation of cascading events: Adaptive islanding with selective under-frequency load shedding. Final Project Report. Power Systems Engineering Research Center. 2008.

[69] Gonzalez-Longatt, D.F.; Available from: http://www.fglongatt.org/Test_Case_IEEE_14.html.

[70] K. R. Wierzbicki: “Statistical estimation of cascading blackout size and propagation with branching processes,” MSc thesis, 2006.

[71] I. Dobson, “Where is the edge for cascading failure?: challenges and opportunities for quantifying blackout risk,” *IEEE Power Engineering Society General Meeting*, Tampa FL USA, Jun. 2007.

[72] Sun, K., D.Z. Zheng, and Q. Lu, Searching for feasible splitting strategies of controlled system islanding. IEE Proceedings-Generation Transmission and Distribution, 2006. 153(1): p. 89-98.

[73] J. H. Chow. Time-scale modeling of dynamic networks with applications to power systems, Springer-Verlag, 1982.

[74] G. N. Ramaswamy, G. C. Verghese, L. Rouco, C. Vialas, C. L. DeMarco. Synchrony, aggregation, and multi-area eigenanalysis. IEEE Transactions on Power Systems. 1995, 10(4): 1986–1993.

[75] J. H. Chow. A nonlinear model reduction formulation for power system slow coherency and aggregation. Proceedings of Workshop on Advances in Control and its Applications: Lecture Notes in Control and Information Sciences. 1996, 208: 282-298.

[76] X. Wang, V. Vittal, G. T. Heydt. Tracing Generator Coherency Indices Using the Continuation Method: A Novel Approach. IEEE Transactions on Power Systems, 2005, 20(3): 1510–1518.

[77] S. Norris, H. Shao and J. Bialek, “Considering voltage stability in preventive islanding,” IEEE PowerTech Conference, Grenoble, France. Jun. 2013.

[78] J. Bialek,, Tracing the flow of electricity. IEE Proceedings-Generation Transmission and Distribution, 1996. 143(4): p. 313-320.

[79] J.W. Bialek and S. Ziemianek. Tracing based transmission pricing of cross-border trades: fundamentals and circular flows. in Power Tech Conference Proceedings, 2003 IEEE Bologna. 2003.

[80] J. Bialek and S. Ziemianek, Tracing Based Transmission Pricing of Cross-Border: Fundamentals and Circular Flows, in IEEE Bologna Power Tech Conference2003, IEEE: Bologna, Italy.

[81] J.W. Bialek, Tracing-based unifying framework for transmission pricing of cross-border trades in Europe. International Conference on Electric Utility Deregulation and Restructuring and Power Technologies, Proceedings, 2000: p. 532-537.

[82] Z. Lin, S. Norris, H. Shao and J. Bialek, “Transient stability assessment of controlled islanding based on power flow tracing,” 18th Power Systems Computation Conference, Wroclaw, Poland. Aug. 2014.

[83] F. Milano, Power System Analysis Toolbox Documentation for PSAT version 2.0.0 β_1, Dec. 2006.

[84] F. Milano, Power System Analysis Toolbox Quick Reference Manual for PSAT version 2.1.2, June 26, 2008.

[85] C. J. Mozina, M. Reichard and Z. Bukhala, et al, “Coordination of Generator Protection with Generator Excitation Control and Generator Capability,” *62nd Annual Conference for Protective Relay Engineers*, pp. 150-164, Mar. 2009.

[86] E. Pajuelo, R. Gokaraju and M.S. Sachdev, “Coordination of Overexcitation Limiter, Field Overcurrent Protection and Generator Control,” *Power and Energy Society General Meeting*, Jul. 2010.

[87] Instruction leaflet. Type CV frequency compensated voltage relays. ABB, Jun. 2008.

[88] NR Electric Co., Ltd. RCS-9400 Generator excitation system.

[89] P. Crossley. Introduction to overcurrent protection. Lecture notes. University of Manchester, 2009.

[90] Distance protection. Network Protection and Automation Guide.

[91] D.A. Tziouvaras and D. Hou, “Out-of-step protection fundamentals and advancements,” *57th annual conference for protective relay engineers*, Apr. 2004.

[92] A report to the power system relaying committee of the IEEE power engineering society. Power swing and out-of-step consideration on transmission lines. IEEE PSRC WG D6, 2005.

[93] M. Pavella and P. G. Murthy. *Transient stability of power systems*, John Wiley & Sons Ltd., ISBN: 0 471 94213 8.

[94] P. McNabb and J. W. Bialek, “A priori transient stability indicator of islanded power systems using extended equal area criterion,” *IEEE Power Engineering Society General Meeting*, San Diego, CA. Jul. 2012.

[95] Y. Xue and M. Ribbens-Pavella, “Critical cluster identification in transient studies,” IEEE Proc, 148, Pt-C, 216,231, 1993.

[96] H. Shao, S. Norris, Z. Lin and J. Bialek, “Determination of when to island by analysing dynamic characteristics in cascading outages,” IEEE PowerTech Conference, Grenoble, France. Jun. 2013.

[97] Y. Xue, Th. Van Cutsem and M. Ribbens-Pavella, “A simple direct method for fast transient stability assessment of large power systems,” *IEEE Trans. Power Systems*, vol. 3, no. 2, pp. 44-52, 1988.

[98] Y. Xue, Th. Van Cutsem and M. Ribbens-Pavella, “Extended equal area criterion, justification, generalizations and applications,” IEEE Trans. Power Systems, vol. 4, no. 1, 1989.

[99] Y. Xue, “Fast analysis of stability using EEAC and simulation technologies,” International Conference on Power System Technology, Beijing, Aug. 1998.

[100] Y. Xue, Y. Zhang, Z. Guo, P. Rousseaux, L. Wehenkel, M. Pavella, M. Trotignon, A. Duchamp and B. Heilbronn, “Dynamic extended equal area criterion: Part 2. Embedding fast valving and automatic voltage requlation,” IEEE/NTUA Athens Power Tech Conference, Sep. 1993.

[101] Y. Xue, Y. Luo, F. Xue, W. Zhu, K. Yang and J. Jiang, “Online transient stability assessment in operation: DEEAC in northeast China power system,” IEEE Computer, Communication, Control and Power Engineering, Beijing, Oct. 1993.

[102] Y. Xue, L. Wehenkel, R. Belhomme, P. Rousseaux, M. Pavella, E. Euxibie, B. Heilbronn and J. F. Lesigne, “Extended equal area criterion revisited,” IEEE Trans. Power System, vol. 7, no. 3, Aug. 1992.

[103] P. W. Sauer and M. A. Pai. Power System Dynamics and Stability, Prentice Hall, Inc., ISBN: 0 13 678830 0.

[104] D. Ernst, D. Ruiz-Vega, M. Pavella, P. M. Hirsch and D. Sobajic, “A unified approach to transient stability contingency filtering, ranking and assessment,” IEEE Trans. Power System, vol. 16, no. 3, Aug. 2001.

[105] D. Ruiz-Vega and M. Pavella, “A comprehensive approach to transient stability control: part 1-near optimal preventive control,” IEEE Trans. Power System, vol. 18, no. 4, Nov. 2003.

[106] D. Ruiz-Vega and M. Pavella, “A comprehensive approach to transient stability control: Part 2-open loop emergency control,” IEEE Trans. Power System, vol. 18, no. 4, Nov. 2003.

[107] D. Ruiz-Vega, A. R. Messina and M. Pavella, “Online assessment and control of transient oscillations damping,” IEEE Trans. Power System, vol. 19, no. 2, May 2004.

[108] A. Pizano-Martinez, C. R. Fuerte-Esquivel and D. Ruiz-Vega, “A new practical approach to transient stability-constrained optimal power flow,” IEEE Trans. Power System, vol. 26, no. 3, Aug. 2011.

[109] M. A. Pai, Energy Function Analysis for Power System Stability, Boston: Kluwer Academic Publishers, 1989.

[110] V. Ajjarapu and B. Leonardi. Online voltage stability margin monitoring using synchrophasor measurements and statistical multi-linear regression models. Iowa State University and Washington State University, 2010.

[111] D. Montgomery, E. Peck and G. Vining. Introduction to linear regression analysis. 4th edition, Hoboken, N.J., Wiley-Interscience, 2006.

[112] A. Alessandri, S. Grillo, S. Massucco, F. Silvestro and G. Vimercati, “ANN application for on-line power system security assessment,” 9th International Conference on Probabilistic Methods Applied to Power Systems. KTH, Stockholm, Sweden. 2006.

[113] A. Arulampalam and T. K. Saha, “Fast and adaptive under frequency load shedding and restoration technique using rate of change of frequency to prevent blackouts,” IEEE Power and Energy Society General Meeting, Minneapolis, Jul. 2010.

[114] J. A. Laghari, H. Mokhlis, A. B. Halim Abu Bakar, M. Karimi and A. Shahriari, “An intelligent under frequency load shedding scheme for islanded distribution network,” IEEE International Power Engineering and Optimization Conference, Melaka, Jun. 2012.

[115] H. You, V. Vittal and Z. Yang, “Self-healing in power systems: an approach using islanding and rate of frequency decline-based load shedding,” IEEE Trans. Power System, vol. 18, no. 1, Feb. 2003.

[116] X. Ding and P. A. Crossley, “Islanding detection for distributed generation,” IEEE Powertech Conference, St. Peterburg, Jun. 2005.

[117] A. Danandeh, H. Seyedi and E. Babaei, “Islanding detection using combined algorithm based on rate of change of reactive power and current THD techniques,” Asia-Pacific Power and Energy Engineering Conference, Shanghai, Mar. 2012.

[118] B. Liu, D. Thomas, K. Jia and M. Woolfson, “Advanced ROCOF protection of synchronous generator,” IEEE PES Innovative Smart Grid Technologies, Hilton Anaheim, Jan. 2011.

[119] J.C.M. Vieira, W. Freitas, Z. Huang, W. Xu and A. Morelato, “Formulas for predicting the dynamic performance of ROCOF relays for embedded generation applications” IEE Generation, Transmission and Distribution, vol. 153, no. 4, Jul, 2006.

[120] C. D. Vournas, P. W. Sauer and M. A. Pai, “Relationships between voltage and angle stability of power systems,” Electical Power and Energy Systems, vol. 18, no. 8, Feb. 1996.

[121] X. Yue and V. M. Venkatasubramanian, “Algorithms for detection of static voltage instability in power systems using synchrophasors,” 43rd Hawaii International Conference on System Science, 2010.